Faculté des bioingénieurs

Impact of artificial surfaces on Urban Heat Island (UHI) effect on the city of Louvain-la-Neuve

Study of the thermal radiance of materials and possible differentiation of surfaces from a TIR image

Auteur : Romane Maroye

Promoteur(s) : Pierre Defourny & Julien Radoux

Lecteur(s) : Sophie Bontemps & Xavier Draye

Année académique 2023-2024

Mémoire de fin d'études présenté en vue de l'obtention du diplôme de Bioingénieur en sciences et technologies de l'environnement

Acknowledgements

I would like to express my gratitude, first and foremost, to Prof. Pierre Defourny, my thesis supervisor, for his interesting proposal of subject, his guidance and support. In particular, I am sincerely thankful for the trust he placed in me by agreeing to supervise my study while I was on Erasmus at EPFL for the first term.

I extend my thanks to Dr. Julien Radoux for his guidance, availability, oversight, and invaluable advices throughout this research.

I would also like to express my gratitude to Ms. Sophie Bontemps and Prof. Xavier Draye, who agreed to read my study.

Moreover, I would like to thank the Earth and Life Institute of UCLouvain for the availability of the data.

I would also like to thank my parents for proofreading my study, offering their guidance and always supporting me. Additionally, I extend my appreciation to my brother, my sister, my grandparents and Martin Baltes for their support throughout my 5 years of study.

Table of Content

Table of figures

Table of tables

List of abbreviations

ANOVA	Analysis Of Variance
GHG	Greenhouse gases
IPCC	Intergovernmental Panel on Climate Change
LLN	Louvain-la-Neuve
NIR	Near-Infrared
SVF	Sky View Factor
SWIR	Shortwave-Infrared
TIR	Thermal Infrared
UHI	Urban Heat Island
VNIR	Visible and Near-Infrared

Introduction

The global climate has shown signs of change linked to increasing concentrations of greenhouse gases in the atmosphere. These changes include an increase in surface air temperature, changes in the spatial and temporal patterns of precipitation and an increase in the frequency of extreme events such as droughts and floods. However, the rise in surface air temperature is considered to be the most obvious change in the world's climate. According to the Intergovernmental Panel on Climate Change (IPCC), the rise in surface air temperature will tend to continue in the future as greenhouse gas (GHG) emissions increase (Sachindra et al., 2016).

In addition to this increase in temperature and the frequency of heat waves, cities will be more vulnerable due to the presence of the urban heat island (UHI) effect. The urban heat island is characterised by a higher air temperature in urban areas compared to surrounding rural areas (Santamouris, 2020). This difference in air temperature is due to the transformation of natural surfaces into artificial areas, which modifies the energy balance. It is also caused by the input of energy from human activities, in addition to solar energy. The energy balance disruption varies according to the types of urban development and the properties of their materials (Hassani, 2023).

The elevation of temperature associated with the UHI effect has several impacts on the environment.

Rising temperatures in cities have an impact on air and water quality. Indeed, all activities in cities lead to the production of harmful pollutants (ozone and fine particles). These pollutants become more concentrated due to the increased heat and the urban landscape, which prevents their dispersion.

Additionally, the UHI effect can elevate the temperature of runoff water, consequently affecting water quality in aquatic ecosystems. This alteration influences the biological and chemical processes within these systems, impacting water quality and disrupting the ecosystem. As a result, local fauna is affected in terms of reproduction and metabolism (Phelan et al., 2015). The UHI phenomenon also impacts biodiversity. According to the IPCC, climate change presents a threat to biological and ecological systems, impacting biodiversity, ecosystems and the delicate balance of nature (Kjellstrom et al., 2010).

The UHI effect also impacts human health.

The elevated temperature caused by the UHI contributes to deteriorating air quality, resulting in impacts on the health and comfort of urban residents. The rise in temperature enhances the production of tropospheric ozone, formed through the interaction of motor vehicle emissions (nitrogen oxides and volatile organic compounds) with solar UV radiation. Ground-level ozone exposure leads to respiratory tract irritation and mortality from heart and lung diseases. Increased exposure to air pollution may also result from elevated respiration as a physiological response to heat exposure (Kjellstrom et al., 2010).

The increased temperatures are also associated with an increased mortality rate due to effects on the cardiovascular and respiratory systems among urban residents. For example, in New England an elevation of 1°C in the average summer temperature corresponds to an estimated overall increase in mortality of 1%. In densely populated cities such as Hong Kong, Bangkok, and Delhi, increases in mortality ranging from 4.1% to 5.8% are observed for a 1°C rise above a temperature threshold of approximately 29°C. Thus, individuals exposed to UHI have higher risk of developing respiratory diseases, along with higher rates of cardiovascular and respiratory morbidity. This is because exposure to heat leads to a rise in core body temperature, an increase in heart rate, a shift in blood flow from the central organs to the skin, increased sweating and associated dehydration if replacement fluid intake is inadequate. Furthermore, there is also a risk of cardiac thrombosis due to dehydration in high temperatures and potential endothelial dysfunction (Shi et al., 2015; Kjellstrom et al., 2010; Wong et al., 2013).

Furthermore, UHI exacerbates the intensity and duration of heatwaves, significantly impacting the health of populations by elevating heat stress and mortality rates. An illustrative example is the 2003 heatwave in Europe, which resulted in approximately 70 000 deaths in Europe, with 15 000 in France alone. There was a discernible difference in excess mortality rates between urban and rural areas. Small medium-sized towns experienced a rate of 40%, while larger metropolitan area such as Paris and Lyon experienced respectively 141% and 80% more deaths. During this heatwave, an increase of 0.5°C above the average minimum night-time temperature doubled the risk of death in the elderly (Sachindra et al., 2016; Kjellstrom et al., 2010; Laaidi, K., 2012; Wong et al., 2013).

Finally, UHI also impacts energy consumption by increasing it. The warming of cities requires the use of air conditioning for cooling, which in turn consumes significant amounts of energy resources. The total electricity consumption showed an increase of between 0,5% and 8,5% per degree of temperature increase per person (Santamouris et al., 2015). The production of this additional energy involves the consumption of fossil fuels, which emits greenhouse gases (GHG) into the atmosphere, creating a positive feedback effect that further increases the UHI effect (Santamouris, 2020).

Given the harmful effects of urban heat islands, it is crucial to understand the factors influencing this phenomenon in order to mitigate its impacts. The emissivity of the surface material which is the ability of a material to emit thermal radiation, is one of these key factors. This study focuses on the city of Louvain-la-Neuve. It examines how Thermal InfraRed (TIR) images allow to determine the emissivity of the various surface materials used in this city.

Different types of artificial surfaces in Louvain-la-Neuve are first identified, based on on-site surveys as well as on optical images. Their thermal radiance values are then measured based on TIR images. Finally, using these measured values, the possible differentiation between the surface materials is investigated. By identifying the location and the associated emissivity of such various material surfaces, this study aims to provide support for urban management for reducing the impact of UHI.

Chapter 1. State of the art – Literature review

This section delves into the state of the art regarding Urban Heat Island (UHI) phenomenon. Firstly, it provides a definition of the phenomenon along with an explanation of its causes. Subsequently, it elucidates the fundamental concepts of electromagnetic radiation, including infrared radiation. Following that, a section is dedicated to exploring different types of artificial surfaces such as roof and ground covering materials and their specific characteristics. Finally, various methods employed for measuring UHI are elucidated.

1.1 Urban Heat Island (UHI) effect

1.1.1Definition and energy balance of UHI

The urban heat island (UHI) effect is a phenomenon defined by the air temperature difference between a city and the surrounding rural areas, with the temperature generally higher in the city. This difference has been evaluated in European cities and can vary between 1 and 10°C, with an average maximum value of 6°C (Santamouris, 2020).

The intensity of the phenomenon of UHI is most often defined as the difference between simultaneous air temperatures in an urban area (T_{urban}) and air temperatures in surrounding rural (T_{rural}) areas. (Yow, 2007)

$\Delta T = T_{urban} - T_{rural}$

Different types of UHI have been considered, depending on the definition of the location where these temperatures are observed:

- Boundary Layer Urban Heat Island (BLUHI) is based on air temperature measured well above the height of buildings in cities;
- Canopy Layer Urban Heat Island (CLUHI) is based on the near-surface air temperature measured below roof height;
- Surface Layer Urban Heat Island (SUHI) is based on the temperature of the soil below ground surface (Stewart et al., 2021; Branea et al., 2016).

The UHI affects the lower layers of the atmosphere and can be explained by different disruptions in the energy within the urban and rural surfaces. Indeed, due to differences in sources and losses of energy, the energy balance is generally modified in urban areas compared to rural areas (Piegon et al., 2008).

The energy balance of an urban area is established for a control volume from the ground to the top of the building.

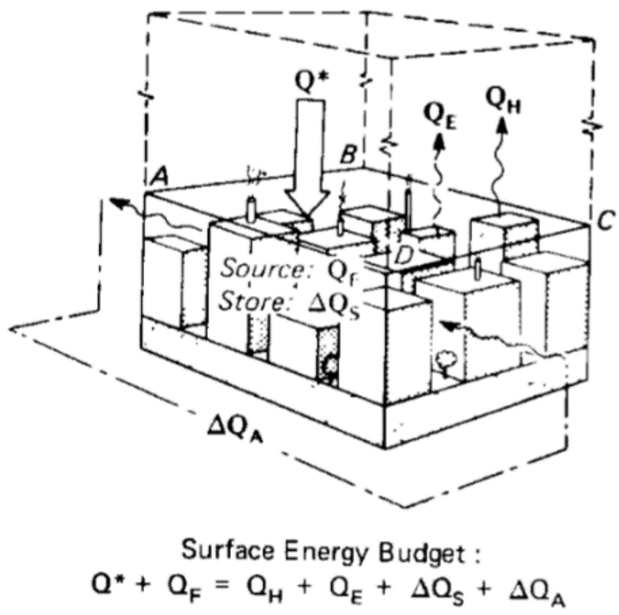

Figure 1: Schematic depiction of terms involved in energy balance of the urban surface (Oke, 1988)

The energy balance is then expressed by the following equation (Pigeon et al., 2008; Oke, 1988):

$$Q^* + QF = QH + QE + \Delta QS + \Delta QA$$

where

Q* = Net all-wave radiation received by the surface [W/m^2]. It is positive when the surface gains energy (day) and negative when it loses energy (night).

$Q^* = K\downarrow - K\uparrow + L\downarrow - L\uparrow$ where

- $K\downarrow$ = Incoming short-wave radiation
- $K\uparrow$ = Reflected short-wave radiation

Short wave radiation corresponding to solar radiation (0.15 µm - 3.0 µm)

- $L\downarrow$ = Incoming long-wave radiation
- $L\uparrow$ = Outgoing long-wave radiation (emitted and reflected by a surface)

Long-wave radiation corresponding to infrared radiation (3.0 µm - 100 µm)

QF = Heat release by anthropogenic combustion, always positive,

QH = Turbulent sensible heat flux, corresponding to the heat flow between the earth's surface and the atmosphere,

QE = Turbulent latent heat flux, corresponding to the flow of water vapour between the earth's surface and the atmosphere,

ΔQS = Net heat storage,

ΔQA = Net heat advection.

The alteration of the energy balance in urban areas is coming from the high heat capacity of urban surfaces, the lack of vegetation, heat trapping by urban geometries, low wind speed in urban areas and anthropogenic heat released from human and industrial activities (such as road traffic, heating of buildings…). Cities are generally highly urbanised and densely populated compared to rural areas (Santamouris, 2020).

Urbanisation is linked with the processes of the substitution of natural materials by artificial ones such as buildings, sidewalks, roads, parking, and so on (Oke, 1982). These materials absorb and re-emit more of the sun's heat than natural surfaces. The fraction of heat re-emitted varies according to the thermal properties of the materials. This process creates a difference in the equivalent temperatures between the city and the surrounding natural area.

1.1.2 Factors impacting the UHI

The intensity of the UHI can vary according to certain factors: the size of the city, the structure of the city and the building density, the thermal properties of artificial surfaces, the vegetation, the weather conditions, the nature of the activities carried out in the city, and the presence of water bodies (Sachindra et al., 2016).

- The structure of the city has an effect on the UHI. If the structure tends to act as an obstruction to the ventilation of urban air, it increases the effect of UHI. By the same theory, if building density is high, ventilation will be difficult, increasing the UHI effect. The urban layout, featuring narrow streets, hinders the cooling of surfaces such as roads and walls. This limitation arises from a reduction in net radiative losses, crucial for dissipating accumulated heat, due to the diminished Sky View Factor (SVF), which normally acts as a potent natural radiative sink (Pigeon et al., 2008).

  The SVF describes the fraction of sky visible, its value ranging from 0 to 1. A low sky view factor, meaning lesser canopy openness, tends to trap reflected radiations, as depicted in Figure 2. Consequently, these radiations are less effectively transmitted to the atmosphere, reducing the city's albedo and trapping (Choi et al., 2018). In addition, the city’s geometry can affect wind circulation, leading to the accumulation of heat and consequently an increase in temperature. Other parameters of the city such as the roughness and porosity can influence the wind circulation and so the UHI effect (Choi et al., 2018).

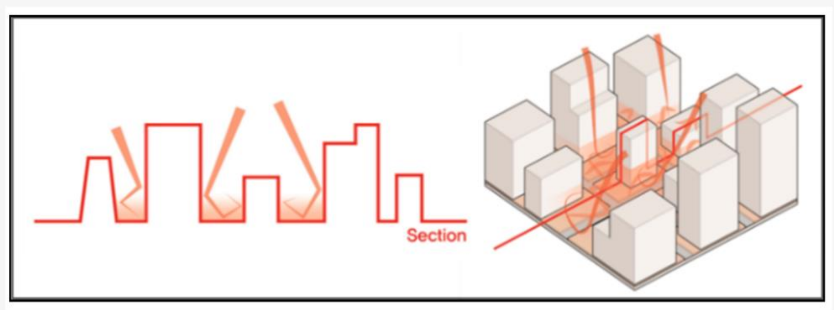

Figure 2 : Illustration of solar radiation trapping effect in urban areas (Choi et al., 2018).

- Another important parameter is the thermal properties of the material used, such as emissivity and albedo, which impact the energy balance. The thermal behaviour of materials of urban surfaces tends to absorb solar and infrared radiation and subsequently release the accumulated heat into the atmosphere through convection and conduction processes, thereby increasing the ambient temperature (Santamouris, 2011). Regarding the albedo, it describes the average reflectance of surfaces, representing the ratio of reflected solar energy flux to incident solar energy flux. It is measured on a scale of 0 to 1 and depends on the colour of the surfaces: a surface with a relatively high albedo (>0.75) is light-coloured and a surface with a low albedo (<0.25) is generally dark-coloured (Hassani, 2023).

  As a result, surfaces with high albedo are highly reflective, absorbing less energy and bouncing it back to the atmosphere. On the other hand, if the albedo is low, the surface will store a lot of energy and the urban temperature will increase.

  Regarding the emissivity, it is the ability of a material to emit thermal radiation compared to an ideal black body at the same temperature. It will be more explained in Chapter 1.2.2.

- In addition, cities are generally sparsely vegetated, and the lack of vegetation reduces the city's cooling potential. First, because plants and trees provide shade which prevents the sun's rays from hitting the ground. Floor and facade coverings that absorb less energy during the day will release less heat at night. Secondly, plants and trees cool the air through evapotranspiration (Stewart et al., 2021; Branea et al., 2016; Hassani, 2023). Consequently, urban vegetation has a mitigating impact on air temperature during both summer and winter periods, playing an important role in improving cooling rates. Enhancing vegetation proves to be a valuable solution compared to urban surfaces since vegetated surfaces exhibit significantly lower temperatures compared to non-permeable urban surfaces (Choi *et al.*, 2018).

- Anthropogenic activities produce a flow of anthropogenic heat from road traffic, heating, and industrial waste, among other sources. This anthropogenic heat flow is greater in urban areas than in rural areas due to the concentration of population and activities. This heat input has an impact on the UHI effect and should not be neglected. It is estimated to account for between 5 and 8% of the total heat flow in most cities and can sometimes reach very high values (Hassani, 2023).

- Weather conditions significantly influence the UHI effect. High wind speeds and cloud cover contribute to reducing its intensity whereas clear skies and calm winds are conducive for nocturnal UHI development. Clouds play a crucial role in altering nocturnal radiative cooling, a process during which the UHI forms (Pigeon et al., 2008; Yow, 2007).

  An illustration of this factor is given in Figure 3.

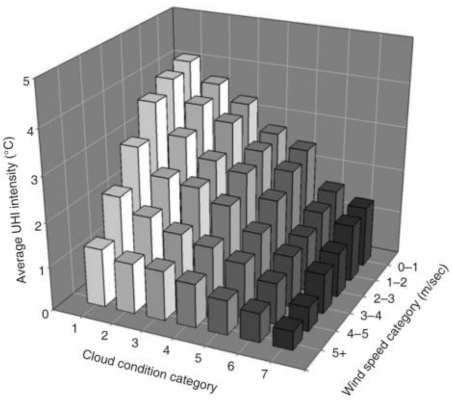

Figure 3 : Intensity of UHI depending on cloud condition and wind speed. In terms of the cloud axis, category 1 represents clear conditions, while category 7 represents completely overcast conditions. (Yow, 2007).

- The presence of water bodies, such as river or groundwater, also plays a role in influencing the UHI effect by lowering air temperatures through water evaporation (Stewart et al., 2021; Choi et al., 2018).

1.1.3 Typical patterns of UHI

The UHI displays temporal variations, featuring a consistent daily pattern illustrated in Figure 4, with its intensity being more intense during the night than during the day.

It amplifies during the nocturnal period, responding to a less effective cooling rate in highly urbanized areas compared to peripheral zones. This is due to the release of accumulated energy from the urban canopy into the atmosphere, sustaining convective heating that hinders nocturnal cooling. In most cases, the peak UHI intensity appears a few hours after sunset, followed by a rapid decrease after sunrise. The UHI intensity diminishes with increasing wind speed (Pigeon et al., 2008).

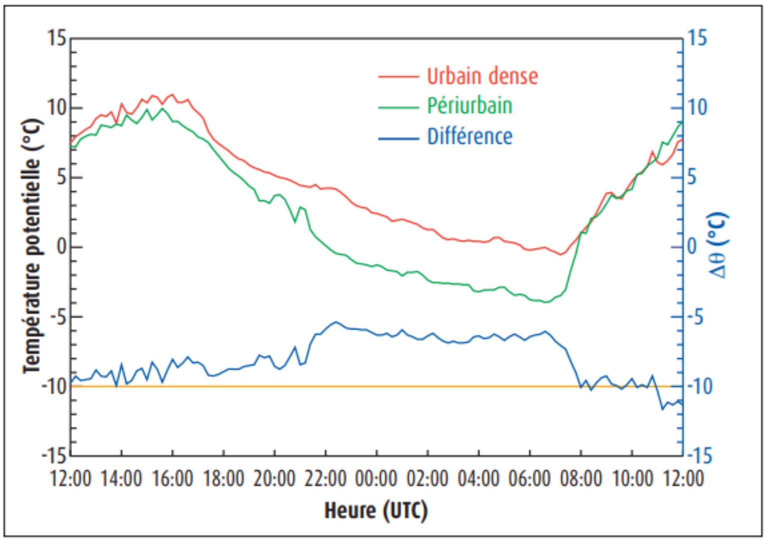

Figure 4 : Change in temperature at two points in Toulouse on 25 February 2005, during the Capitoul campaign (Piegon et al., 2008)

Seasonal patterns, as observed in the study of Pigeon et al. (2008), indicate that UHIs are more prevalent in summer, tend to form later in winter, and exhibit a slower decrease in intensity during the morning. Additionally, UHIs are weaker and less frequent during rainy periods.

1.2 Energy and Energy transfer

The energy can be transfered through different processes (radiation, convection and conduction) in different forms such as radiation, sensible and latent heats. In this master thesis, the relevant energy transfer process is the radiation.

1.2.1 Radiation

All objects with a temperature above absolute zero Kelvin emit electromagnetic radiation from their surface (Avdelidis & Moropoulou, 2003).

- The electromagnetic spectrum refers to the intensity of a mix of electromagnetic waves based on wavelength or frequency. The speed of expansion of electromagnetic waves equals the speed of light, expressed as

  $\lambda \cdot f = c$, with

  - the wavelength (λ),
  - the frequency (f)
  - and the light speed (c)
- This spectrum spans a wide range of electromagnetic radiation based on their wavelength which can be separately used for various purposes by different industrial sectors.
- Electromagnetic radiation follows physical principles like diffraction and reflection.

The human eye can be considered as a remote sensor of this spectrum, although it only operates in a limited spectral range, the visible electromagnetic spectrum.

The amount of electromagnetic radiations is directly proportional to the object's intrinsic temperature (Optris, n.d. ; Antoine & Lopez, 2017) in the absence of any other source of energy. A black body is a theoretical physical object that absorbs all incoming radiation, exhibiting no reflective or transmissive properties. This is described by the parameters $\alpha = \varepsilon = 1$, with α the absorption and ε the emissivity.

The spectral distribution of energy emitted by a black body, as a function of its temperature, can be described by the Planck's law. In a black body, electromagnetic radiation at a specific wavelength depends only on its surface temperature. This phenomenon is expressed through the spectral radiance energy, denoted as B_{λ}, which varies with wavelength (Antoine & Lopez, 2017, Dubuisson et al., 2017; Marr & Wilkin, 2012)

$$\text{Planck's law}: \; B_{\lambda} = \frac{2hc^2}{\lambda^5} \frac{1}{exp^{hc/(\lambda kT)} - 1} \; [W/m^2 sr\ m]$$

where

- $k = 1{,}38.10^{-23}$ [J/K], Boltzmann's constant
- $h = 6{,}62.10^{-34}$ [J.s], Planck's constant
- $c = 3.10^{8}$ [m/s], the light speed

For a blackbody, the brightness temperature is the temperature at which it emits the same luminance as the observed surface. Therefore, when the value of the spectral radiance energy is known, it becomes possible to calculate the brightness temperature of the object. This brightness temperature corresponds to the temperature that the object's temperature would be if it behaved as a blackbody, emitting the same amount of energy (Antoine & Lopez, 2017).

1.2.2 Emissivity

In reality, bodies don't behave with the same properties as a blackbody; we call them grey bodies.

Emissivity, ε, is a variable that quantifies the relationship between actual radiation and that of a blackbody, ranging from zero to one. The emissivity is the ratio between the spectral radiance of an object and the spectral radiance of a blackbody at the same temperature (Dubuisson et al., 2017; Avdelidis & Moropoulou, 2003).

Surface temperature and emissivity are interconnected through the radiative transfer equation, expressed in the radiation heat transfer equation of Stefan Boltzmann's law for a Gray body (Green & Perry, 2008) :

$$q = \varepsilon\sigma T^4 \ [W/m^2]$$

where

- q= radiation heat transfer,
- ε = emissivity (between 0 and 1)
- σ = 5.6697×10^{-8} W/m^2K^4, Stefan–Boltzmann constant

Precise surface temperature values cannot be retrieved unless surface emissivity is accurately characterized. A deviation of 0.01 units in emissivity introduces an error of 0.5°C in temperature. Therefore, ensuring the accurate determination of emissivity for urban surfaces is crucial, given the highly heterogeneous nature of a city, with materials possessing emissivity below 1 (Sobrino et al., 2012).

The emissivity value depends on the material properties, its surface, temperature, wavelength and measuring angle:

- Materials that are not metallic tend to exhibit a consistently high emissivity, regardless of the surface texture, particularly in the long-wave spectral ranges.

Regarding plastic materials, their transmission rate varies according to wavelength. It is inversely proportional to thickness, with thin materials being more transmissive than thick ones. Optimal measurements can be taken at wavelengths where transmissivity is nearly zero, independent of thickness (Optris, n.d.).

- Metallic materials, on the other hand, tend to have low emissivity, which is highly dependent on the consistency of the surface and decreases at higher wavelengths (Optris, n.d.). Metallic surfaces, with their low emissivity, have high reflectance and act as a mirror (Avdelidis & Moropoulou, 2003). Measuring the temperature of a metallic material can give variable and unreliable results. It is important to choose an appropriate temperature measurement device. Infrared radiation must be measured at a specific wavelength and in a specific temperature range, in which metallic materials have a relatively high(er) emissivity. It is preferable to use the shortest possible wavelength, as measurement error increases in correlation with wavelength. For example, the best wavelength at high temperatures is 0.8 to 1 µm for metals (Optris, n.d.).

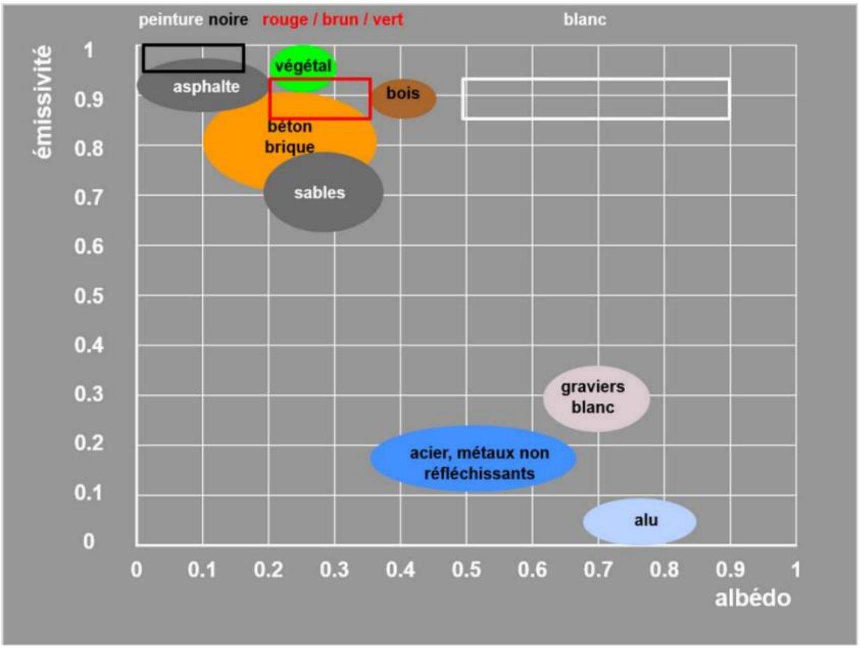

Figure 5 : Link between emissivity and albedo of materials (Hassani, 2023)

1.2.4 Infrared radiation

The infrared radiation, a small part of the spectrum between the visible and the microwaves, ranges from around 0.78 µm to approximately 1000 µm.

Infrared radiation, wavelengths from 0.7 to 14 µm, is relevant for measuring surface temperature because the amount of radiative energy emitted by the object at ambient temperature is higher at 8-14 µm. As depicted in Figure 6, there is a noticeable peak in radiative energy at ambient temperature above 10 µm (λ_{max} = 9,66 for 300K = 27°C). This characteristic underscores the significance of infrared radiation for accurate temperature identification (Antoine et al., 2017). The Wien's displacement law stipulates that the wavelength for maximum intensity is inversely proportional to the absolute temperature (Green & Perry, 2008).

Wien's equation : $\lambda_{max} = \frac{2.89710^{-3}}{T} \quad [m]$

where

- $T =$ temperature of the blackbody
- $2.89710^{-3}[mK] =$ Wien's constant

It is worth mentioning that near-infrared (NIR) and shortwave-infrared (SWIR) wavelength are influenced by reflective properties of the surface and can not be used to estimate the temperature, unlike the thermal infrared.

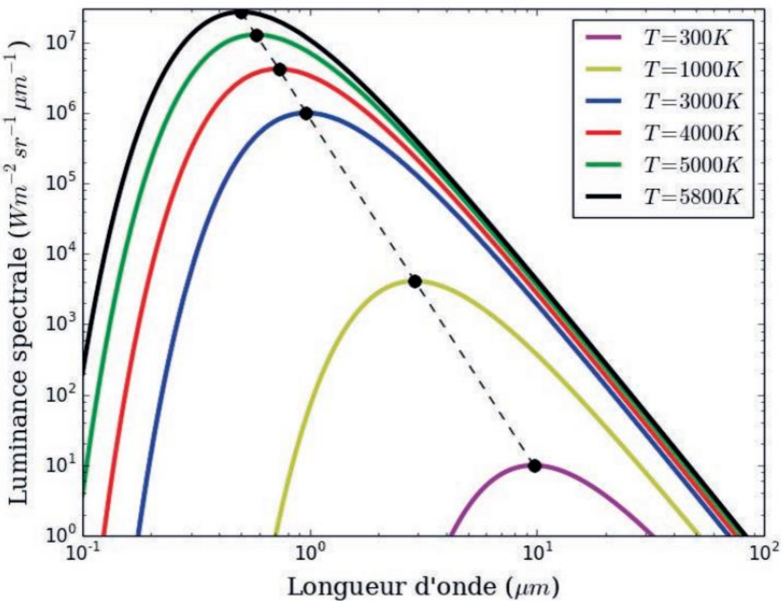

Figure 6 : Spectral distribution of the luminance energy emitted by a blackbody, calculated from Planck's law for a temperature T varying from 300 to 5800 K and presented on a log-log scale (Dubuisson et al., 2017).

- Infrared radiation is a type of electromagnetic radiation whose radiant energy cannot be seen by the human eye.

- It can be detected by sensors such as infrared cameras which can capture the heat emitted by the object, to produce an image reflecting temperature variations (Antoine et al., 2017).
- The camera uses an optical lens. The beams are focused on the object, which generates an electrical signal proportional to the radiation. The signal is then amplified and transformed into an output signal proportional to the object's temperature (Optris, n.d.).
- The obtained temperature represents the brightness temperature, equivalent to a blackbody's temperature, without considering emissivity (Antoine et al., 2017).

1.3 Infrared thermography sensing

In the context of climate change and the UHI effect accompanying this change, it is crucial to explore the environmental impacts caused by different infrastructures (Chui et al., 2018).

- In order to mitigate UHI effect, reducing the surface temperature also decreases air temperature within the lower boundary layer through convective heating from below.
- The materials used in cities have a significant influence on the urban heat island effect as the surface temperatures of infrastructures vary based on their constituents. Indeed, there are significant temperature differences between different surface materials receiving the same insolation.

The main factors leading to high urban surface temperatures on a large scale include low-albedo surfaces, the absence of vegetation, the angle of solar incidence on a surface, and light trapping. Indeed, white surfaces with high albedo values tend to have lower surface temperatures. Vegetation also maintains a lower temperature through evapotranspiration, enabling plants to self-regulate (Chui et al., 2018).

Hence, it is crucial to determine the surface temperature of materials in urban areas. Surface temperatures are established through the detection of longwave or thermal infrared radiation emitted by all terrestrial matter (Chui et al., 2018).

Remote sensing can offer a comprehensive overview of urban areas and enable the generation of urban maps to determine physical parameters such as surface temperature (Sobrino et al, 2012), which is particularly relevant in the context of UHI.

In the past, different remote sensing technologies have been used based on various physical properties, including acoustic, magnetic, seismic, chemical, and electromagnetic (EM) characteristics (de Loor, 1970).

Today infrared thermography, a common remote sensing method, uses infrared radiation emitted by an object to identify and quantify its surface temperature. This method involves aerial flights using thermal infrared cameras to capture infrared radiation or the so-called temperature of brightness. Subsequently, corrections are applied to infrared thermograms to obtain the real surface temperature.

To achieve this, several parameters must be taken into account including the surface’s emissivity, the heat flux coming from the environment and, possibly, reflected by the studied surface and the atmospheric transmission factor (Candoré, 2008).

1.4 Variety and characteristics of ground covering materials.

It is therefore crucial, to pay attention to the materials used in urban areas. As urban areas are densely built up, ground is highly covered by artificial surfaces such as construction materials.

This section focuses on materials that are covering ground surfaces.

1.4.1 Different ground covering materials.

The main constructions materials used in Belgium for ground coverings are concrete, asphalt, cobblestones of natural stone and gravels (Becosan, 2020).

Concrete is the result of mixing coarse aggregate (gravel) with fine aggregate (sand), cement and water. It is used for roads (Becosan, 2020).

Asphalt is mainly composed of natural bitumen (hydrocarbons), which are refined during the industrial process of oil distillation. It is dark in colour and varies in consistency, ranging from solid to semi-solid or liquid (Becosan, 2020).

Cobblestones are worked stones characterised by their rectangular shape. This paving material can be made from granite or basalt, which are very resistant rocks. For town improvements, such as those used for pedestrian crossings and pavements, they are more often made from concrete, with various colour pigments (Becosan, 2020). In the Walloon Brabant region of Belgium, old cobblestones roads are usually made from local stones, such as sandstone, porphyry or limestone, which are abundant in the region. Belgian blue stones, which are more expensive, are more commonly used privately (Pierre & sol, n.d.).

In addition to these building materials, it is common to find other materials in urban environments, such as gravel and wood. Wood, for example, is often used in the construction of terraces, footbridges and similar structures in urban environments.

The following table shows the emissivity values of the different ground cover materials.

Table 1 : Table of emissivity for ground covering (Moretti et al., 2021; Omega Engineering, n.d ; Thermometer.eu, 2024 ; Vleck, 1982 ; Zhong et al., 2022).

Ground Material	Emissivity ε
Asphalt (38°C)	0.93
Basalt (20°C)	0.72
Concrete	0.91
Granit	0.96
Gravel (38°C)	0.90
Limestone (38°C)	0.95
Sandstone (38°C)	0.67
Wood (Low temperature)	0.80-0.90

1.4.2 Fluctuation of ground covering emissivity and surface temperature due to moisture content

It is essential to correctly identify the emissivity, since a 1% uncertainty in the emissivity value could lead to a 0.5°C uncertainty in the surface temperature under moderate conditions and up to 1°C in less humid and warmer situations (Sobrino et al., 2012). This is why the study of Zhong *et al.*, (2022) focuses on the effects of surface moisture content on thermal infrared emissivity of urban underlying surfaces. This study is based on impervious (concrete paving, granite paving and asphalt) and permeable (red clay brick paving, permeable brick paving, gravel road, grass, shrubs and soil) urban materials.

The spectral characteristics of the surfaces before and after watering were studied (Zhong et al., 2022). The surfaces were separated and studied at two different times. First in the afternoon, when the sun's rays were less intense, enabling to capture the dry, wet and water film states.

The emissivity spectra for granite paving stones, red clay paving stones, asphalt road and soil, showed three states, shown in Figure 7: dry (blue line), after watering, a film of water formed on the surfaces (red line), wet, after some of the water had evaporated (green line). The spectrum of pure water was plotted (yellow line) for reference.

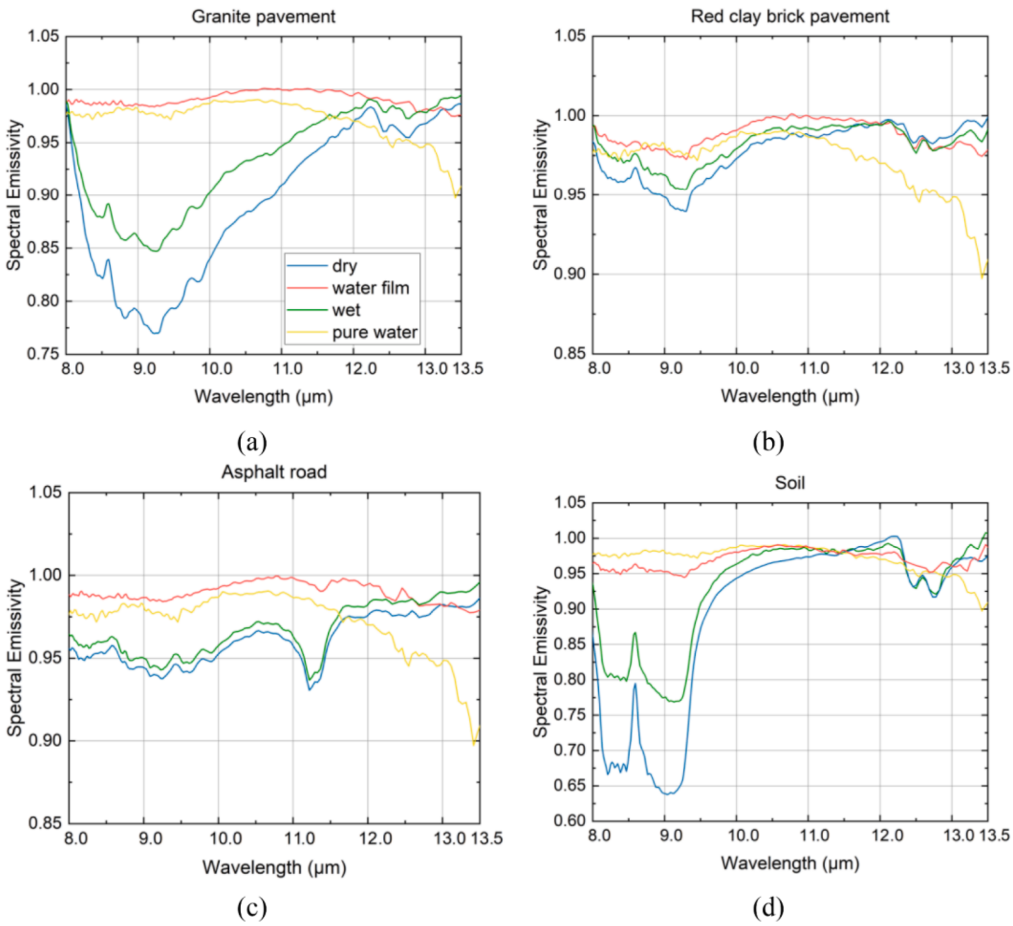

Figure 7 : Emissivity spectra (8.0–13.5 μm) for the permeable surfaces (Zhong et al., 2022)

Then, at midday, when the sun's rays were more intense, allowing only the dry and water film states to be captured. The emissivity spectra for the surfaces (concrete paving, permeable paving, grass, shrubs and gravel road) showed two states due to the faster evaporation. As shown in figure 8: dry surfaces (blue line), a film of water formed (red line). Similarly, the spectrum of pure water was plotted (yellow line).

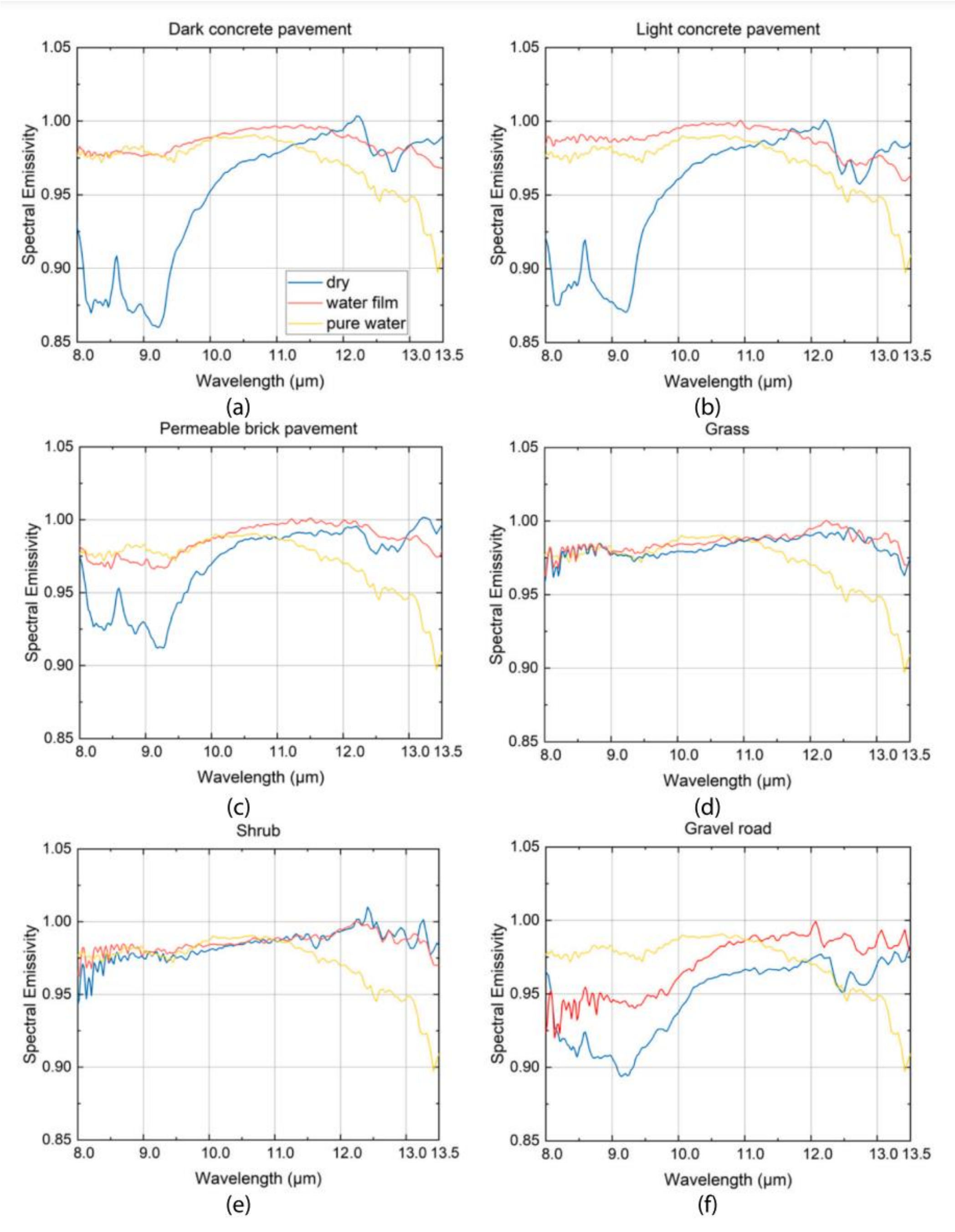

Figure 8 : Emissivity spectra (8.0–13.5 µm) for the impermeable surfaces (Zhong et al., 2022)

The Figure 7 and Figure 8 exhibit variations of the emissivity depending on the soil moisture content. The surface moisture content has little effect on the emissivity of permeable soils and a significant effect on the other soils. The variation in emissivity observed for concrete paving, granite paving, asphalt roads and soil exceeded 0.02 before and after watering, resulting in temperature fluctuations of 0.9, 2.1, 1.0 and 2.3°C, respectively. Differences in precipitation could induce distinctive variations in emissivity, even for surfaces composed of similar materials (Zhong *et al.*, 2022).

The study by Mohammad and Goswami (2021) examines the impact of soil moisture on surface temperature variations. Higher soil moisture is associated with lower UHI intensity. This is because the supply of soil moisture makes a significant contribution to surface cooling during the day, as the evaporation of water in moist soils consumes energy. Moist soils have a greater capacity to absorb and store heat during the day and release it slowly at night. Releasing heat more slowly contributes to slower and more moderate temperature variations compared with dry soil (Mohammad and Goswami, 2021).

1.5 Variety and characteristics of roof types in Wallonia

1.5.1 Different roofs in Wallonia

As described previously, the composition of urban infrastructures holds significant importance within UHI context. Exploring the spectral properties of urban materials is beneficial to assess the heating and cooling effects of urban materials in UHI mitigation strategies. One of the most crucial properties to consider is the emissivity of materials.

Accurately characterising the emissivity of different types of roofs is essential, given the significant variations between different materials. With this nuanced understanding of emissivity, these values can be used accurately, ensuring precise calculations of the contribution of each material to the energy balance. It is therefore important to look at the different types of roofs in the study area.

This study is dedicated to Belgium, and more precisely to Louvain-la-Neuve, in Wallonia. Roofing materials in Wallonia exhibit a large diversity. This is due to the large number of geographical sub-regions, the development of Wallonia and its strong economic connections with the surrounding countries of Europe (Wyard, 2023).

In the study performed by Wyard (2023), the Walloon Roof Material (WaRM) spectral library reflects the diversity of roof materials used in Wallonia:

- There are 26 types of roofs identified in the study in Wallonia and the spectral ranges from 350 to 2500nm.
- The 26 different types of roofs can be distributed in 7 classes of roofing materials, as illustrated in Figure 9 : metals, tiles, slates, membranes, PVC, solar panels, and corrugated (asbestos-cement) sheets.

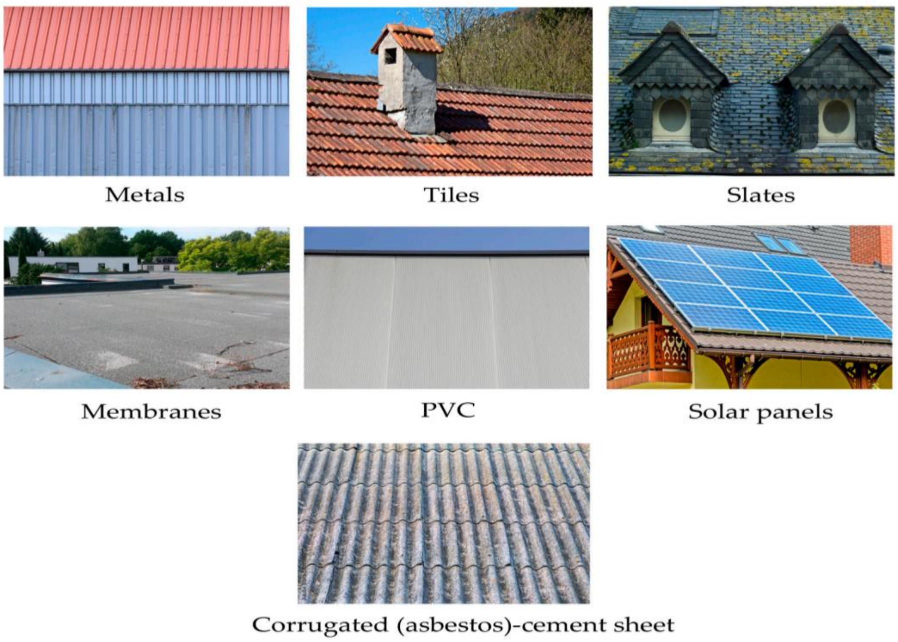

Figure 9 : Example of the 7 different classes of roof type from the WaRM (Wyard, 2023)

The following table provides an inventory of the 26 main roof types identified in Wallonia and the distribution in their respective class according to Wyard, 2023.

With this distribution, we create subclasses within the roof type class. We may observe that, for example, the Metal Class includes 4 different metals and 7 roof types (sub-classes of the Metal class).

Table 2 : 26 main roof materials used in Wallonia and associated class (Wyard, 2023).

Roof Material	Class
Aluminium—Black painting	Metal
Aluminium—Grey painting	Metal
Aluminium—Natural	Metal
Lead—Natural	Metal
Steel—Black painting	Metal
Steel—Grey painting	Metal
Steel—Orange painting	Metal
Zinc—Natural	Metal
Artificial slate with asbestos—Brown colour	Slate
Artificial slate without asbestos—Anthracite colour	Slate
Artificial slate without asbestos—Brown colour	Slate
Artificial slate without asbestos—Light grey colour	Slate
Artificial slate without asbestos—Purple colour	Slate
Natural slate—Anthracite colour	Slate
Natural slate—Purple colour	Slate
Bitumen membrane—Black colour	Membrane
EPDM membrane—Black colour	Membrane
Ceramic tile—Black colour	Tile
Ceramic tile—Brown colour	Tile
Ceramic tile—Orange colour	Tile
Concrete tile—Black colour	Tile
Concrete tile—Brown colour	Tile
Fiberglass roofing panel—Translucent and corrugated	PVC
Polycarbonate panel—Twin wall	PVC
Corrugated asbestos cement sheet	Corrugated cement sheet
Photovoltaic solar panel	Solar panel

1.5.2 Roof reflectance

The spectral library opens up the possibility of detecting roof materials using Earth Observation data.

Each type of roof exhibits unique reflectance spectra, contributing to their distinct characterization. The spectral-reflectance signatures of the different roof types were acquired using an ASD FieldSpec3 Hi-Res spectrometer, under laboratory conditions. This is illustrated in the figures 10, 11 and 12 for the 26 roof types.

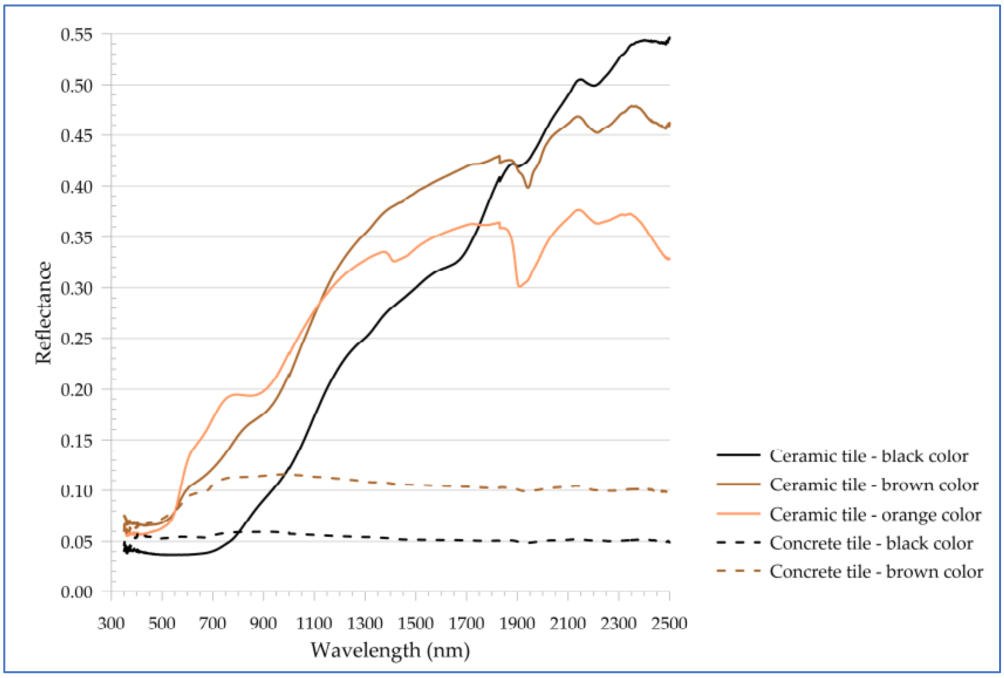

Figure 10 : Reflectance spectra of ceramic and concrete tiles (Wyard, 2023).

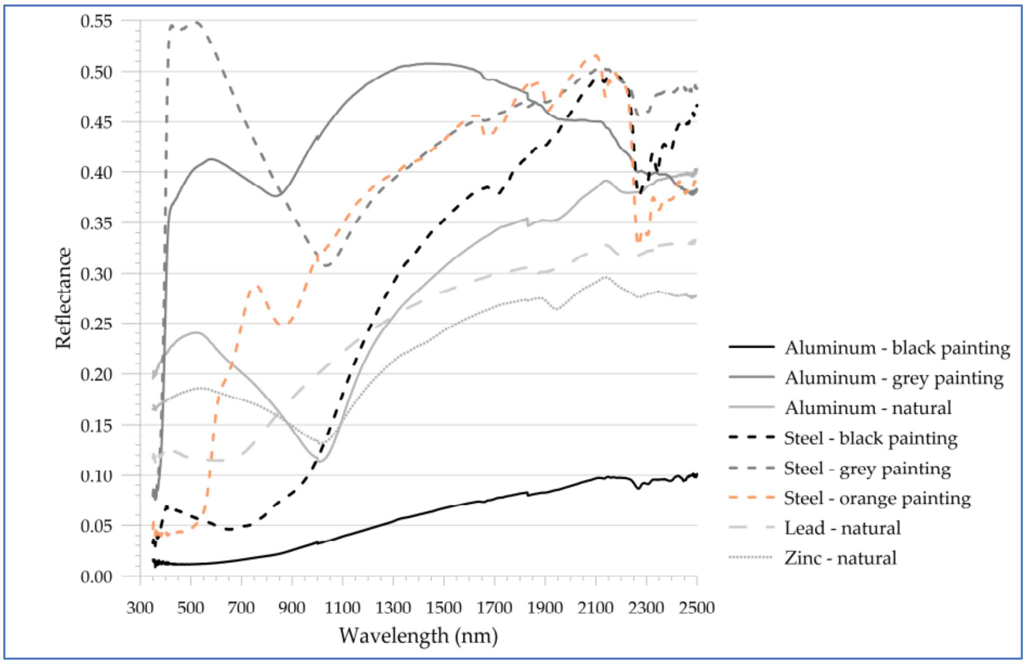

Figure 11: Reflectance spectra of metallic roof materials (Wyard, 2023).

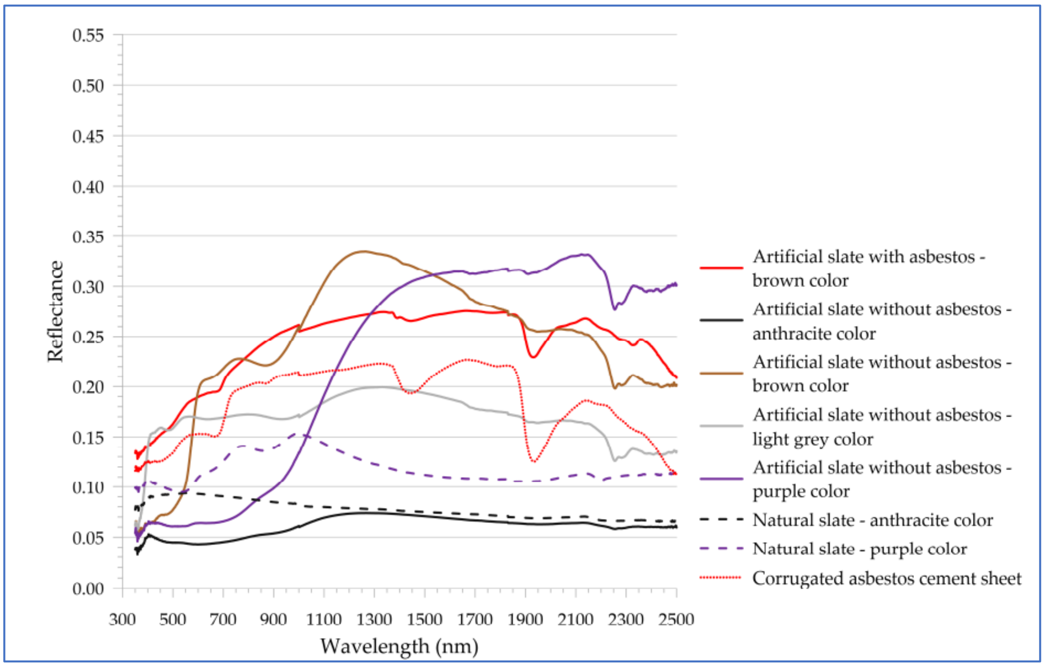

Figure 12 : Reflectance spectra of natural and artificial slates, and asbestos roof materials (Wyard, 2023).

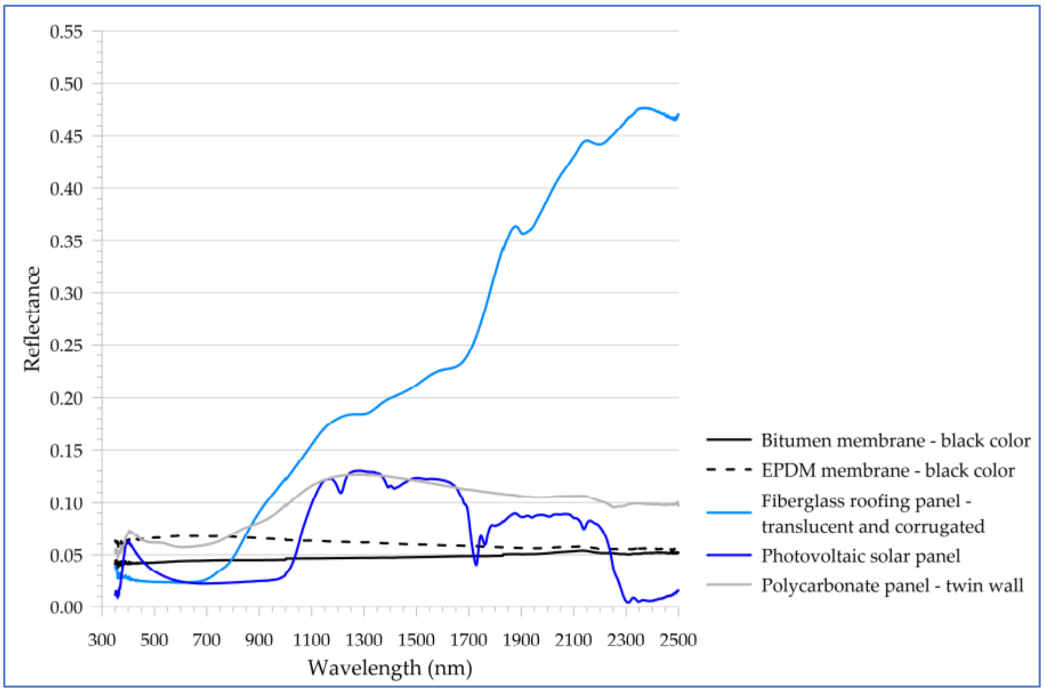

Figure 13 : Reflectance spectra of remaining five roof materials (Wyard, 2023).

In the visible spectral range, the influence of the colour is highlighted. The shortwave-infrared (SWIR) spectral range, which spans from 1 µm to 2.5 µm, is more relevant than the visible range for distinguishing between various materials. Nevertheless, exceptions arise with black materials sharing similar properties and very close spectra, indicating that their spectral signatures lack sufficient distinctiveness. Additional information, such as roof slope and texture, would enhance the identification of different types (Wyard, 2023).

1.5.3 Roof emissivity

The Table 3 presents the overall emissivity values that can be found in the literature review associated to the above 7 classes of roof types with, when necessary, some more specific values for some roof types sub-classes (like Metals and Concrete tiles).

Table 3 : Table of emissivity for roof (Green & Perry, 2008; Omega Engineering, n.d; Plachý, 2019; Subedi et al., 2019; Thermometer.eu, 2024).

Roof Material	Emissivity ε
Metals	
Aluminium	0.04
Steel	0.27
Zinc	0.23
Non-metals	
Ceramic (porcelain)	0.92
Concrete tile—Black colour	0.83-0.87
Concrete tile—Brown colour	0.91-0.94
Slate	0.67-0.80
EPDM membrane—Black colour	0.90
Bitumen membrane	0.92
Fiberglass roofing panel	0.80-0.90
Corrugated asbestos cement sheet	0.96
Polycarbonate panel	0.91-0.93
Photovoltaic solar panel (solar cell cover glasses)	0.70-0.90

The validity of emissivity values may be subject to variations depending on the specific composition of materials, emphasizing the need to verify their accuracy for each particular case.

The exclusion of green roofs from the table is attributed to the dependency of their emissivity on the type of vegetation, typically resulting in higher values due to the presence of plants.

1.6 Methods for assessing the impact of ground covering on UHI in cities

The study of Ibrahim et al., (2018) examined the impact of road coverings on UHI effect in Malaysia. The surface materials analysed in this study are : asphalt, concrete, permeable and the industrialised building system (IBS) StormPav. Surface temperatures, measured using a ThermaCam, were compared with ambient temperatures. The study concludes that asphalt has a significant impact on the UHI phenomenon compared to concrete, permeable pavements, and IBS StormPav.

An other study of Akbari & Rose (2008), used high-resolution aerial colour orthophotography to identified the surface, classified them and calculate their distribution. The aim of assessing the proportion of vegetation, roofs and paved surfaces is to understand their contribution to the UHI. The study estimated the potential change in albedo for different urban surfaces and calculated the resulting impact on ambient temperatures. The potential for increasing the albedo (reflectivity) of roofs and the potential for increasing vegetation to mitigate the UHI are then studied.

1.7 Conclusion of the literature review

This literature review has underscored the significant impact of the UHI effect. It has highlighted the pivotal role of the thermal properties of the urban materials on the urban heat island effect. The main materials used in Wallonia for ground and roof coverings were identified, along with their associated emissivity.

The study by Ibrahim et al., (2018), investigating the impact of road coverings on the UHI effect, involved measuring the surface temperature and comparing it with the ambient temperature.

The study of Akbari & Rose (2008) focused based on aerial orthophotos on the surfaces covering distribution in the city and their albedo.

It seems therefore interesting to evaluate the impact of artificial surfaces on the UHI from another approach using this time a TIR image captured at night to examine the thermal radiance of surface materials.

The city of Louvain-la-Neuve has been chosen for this study which allows by its proximity on site surveys necessary for accurate identification of the surface material In addition, the city being not yet strongly affected by UHI, it provides an opportunity to assess and mitigate future risks of the UHI effect. The findings could provide recommendations for the selection of materials in future urban projects, such as the planned construction of the bicycles corridors (Namur-Brussels), the construction of the Athéna-Lauzelle sustainable neighbourhood, the new parking lots or the continuous renovation and insulation of the seventies and eighties dwelling’s roofs.

Chapter 2. Objectives

In this problematic context of the urban heat island effect, it is crucial to study the levers on which it is possible to act.

It is therefore relevant to focus on the impact of artificial surfaces in cities.

One possibility is to measure the emissivity of materials using a thermal infrared (TIR) map. The main objective of this study is to assess the thermal radiance and indirectly the emissivity of different types of artificial surfaces that contribute to the urban heat island effect. The study aims to determine whether it is possible to recognise surface materials and their emissivity from a thermal infrared image.

The study focused on the city of Louvain-la-Neuve, which has a certain homogeneity in terms of materials used but also has specific construction features that will be taken into account when interpreting the results.

To achieve this, the study aims to determine the emissivity of surface materials by classifying distinct surface material types through an analysis of an available TIR image of Louvain-la-Neuve captured in 2012.

Several sub-objectives will be pursued:

- Categorizing various surface material types by integrating data from both thermal infrared and high-resolution visible images;
- Computing the average thermal radiance value for each surface material type;
- Assessing the differences in thermal radiance values among materials;
- Establish categories of surface materials exhibiting similar thermal radiance values;
- Identifying the advantages of TIR over optical images on the discrimination of surface materials used in Louvain-la-Neuve.

If successful, the identification of these surface materials and their location on available IR images could subsequently assist the cities in evaluating the impact of those artificial surfaces on the UHI and exploring alternative surface coverings to mitigate the UHI effect.

Chapter 3. Materials

3.1 Study area

The study area for this research is Louvain-la-Neuve, a town in the Walloon Brabant region of Belgium. Louvain-la-Neuve is part of the municipality of Ottignies-Louvain-la-Neuve.

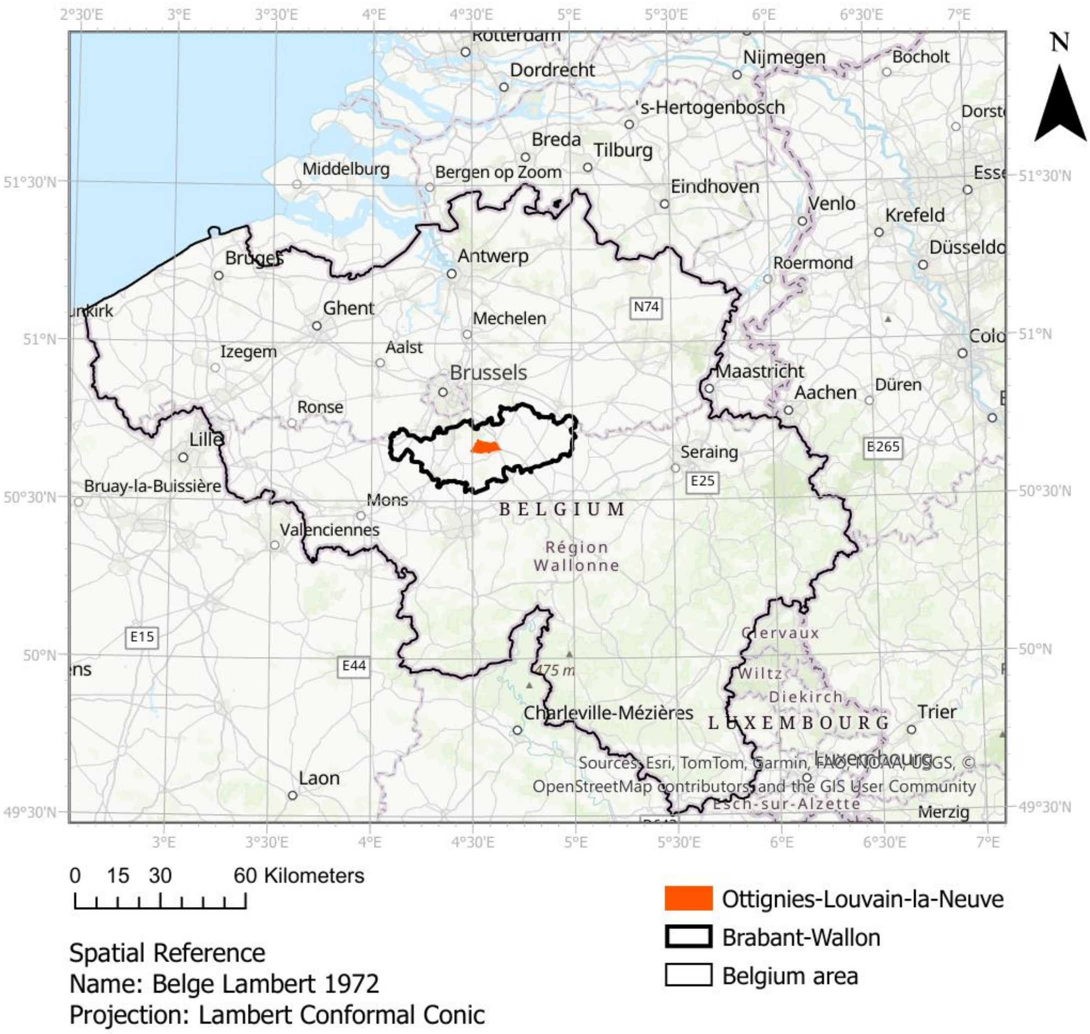

Figure 14 : Location map of Louvain-la-Neuve

The town of Louvain-la-Neuve was built in 1972 following a linguistic conflict between French and Flemish speaking politicians. The student population of the KUL-UCL, the catholic university of Louvan, which dates back to 1425 and is located in Leuven in the Flemish region, was growing considerably. By the end of the 1960s, the presence of French-speaking students and professors was becoming increasingly contested by their Dutch-speaking compatriots. In 1968, the situation took a turn for the worse, with an increasing number of demonstrations accompanied by cries of "Walen Buiten", meaning "Walloons out" in Dutch. The Walloons had to find a solution and decided to create a new student campus in the fields next to the town of Ottignies. This is how the town of Louvain-la-Neuve was created, along with UCLouvain, the Université Catholique de Louvain (Olln, n.d). As a result, this student town has developed rapidly and with very strict urbanism development guidelines, using the same types of building materials. It is home to student accommodation, university buildings, shops and sports and cultural facilities. In addition, single-family homes and apartments building have been built also, creating a town made of a mix of housing types.

This region has been chosen for its high-resolution images provided by the Earth and Life Institute (ELI) at the Université Catholique de Louvain, as they were acquired by the Geomatics Research Lab for the Minerve project (Greenwin, SPW).

For this study, the data used consists of thermal infrared image and optical image from Louvain-la-Neuve (LLN).

3.2 Thermal Infrared image

The following image (Figure 15) is a thermal infrared (TIR) image of Louvain-la-Neuve. This image was captured by an aircraft (D-ISAV type C-402), during a flight conducted on March 20th 2012 between 2:50 and 5:33 am. All the images were combined to form an overall view of Louvain-la-Neuve. The spatial resolution of the image is around 50 cm, with each pixel representing a surface area of 50 cm by 50 cm on the ground. Concerning the sensor, it was a ThermoVision SC-7K6-Dual + NikonD. The altitude during the flight was 3250 ft (about 990,6 m). The two black rectangular shape on the thermal image are anomalies of the captured image, they doesn't represent physically anything and are consider as zone with no data.

This thermal infrared image depicts Louvain-la-Neuve city with thermal radiance values measured in [$W/m^2/Sr$] at the end of the night in winter time to limit any reflected energy. This allows to capture the diversity of thermal inertia characterising the different materials. On this image, the thermal radiance is characterized by pixel darkness levels, where lower values of thermal radiance appear darker and higher values tend towards white. The thermal radiance value depends on the real surface temperature but also on thermal properties of materials, such as the emissivity. The emissivity, which is a central topic in this study, is the ability of a material to emit thermal energy in the form of infrared radiation, compared to a perfect blackbody with an emissivity of 1 (*Cfr.* Chapter 1.2.2).

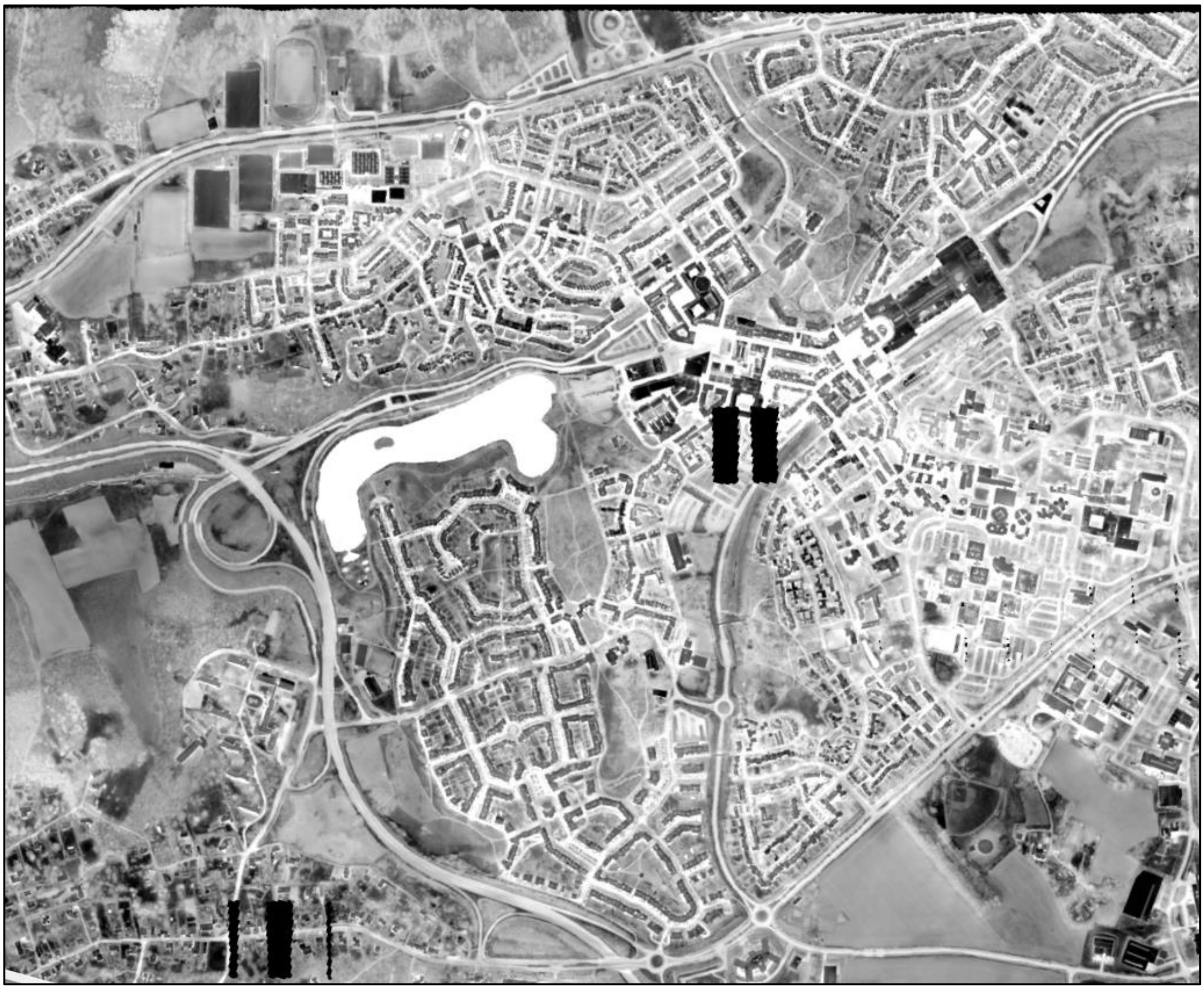

Figure 15 : Thermal Infrared image of Louvain-la-Neuve (ELI, 2012)

3.3 Optical 2012 aerial photo

The first identification of the surface was done on-site, with the use of Google Earth and with an optical image from 2022, Figure 16. This optical image with a resolution of 4 cm was also acquired by the Geomatics Research lab for scientific activities.

Figure 16 : Optical image of Louvain-la-Neuve in 2022 (ELI, 2022)

Then, as the thermal infrared image dates from 2012 and the city changes over time, it was crucial to use maps on WalOnMap with the 2012 dataset, to check whether there had been any changes in the surface since 2012 to avoid any identification errors.

3.4 Weather conditions prior to and during the flight

The Figure 17 shows the weather conditions from 19 to 20 March 2012 using data from Brussel airport. The camera during the flight recorded an outside air temperature of +4°C, which is consistent with the graph. The temperature during the day before the flight was a maximum of 11°C, dropping to a minimum of 2°C at night. Figure 18 shows the cloud covering during the day before the flight at Brussels airport.

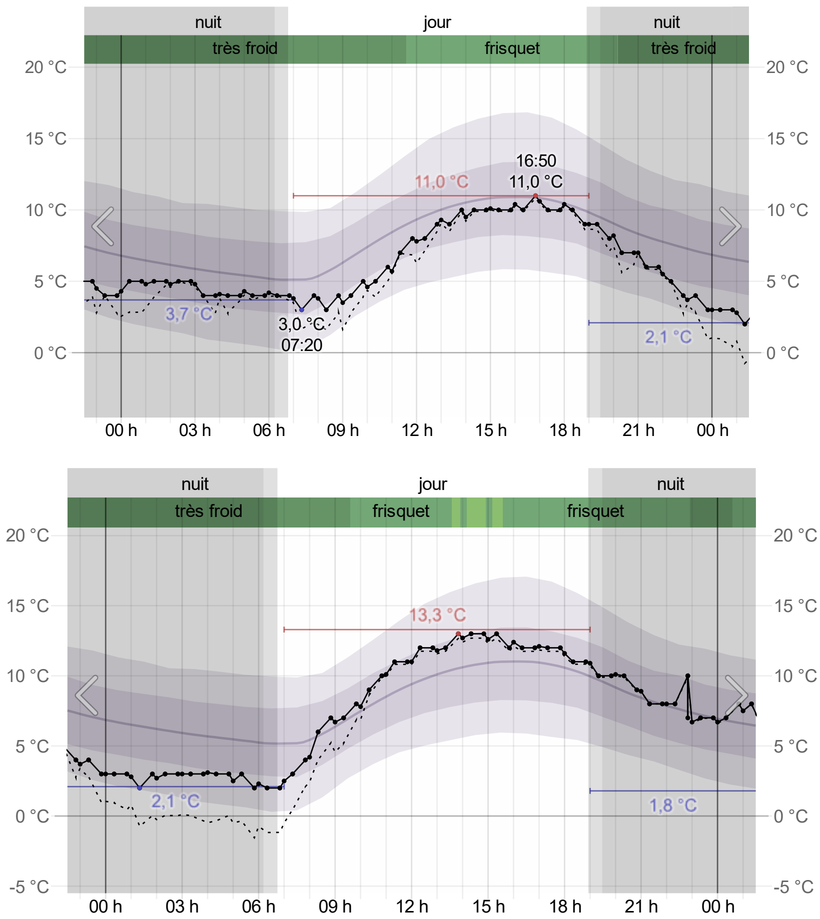

Figure 17 : Temperature of Brussels Airport from 00:00 on the 19th March to 23:59 on the 20th March 2012 (Weather Spark, 2012)

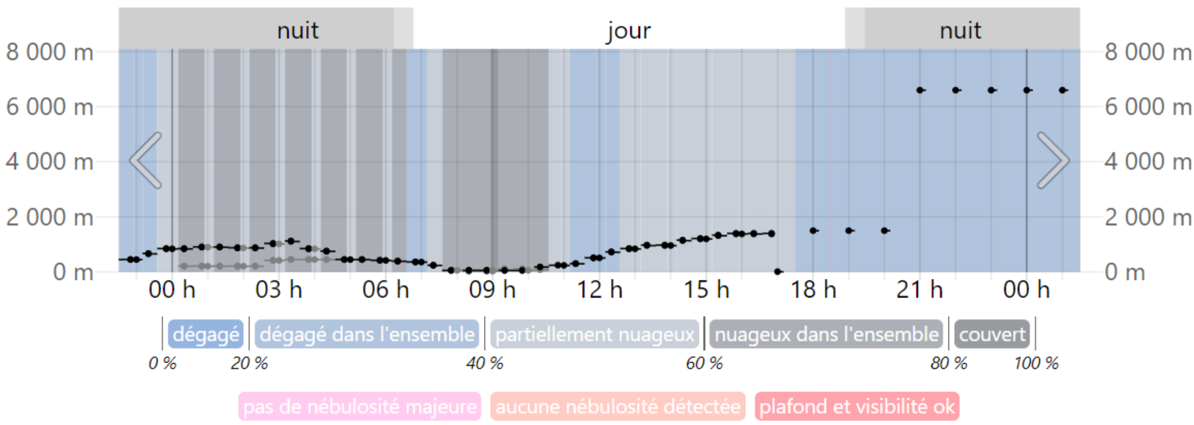

Figure 18 : Cloud covering the day before the infrared image captured, 19th March 2012 at Brussels airport (Weather Spark, 2012)

Figure 19 and Figure 20 show meteorological data for the month of March 2012 at the Uccle station. The figures indicate that it had been raining a few days before the flight, with a low precipitation value of 19 mm the day before the night flight. Regarding the insolation data, the day before the flight was quite sunny with a total of 391 minutes of insulation, which represents 6.5 hours of sun.

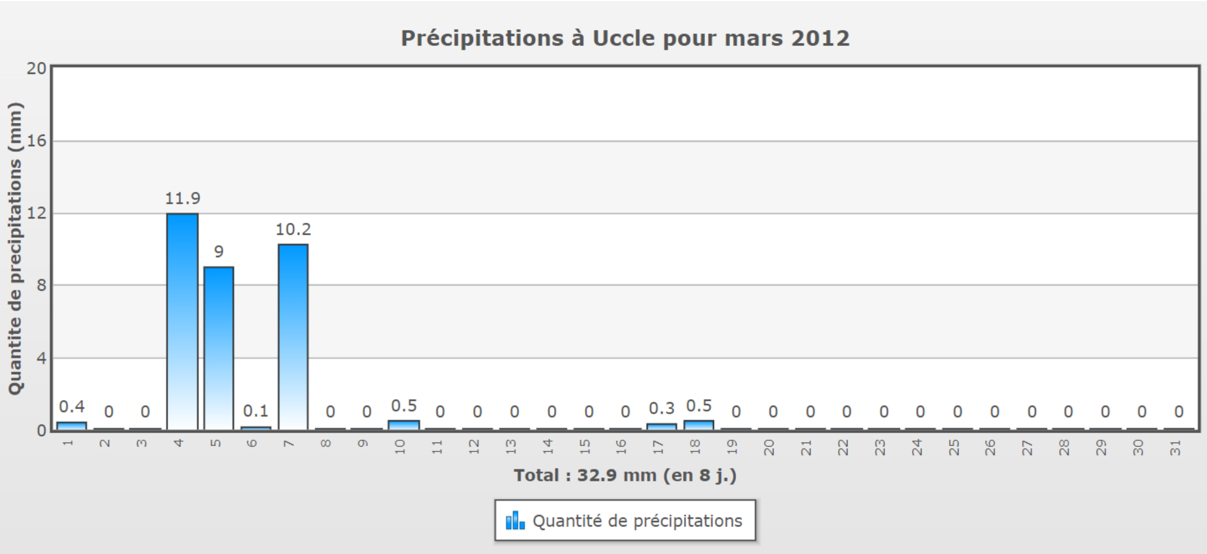

Figure 19 : Summary of March 2012 precipitation at the Uccle station (Mievis, 2012)

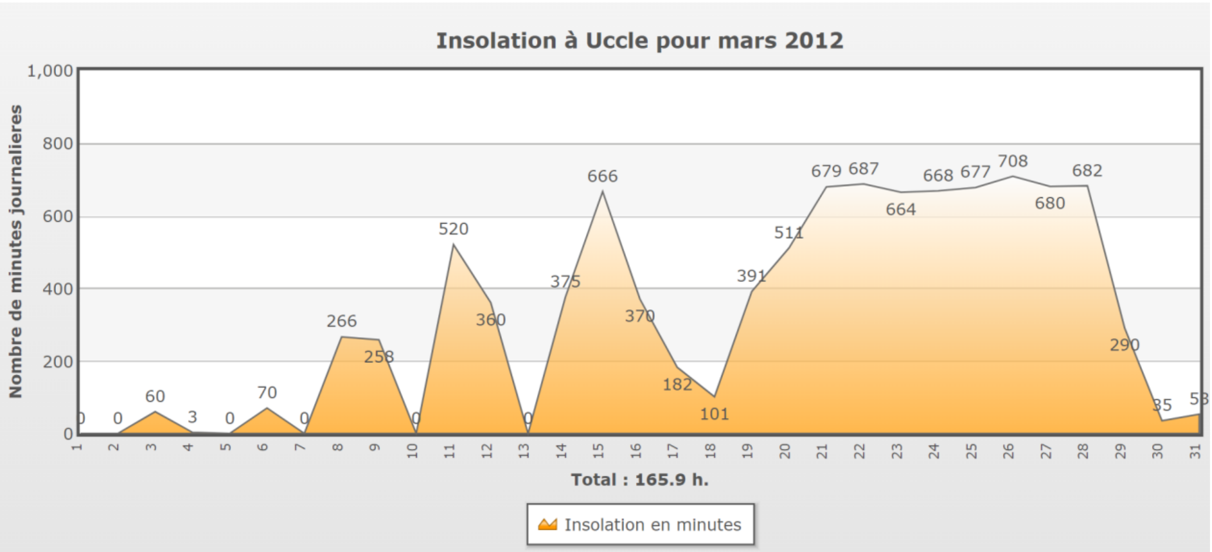

Figure 20 : Summary of March 2012 insolation at the Uccle station (Mievis, 2012)

These meteorological conditions of observation were very good because of the sun's radiation on the day before the flight and the clear sky during the night, allowing to emit to other space all the radiation (no blocking effect by the clouds) according to the respective emissivity of the bodies, highlighting at the end of the night the thermal behaviour of the various properties (emissivity, inertia).

Chapter 4. Methods and assumptions

In this chapter, the main steps of the method selected will be presented, along with a thorough inventory and justification of the assumptions made in this study.

4.1 Assumptions: Impact of external factors on thermal radiance

In order to define the exploitation strategy of this thermal infrared image to assess the materials thanks to their emissivity, it is important to verify a number of assumptions.

4.1.1 Assumption 1 : no solar reflectance

Assumption 1: "There is no solar reflectance to be taken into account."

Given that the thermal infrared image was taken during the night, an assumption can be made regarding solar reflectance.

This assumption stems from the fact that the image has been captured during the night, between 3 and 5 AM, when the sunlight was absent, which means that the contribution of solar reflectance to the thermal image is more than negligible. Consequently, the absence of direct sunlight excludes any reflection from surfaces, thus justifying the hypothesis that reflection should not be taken into account in the analysis.

4.1.2 Assumption 2 : uniformity of surface temperature

Assumption 2: "Surface temperature remains uniform across the city."

This assumption is built on the premise that surface temperature variation is minimal across the city. The infrared image was captured at 3 AM in March, which is a period marked by reduced human activity and allowing buildings to cool overnight. However, given that the temperature can drop to 3°C during the night, most residents will heat their homes during this nocturnal period, which can alter the surface temperature of poorly insulated roofs. Another aspect to consider is the shading effect. Does shading affect pixel values for the same material and location? Some tests have been conducted to investigate this.

This assumption, which allows to exclude the variation of surface temperature as a parameter of the thermal radiance, facilitates a direct correlation between the thermal radiance value and the emissivity of surface materials.

4.1.2.1 Insulation effect on roof

To evaluate the importance of rigorous pixel selection to avoid roof insulation effects, a study was conducted on ten slate roofs. First, slate roof have been identified on-site, followed by verification that these materials have remained unchanged since 2012. This latter verification can be performed using the 2012 optical image available on WalOnMap.

Once the surface type was identified, the evaluation of the thermal radiance of slate was done using the TIR image:

- To process the thermal infrared image (in TIFF format), a Geographic Information System (GIS) software, in this case QGIS, was used.
- Then, 10 polygons were drawn around randomly selected pixels and ten others were chosen from the darkest pixels on the roof to mitigate insulation effects.
- The polygons selected comprised about six pixels.
- For each polygon, statistical measures were extracted, including the number of pixels, the mean, the median, the standard deviation, the minimum and maximum values of the pixel values, and therefore of the thermal radiance.

These statistical measures could provide an overview of the relevance and uniformity of the selected pixels.

The statistical data obtained for randomly selected pixels and darkest selected pixels were then analysed using statistical software such as RStudio. The randomly selected data were compared with those considering insulation (darkest) using a Wilcoxon signed-rank test. This non-parametric test is used to compare the two means of paired samples (XLSTAT, 2023). The non-parametric test is chosen because the homogeneity of variances is not met. This comparison helps determine the significance of the insulation effect and whether careful pixel selection is crucial.

4.1.2.2 Shading effect – Inconsistency in pixel values for the same material and location

When analysing the thermal infrared map, pixels with unusual colour variations were observed for the same surface material. This intriguing discovery suggested an effect originating from external factors, resulting in an inconsistency in the pixel values for the same location.

As shown in Figure 21, which is an aerial image of the “Leclercq parking lot”, a parking area located in the centre of LLN, some cars seem to have stayed overnight, appearing very dark.

It can be also observed that the upper part on the image of the “Leclercq parking lot” presents different colour shades between the parking spaces and the road surrounding them. This seems intriguing at first glance because the ground material is the same on the road and the parking spaces, with asphalt everywhere, so the hypothesis of different materials is to be rejected.

Upon closer inspection, a difference in colour can be observed between the parking spaces located at the upper part of the parking lot (closer to the centre) and the more distant parking spaces, which have a colour similar to that of the surrounding road.

The “Leclercq parking lot” is in high demand and often full. A likely explanation for this difference in colour between the parking spaces and the parking road is due to the effect of cars that have remained parked all day, thus preventing sunlight from hitting the asphalt. This hypothesis of shading has been further investigated.

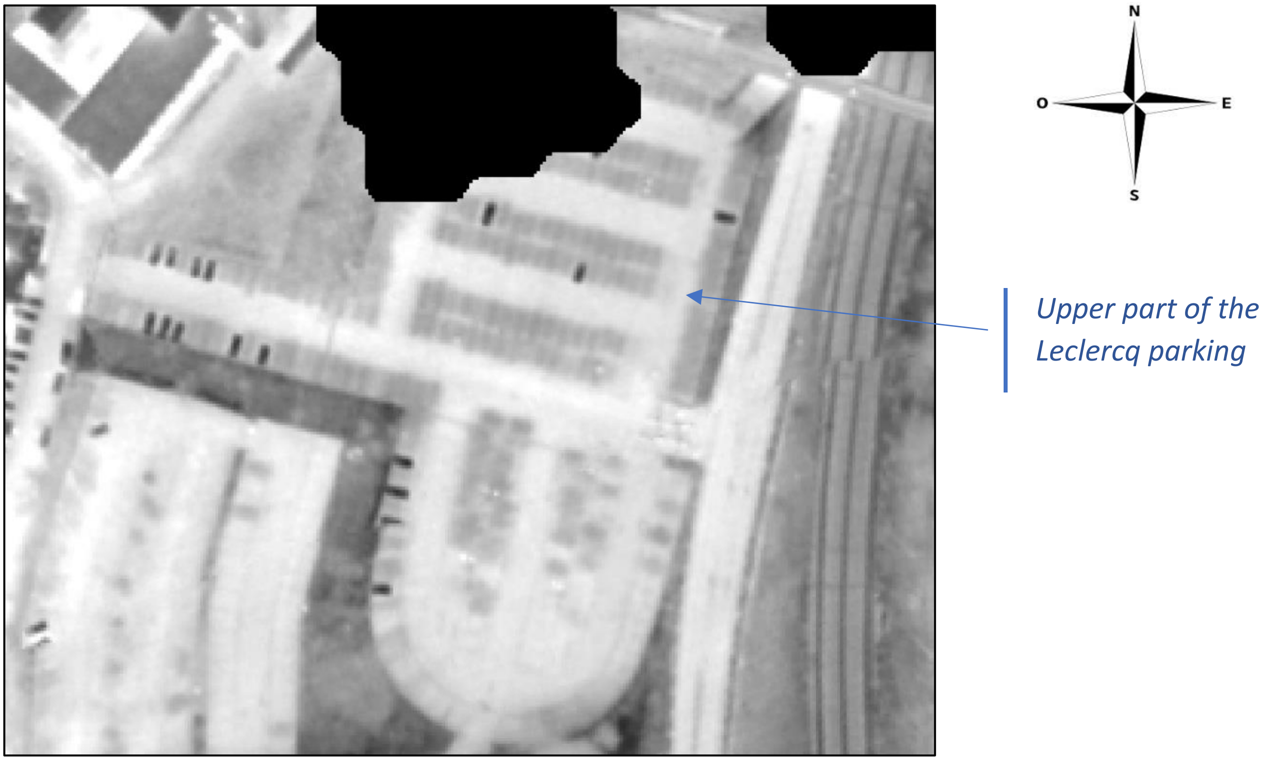

Figure 21: Zoom on parking “Leclercq”

Having identified the hypothesis of the shading effect from cars, it was therefore interesting to check whether relatively tall buildings also have a shading effect on the roads in order to confirm this hypothesis. Therefore, polygons in the area located North of buildings and other polygons in the area located South of buildings were drawn in order to assess whether there was a significant effect between the two locations, as shown in Figure 22.

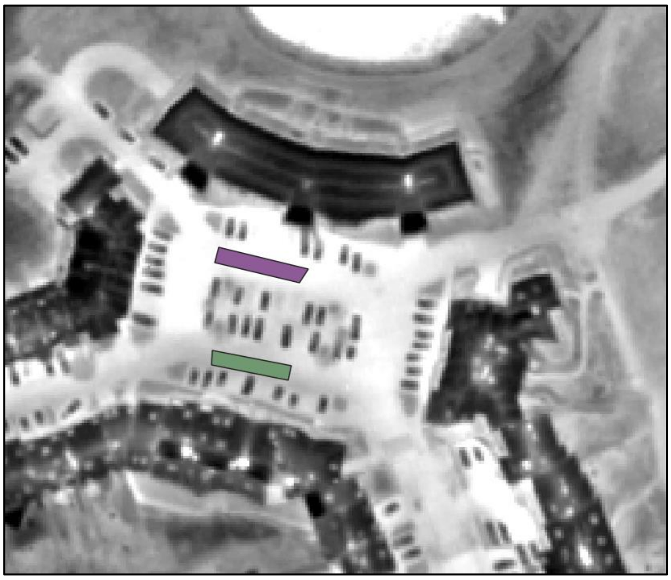

Figure 22: Thermal aerial image of the "Place des peintres" in Louvain-la-Neuve, with a polygon in purple to the south of the buildings and a polygon in green to the north.

4.1.3 Assumption 3 : homogeneity of the environment

Assumption 3 : " The environment in Louvain-la-Neuve is homogeneous; the city's microclimate has no influence on materials.*"*

Before assessing the thermal radiance value of materials across the city, it is essential to assess whether the microclimate of Louvain-la-Neuve influences the thermal radiance value, as outlined in assumption 3. This assumption stems from the understanding that each material has its own emissivity, implying uniform behaviour across different environments.

4.1.3.1 Microclimate

To evaluate this assumption, a sensitivity analysis shall be conducted to verify the absence of a dominant microclimate effect on the thermal radiance value associated with the material.

Therefore, the city has been divided into nine Cartesian zones, as depicted in Figure 23. In each zone, concrete and asphalt surfaces have been selected to examine potential trends in values across the different zones. These two materials were selected based on their distinct visual properties: asphalt, known for its dark colour and concrete, which is light in colour. Identifying concrete and asphalt surfaces in each zone has been done on-site, followed by verification that these materials have remained unchanged since 2012, using the 2012 optical image available on WalOnMap. The sample can not be taken in shadowed areas (*Cfr* assumption 2).

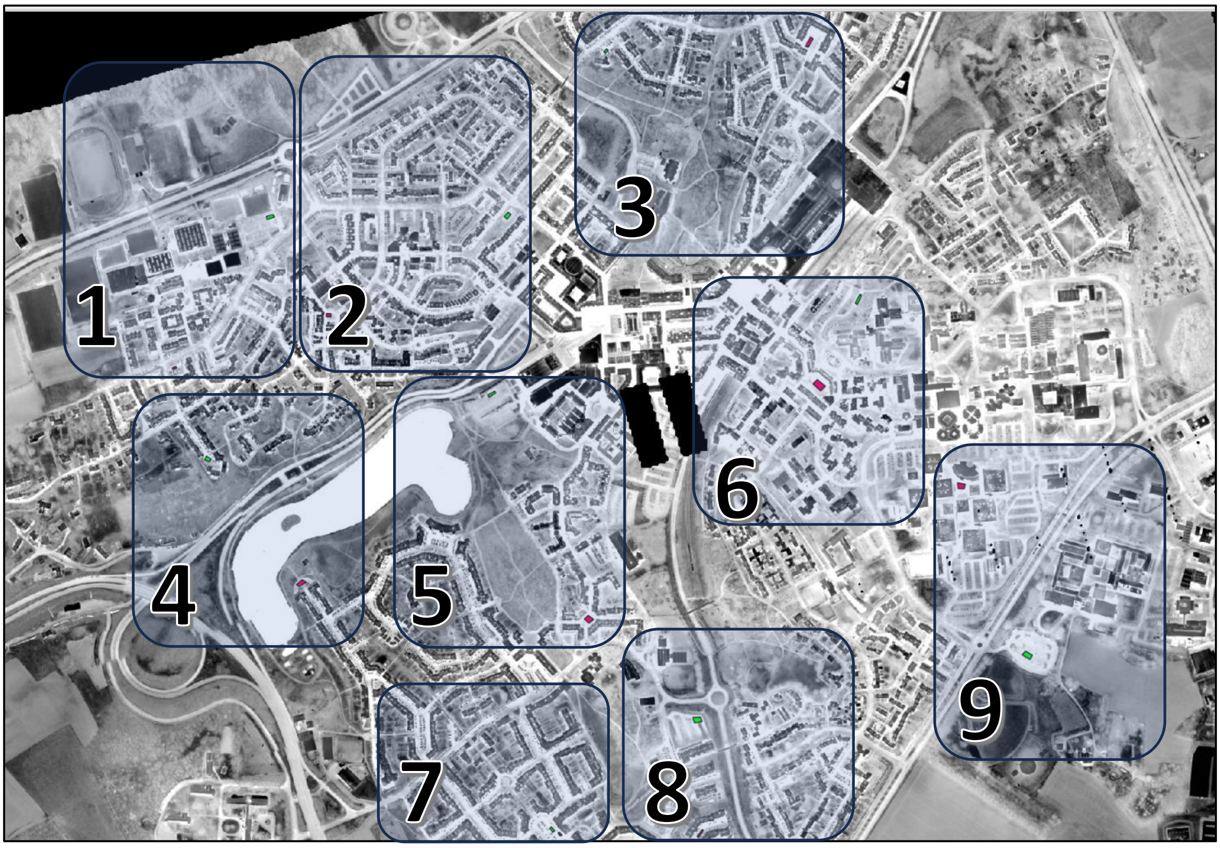

Figure 23 Localisation of the 9 zones in the city of LLN. A polygon of concrete (green) and asphalt (pink) in each zone

- Once the surface's types were identified, the evaluation of the thermal radiance of these surface was done drawing polygons around known material surfaces (concrete and asphalt), forming pixel samples.
- Then, statistical measures were extracted for each polygon, including the number of pixels, the mean, median, standard deviation, minimum and maximum values of the pixel values, and therefore of the thermal radiance. Polygons comprise numerous pixels with a mean of 300 for concrete and 256 for asphalt. It is more pertinent to prioritize the median as the representative value of thermal radiance rather than the mean for these polygons.
- The data was then collated into a single database to group the material values by zone.
- Since each zone contains one mean thermal radiance value per material (concrete and asphalt), this results in two mean values per zone. To assess the possible impact of the zones on the material properties, a Kruskal-Wallis test, a non-parametric test, was performed on the combined materials (asphalt and concrete) as a function of zone. This combined test was used to determine whether variations in the emissivity of the two materials follow similar or different trends depending on the zone, in order to see whether the zone influences the thermal radiation of the materials.

The Kruskal-Wallis test, was chosen because, when comparing more than two group means, this test assesses whether the medians of the distributions of the two materials differ significantly between zones (Robert, 2006). Additionally, it was appropriate in this context because data from different zones are independent, as the zones are located in different areas. It was not possible to perform an ANOVA test due to the limited number of mean values per material per zone, making it impossible to compare variances effectively (Kim, 2014; XLSTAT, 2023).

4.1.3.2 Specificity of LLN : the Platform effect

A particularity of the city of Louvain-la-Neuve is that it was designed to be pedestrianised, with a large proportion of car traffic moving underground. The urban centre was therefore built on a gigantic concrete platform supporting buildings and pedestrian streets. Underneath this platform, there are car parks and roads for cars. The platform is 14.5 hectares in size and 39 cm thick. The entire pedestrian area of the city is paved with Bierges cobblestones of concrete, as depicted in Figure 24 (Olln, 2024). A specific question is whether this platform enhances the UHI effect or not.

Figure 24 : Paving stones of Bierges in concrete at “Place de l’université” in the centre of LLN.

It was therefore important to evaluate whether there is a difference in thermal radiance values between

- the group of paving stones of Bierges that are on the platform;
- the group of paving stones of Bierges that are outside of the platform.

In order to assess the effect of the platform, samples have been taken on the platform and off the platform. 7 samples were taken at locations above the platforms and 8 samples were taken at locations outside the platform. All the samples were taken from areas containing Bierges cobblestones.

Then, a Student's t-test was carried out, to evaluate whether there is a significant difference between the mean values of the two groups, in this case, the two localisations. For the results of a Student's t-test to be valid, the homogeneity of the variances and the normality of the residuals must be respected. Therefore, a Levene test to evaluate the homogeneity of variance and a Shapiro-Wilk test was made to assess the normality of the residuals (Kim, 2014).

4.2 Impact of materials on thermal radiance

Now that the homogeneity of the environment of Louvain-la-Neuve has been established, and that an analysis on the possible platform effect has been conducted, the next step was to identify the various types of surface materials present in the city of Louvain-la-Neuve.

4.2.1 Method applied for the roof types

Survey-based approach (SBA)

Firstly, a survey-based approach was adopted to ensure accurate identification of the different roof types. A site survey was carried out and in addition, residents were asked about the type of roof of their house.

The data on roof types collected from residents were used for two main purposes:

- first, to carry out an initial analysis of the different types of roofs present in Louvain-la-Neuve;
- second, to evaluate the coefficient of thermal radiance for these different types of roofs.

The mains roof types identified were: ceramic, natural slate, artificial slate, artificial slate with asbestos, flat roof and solar panels. The table below shows the number of roofs identified by roof type during the survey-based approach.

Table 4 : Number of roofs identified by type

Type of roof	Ceramic	Natural slate	Artificial slate	Artificial slate with asbestos	Flat roof	Solar panel
Number of roof identified	11	9	4	13	25	18

After this identification of roof types, new layers were generated in QGIS, one for each roof material. To measure the difference in thermal radiance coefficient between roofs, polygons were created on the surfaces of known roofs materials in order to extract small samples of pixels. When selecting pixels on roofs, it is important to select those which are the most representative for the study. Indeed, when selecting pixels on the thermal infrared image, it is essential to consult the 2012 optical image in parallel to identify variations in materials (metal parts, solar panels, etc.) and sources of heat loss (windows or chimneys) in order to exclude any zone affected by significant heat effect.

Figure 25 : Images of a house located on "Rue Haute" in Louvain-la-Neuve, with a thermal infrared image on the left and an optical image from 2012 on WalOnMap on the right.

Then, the pixels with the darkest values (with lower thermal radiance values) for the same surface type were selected, as shown on Figure 26. This approach takes into account the fact that the variation in thermal radiance of the roof may depend on the insulation of the roof.

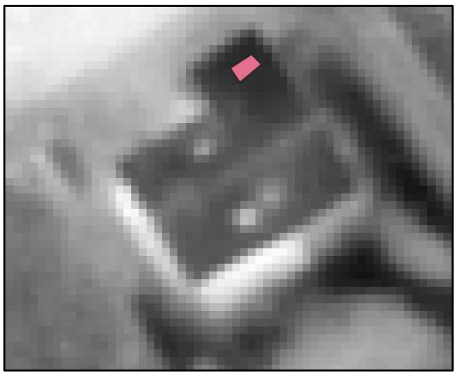

Figure 26 : Selection of the darkest pixels from a slate roof on a house located on "Rue Haute" in Louvain-la-Neuve

The number of pixels selected for each roof type was significantly lower than that selected for the ground covering in assumption 3, with an average number of 6 pixels per roof. For each polygon, again the zonal statistics process was used to calculate statistical values such as the minimum, maximum, mean, median, standard deviation and the number of pixels. These statistics provide quantitative measures of the thermal radiance values for each polygon.

During the selection of pixels using polygons, the standard deviation value of each polygon was verified to guarantee the sample representativity. If the standard deviation was found to be significantly high, exceeding a value of 10, as the range value can vary from 0 to 255, further investigation was conducted to identify the cause. This involved verifying the data on the map and selecting another polygon if necessary to ensure higher accuracy.

Since the standard deviation was very low and there was no significant difference between the median and the mean, the mean was chosen in this case as the representative value of thermal radiance per polygon instead of the median.

In the R software, all the thermal radiance values of a surface material were then plotted in a box plot to show the distribution and median of the material's thermal radiance. Once the thermal radiance value of materials was found quite similar, a test was done in order to see if only one category could be representative of several materials.

- This was the case for example for artificial slate, artificial slate with asbestos and natural slate. An ANOVA (Analysis of Variance) test was carried out to see if there was a significant difference between the mean values of the 3 different types of slate.
- For a comparison of more than two group means, the one-factor analysis ANOVA is the appropriate method rather than the t-test (Kim ,2014). This is why this method is used, in this case there are 3 groups to evaluate, representing the 3 types of slate.
- For the results of an ANOVA test to be valid, the homogeneity of the variances and the normality of the residuals must be respected (Kim, 2014).
- Therefore, a Shapiro-Wilk test was made to assess the normality of the residuals and a Levene test to evaluate the homogeneity of variance.

Photointerpretation-based approach (PIBA)

The data collected from the residents was used to create a field database, providing first a valid qualitative view of the areas identified. However, in terms of quantity, these data were not sufficiently consistent. A photointerpretation-based approach was therefore required to validate their quantitative accuracy.

As the ceramic and slate are easily recognisable on an optical image, a new database containing 50 ceramic roof polygons and 50 slate roof polygons was created, based on the 2012 optical image on WalOnMap and Google Earth.

Comparison between the survey-based and photointerpretation-based approaches

The boxplots of the survey-based and photointerpretation-based data (done for both ceramic and slate roofs) were then plotted to visually assess their similarity or differences. In order to statistically compare the data of the two approaches, a Student's t-test was carried out.

As there are only two means to compare, an ANOVA test can not be done in this case. A Student’s t-test was used to evaluate if the difference between the two means could be considered significant or not. For the Student's t-test to be valid, the homogeneity of the variances must be ensured and the distribution must be normal, as is the case for the ANOVA test. Therefore, Shapiro-Wilk and Levene tests had to be performed.

Comparison of optical and thermal infrared for differentiating ceramic and slate.

In order to identify the potential contribution of thermal imaging to optical imaging, it seemed appropriate to compare the effectiveness of optical and thermal imaging in distinguishing between ceramic roofs and slate roofs. Thus, the difference in separability of the two materials by thermal infrared and optical data was evaluated.

To assess this, regarding the optical data, 20 polygons representing ceramic and slate roofs were delineated in the same way as explained above, but on an optical image presented in Figure 16 in Chapter 3.3. As the image is in the visible range, band 1 (red), band 2 (green), and band 3 (blue) values were extracted from the polygons. For the ceramic and slate TIR data, the data from the survey-based analysis were reused.

Once the data had been extracted, multivariate statistics, including the Mahalanobis distance and the Bhattacharyya, were employed to evaluate separability.

- The Mahalanobis distance measures the distance between two sets of points, taking into account the variances and covariances of the variables. It is calculated using the inverse of the variance-covariance matrix of the data (De Maesschalck et al., 2000).
- The Bhattacharyya distance measures the similarity between two probability distributions and is influenced by both the mean and variance of the two-class sample distribution. It provides an accurate estimation of classification error and is particularly useful as a metric for assessing class separability (Choi, 2003).

The distances obtained for the TIR and optical data were then compared to determine which of the two methods was giving a better separation of roof types.

4.2.2 Method applied for the ground covering

Concerning the ground covering, the identification of the materials has been done on-site, on Google Earth and checking with optical images of 2012 on WalOnMap for any changes in materials between 2012 and now.

It is important to note that the platform located in the city centre could have an impact on thermal radiance values. It was therefore essential not to include the pixels of this platform in this first analysis of surfaces covering the ground. Three different types of ground covering have been identified: asphalt, concrete and cobblestones.

Figure 27 : Cobblestones

Figure 28 : Asphalt

The concrete category encompasses all surface coverings containing concrete, including pavements, roads, parking lots, and other similar urban structures.

Figure 29 : Different types of concrete pavement captured in Louvain-la-Neuve

The thermal radiance value has been calculated for each ground covering as explained previously in the explication of assumption three.

The values of thermal radiance for each ground covering materials have been plotted into boxplot to visually compared them. Then, a test has been conducted to evaluate the differences between the means of the data.

A Kruskal-Wallis test was performed because one of the conditions for an ANOVA test was not met : the distribution of the value observed for concrete was not normal. This test analyses the hypothesis that two variables have the same mean. This test was used to evaluate the differences between the mean thermal radiance values of concrete, asphalt and pavement.

4.2.3 Analysis on other surfaces particularities

This final section examines additional infrared particularities identified in the thermal infrared image. These observations serve to highlight the effectiveness of thermal imaging in different contexts compared to optical multispectral reflectance. This comparison utilised both thermal infrared and optical imaging. The section first examines metals (such as cars and metal roofing sheets), the differences between railways and roads, and footbridges.

Chapter 5. Results

This section presents the results, which are discussed in Chapter 6.

5.1. Impact of external factors on thermal radiance

5.1.1 Assumption 1 : no solar reflectance

Assumption 1: "There is no solar reflectance to be taken into account. "

There was no other source of energy and therefore no real reason to verify this assumption which is obvious as the IR image was captured in the middle of the night, at 3PM. This period of the night was ideally selected to be far from the sunset and sunrise in March.

5.1.2.1 Verification of assumption 2 : the insulation effect

The results of the comparison between randomly selected polygons and polygons selected for their insulation effects on the thermal radiance values of slate roofs are presented.

Table 5 : Comparison of thermal radiance between the darkest polygons and randomly selected polygons on slate roofs

Insulation?	Taken into account	Not taken into account
Thermal radiance value [W/m²]	39.20	72.59

The Shapiro Wilk normality tests show that the data are normally distributed, with p-values greater than 0.05. However, the Barlett test shows that the variances of the two groups (with and without insulation taken into account) are not homogeneous. This justifies the use of a non-parametric test, such as the Wilcoxon signed-rank test, which does not assume that the variances are homogeneous. The Wilcoxon signed-rank test, with a p-value of 0.002 reveals a significant difference between the thermal radiance values of roofs with and without insulation (XLSTAT, 2023). This indicates that the effect of insulation on the thermal radiance of roofs is statistically significant.

5.1.2.2 Verification of assumption 2 : shading effect

Regarding the effect of the cars, the homogeneity of the variance wasn't respected, consequently, a Student's t-test couldn't be conducted.

Therefore, a Welch's test was conducted to evaluate the differences between the means of the two groups. With a p-value of 0.033, which is less than 0.05, we can reject the null hypothesis that there is no significant difference between the means of the two groups. The results indicate a significant difference. The mean for areas with car shadows is 145.01, while the mean for areas without car shadows is 159.74.

Table 6 : Table of the mean thermal radiance value for in the shadow and out of the shadow of the cars, in [W/m²]

	Shadow of the car	**No shadow of the car**
Mean thermal radiance value [W/m²]	145.01	159.74

In conclusion, the presence of cars in the parking during the day before had a significant impact on thermal radiance values measured at the end of the night and decreases the heat release during the night.

Regarding the effect of buildings, a Levene's test and a Shapiro-Wilk test were carried out to assess the conditions necessary for a Student's t test. As the homogeneity of variance was not met with a p-value of 0.0066, a Student's t test could not be performed.

A Welch's test was therefore carried out, the results giving a p-value of 0.0016, which is less than 0.05. Thus, the null hypothesis that there is no significant difference between the means of the two groups can be rejected. The averages therefore have significantly different values, with an average of 159.54 for the pixels located in the shadow of the building and an average of 229.26 for the pixels located to the south of the buildings.

Table 7 : Table of the mean thermal radiance value for in the shadow and out of the shadow of the buildings, in [W/m²]

	Shadow of the building (North)	**No shadow of the building (South)**
Mean thermal radiance value [W/m²]	159.54	229.26

5.1.3.1 Verification of assumption 3 : homogeneity of the environment

Assumption 3 : "The environment in Louvain-la-Neuve is homogeneous; the city's microclimate has no influence on materials." The following plot illustrates the different values of mean thermal radiance value for asphalt and concrete depending on the zone:

For asphalt, the mean thermal radiance value is 202.6 with a standard deviation of 11.09.

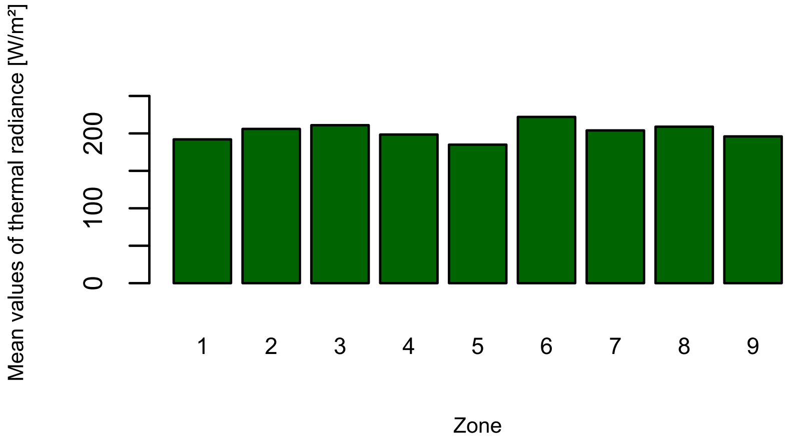

Figure 30 : Barplot of mean thermal radiance value for asphalt by zone (in green)

For concrete, the mean thermal radiance value is 205.1 with a standard deviation of 9.9.

Figure 31 : Barplot of mean thermal radiance value for concrete by zone (in purple)

With the Kruskal-Wallis test, the null hypothesis (H0) is that there is no significant difference between the thermal radiance means in the different zones. If the p-value is smaller than 0.05, it rejects the null hypothesis, indicating a significant difference. In this case, the Kruskal-Wallis test evaluated the effect of the zone on the combined materials (concrete and asphalt) and obtained a p-value of 0.4704, which is greater than 0.05. This indicates insufficient evidence to reject the null hypothesis (H0).

We can thus conclude that, the thermal emissions of the materials do not appear to be significantly influenced by the different zones of the city.

5.1.3.2 Verification of assumption 3 : a possible platform effect

The results of the analysis of the effect of the platform on the thermal radiance value of the paving stones of Bierges are presented below in Table 8.

All the samples were taken from areas containing Bierges cobblestones in concrete, as these cobblestones cover the entire pedestrianised area of Louvain-la-Neuve.

Table 8 : Comparison of thermal radiance coefficients on and off the platform

	On the platform	**Off the platform**
Thermal radiance value [W/m²]	243.13	217.97
Standard deviation	10.67	10.88

These measurements indicate a slight tendency for the soil to exhibit higher thermal radiance values when it is on the platform compared to when it is off the platform. A graph showing the different thermal radiance values captured can be found in Appendix 7.4.1.

In order to confirm whether or not there is a significant difference between the two variables, a Student's t-test was carried out. The Student's t-test is valid if both the homogeneity of the variances and the normality of the residuals are respected.

The results of the Shapiro-Wilk test to assess the normality of the residuals show a p-value of 0.5159 for the data on the platform and 0.2203 for the data off the platform. With p-value higher than 0.05, these Shapiro-Wilk normality tests did not reject the null hypothesis (H0) at the 5% significance level, indicating that the samples can be considered as coming from normally distributed populations.

Then, a Levene test was made to evaluate the homogeneity of variance. If the p-value is smaller than 0.05, it rejects the null hypothesis. As the Levene test gave a p-value of 0.9319, it confirmed the null hypothesis. The variances of the data can then be considered as homogeneous.

Finally, these two valid conditions allowed for a valid Student's t-test to be conducted. The null hypothesis indicates no significant difference between the means of the two groups. The Student's t-test gives us a p-value of 0.0006, which is clearly less than 0.05, indicating that the mean values of thermal radiance are statistically different between areas with and without a platform, with a mean value of 243.13 on the platform and 217.97 off the platform. In conclusion, there is an effect of the platform on thermal radiance.

5.2 Impact of materials on thermal radiance

5.2.1 Roof materials results

Survey-based approach

Table 9 presents the number of roofs identified per type and the number of pixels per roof type selected for the survey based approach.

Table 9 : Number of roofs identified and the number of pixels selected for each roof type for the survey-based approach

Roof type	Ceramic	Artificial asbestos slate	Natural slate	Artificial slate	Flat roof	Solar panel
Number of roof identified	11	13	9	4	25	18
Total number of pixels selected	49	50	35	11	836	139

The data on roof types was leveraged to create boxplots, as shown in Figure 32, for each type of roof. By examining the different boxplots on Figure 32, one can discern the typical range of thermal radiance values for each specific roof type.

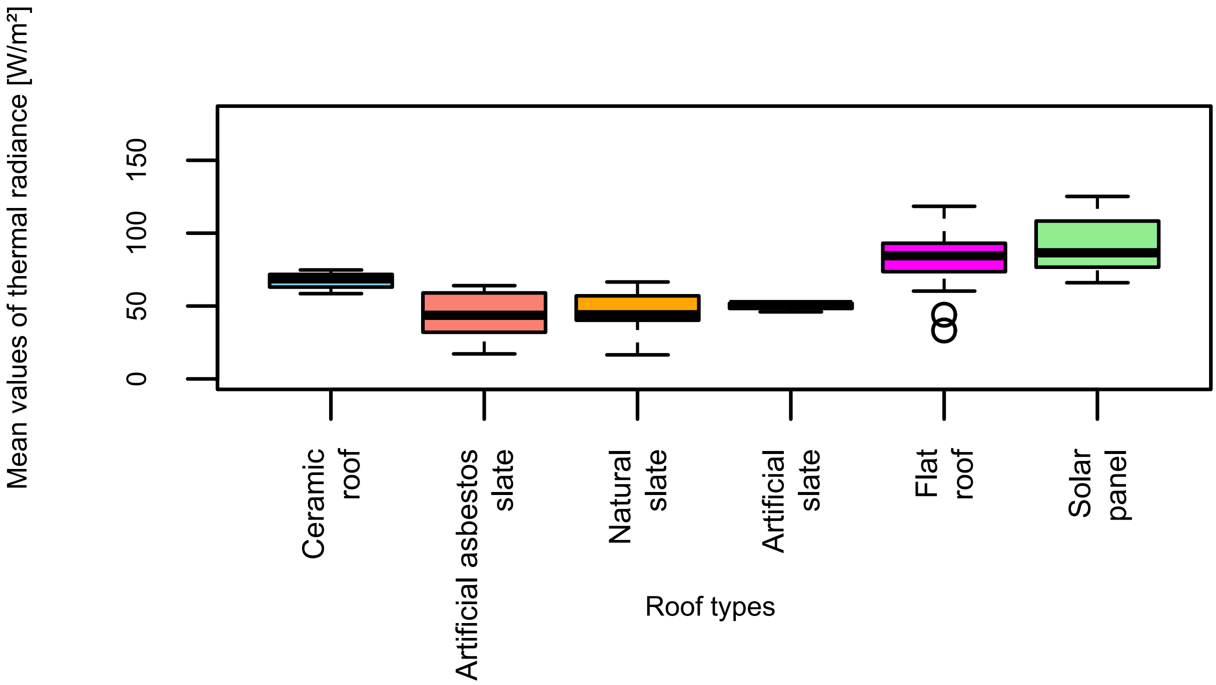

Figure 32 : Boxplot of the different roof types in Louvain-la-Neuve

Table 10 presents the mean values and the 95% confidence interval measured for each roof type.

Table 10 : Mean thermal radiance values and 95% confidence intervals for each roof type

Roof type	Ceramic	Artificial asbestos slate	Natural slate	Artificial slate	Flat roof	Solar panel
Mean thermal radiance value [W/m²]	67.38	44.42	44.96	50.13	83.60	92.08
CI 95%	[63.8;70.9]	[34.9;54]	[31.1;58.8]	[45.6;54.7]	[75.3;92]	[82.5;101.7]

The three types of slate roofs exhibit the lowest radiance values, while ceramic roofing shows slightly higher values compared to slate. In contrast, flat roof and solar panels display significantly higher values.

No notable differences were observed among the three types of slate roofs, namely artificial slate, artificial slate with asbestos, and natural slate. Therefore, a test was conducted to determine if there is a significant difference between the means.

An ANOVA test was carried out to see if there was a significant difference between the mean values of the 3 different types of slate. For the results of an ANOVA test to be valid, the homogeneity of the variances and the normality of the residuals must be respected.

To assess the normality of the residuals, a Shapiro-Wilk test was done which stipulates that: (Ducay, 2017)

- H0: the sample follows a normal distribution.
- H1: the sample does not follow a normal distribution.

If the p-value (Pr(>F)) is smaller than 0.05 (common significance level), it rejects the null hypothesis (H0).

The results of the Shapiro-Wilk test gave a p-value of 0.255 for artificial slate, 0.262 for natural slate and 0.212 for artificial slate with asbestos. In each case, the Shapiro-Wilk normality test did not reject the normality hypothesis (H0). This indicates that the samples can be considered as coming from normally distributed populations.

Then, a Levene test was made to evaluate the homogeneity of variance (O'Neill and Mathews, 2002).

- H0 : The variances of the groups are equal, $\sigma_1^2 = \sigma_2^2 = \sigma_3^2$
- H1 : At least one group variance is different, $\sigma_i^2 \neq \sigma_j^2$ for some $i \neq j$

If the p-value is smaller than 0.05, it rejects the null hypothesis. The Levene test gives a p-value of 0.0519, suggesting marginal homogeneity in variances between the three slate groups.

The validity of the ANOVA test is therefore confirmed by these two conditions. The ANOVA test stipulates that:

- H0 : There are no significative differences between the means of the groups.
- H1 : There are significant differences between at least two groups.

The results for the three types of slate gave a p-value associated with this F statistic of 0.811, which is greater than 0.05, indicating no significant difference between the averages for the different types of slate. Therefore, it is pertinent to group them into a single category: slate.

The three slate types are then combined in the red boxplot on the right of the Figure 33. The mean thermal radiance value for the union of slate is 45.49 [W/m^2].

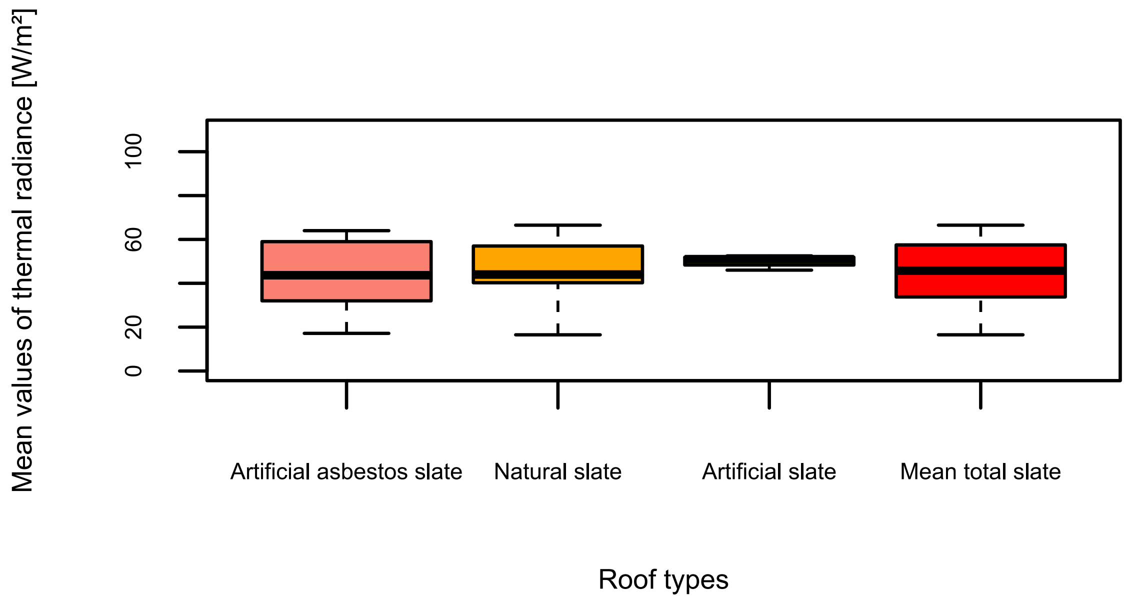

Figure 33: Boxplot of the three different types of slate roofs with the overall mean value for all slate roofs

The Figure 34 illustrates the final four types of roofing materials: ceramic, slate, flat roof and solar panel.

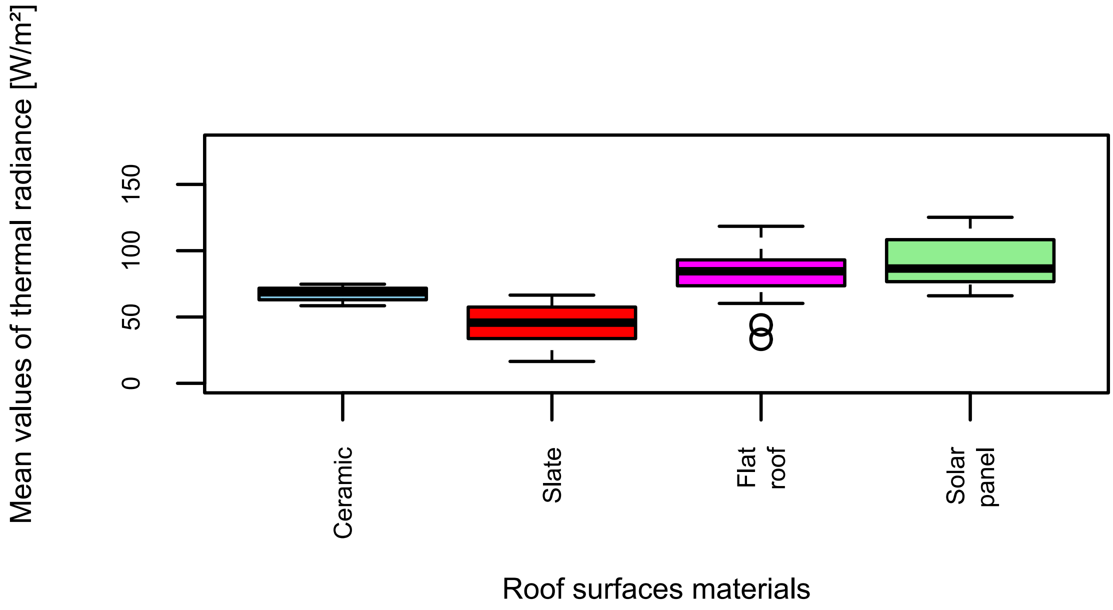

Figure 34 : Comparison of the thermal radiance value of the four different types of roofs : ceramic, slate, flat roof and solar panel.

Comparison of the survey-based (SBA) and photointerpretation-based (PIBA) approaches for ceramic and slate.

Results of the survey-based and photointerpretation-based approaches are visually compared on Figure 35.

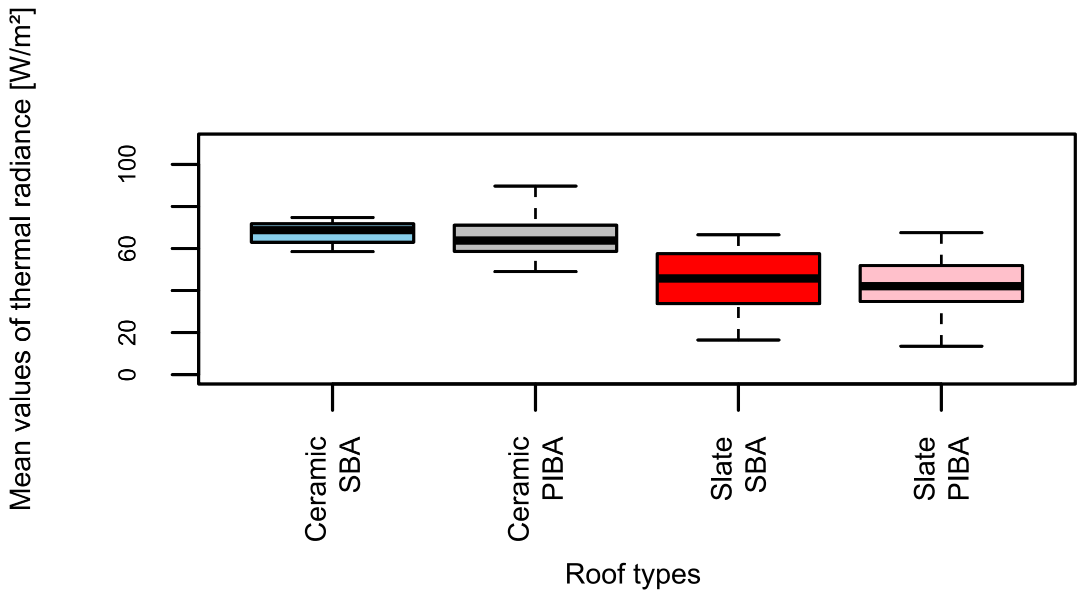

Figure 35 : Comparison of the survey-based (SBA) and photointerpretation-based (PIBA) data for ceramic and slate roofs

The results of the Shapiro-Wilk tests show that the p-values for each group are all greater than 0.05, indicating that the data follow a normal distribution.

Concerning the Levene test on the homogeneity of variances, the null hypothesis of homogeneity of variances for the two comparisons cannot be rejected. Slate has a p-value of 0.1998 and ceramic 0.109. In both cases, the p-values are greater than 0.05, which means that the variances of the groups can be considered homogeneous.

These two valid conditions allowed for a valid Student's t-test to be conducted. The results are as follows: regarding the slate test, the p-value of 0.2843 is above the 0.05 threshold, suggesting no evidence to reject the null hypothesis of no differences between the means, which means that the difference between the means is not statistically significant. Regarding the ceramic test, the p-value of 0.3802 means that the means are not significantly different.

The average values for the survey-based and photointerpretation-based data of ceramics and slate are summarized in the table below.

Table 11 : Survey-based and photointerpretation-based thermal radiance coefficient of ceramic and slate in [W/m^2]

	Survey	Photointerpretation
Ceramic	67,38	64,85
Slate	45,49	41,99

In conclusion, there is no significative difference between the survey-based and photointerpretation-based mean values for both materials. This means that the photointerpretation-based identification of these materials does not bias the estimation of radiance.

Comparison of optical and thermal infrared for differentiating ceramic and slate.

The results of the Mahalanobis distance show a distance of 2.094 for thermal infrared data while for optical data, it is 4.2687. The method that gives the greatest distance indicates a better separability of ceramic and slate roofs. The results of the Bhattacharyya distance show a distance of 0.5721 for thermal infrared data while for optical data, it is 2.79.

The results of the two experiments are in the Table 12 below.

Table 12 : Results of the Mahalanobis and Bhattacharyya distance for thermal infrared and optical data

	TIR	Optical
Mahalanobis	2.09	4.27
Bhattacharyya	0.57	2.79

5.2.2 Ground covering results

The ground coverings in Louvain-la-Neuve are mainly composed of asphalt, concrete and cobblestones. Table 13 presents the number of polygons created for each ground covering as well as the number of pixels selected for each ground covering type.

Table 13 : Number of polygons created for ground covering and the number of pixels selected for each ground covering type.

Ground covering type	Concrete	Cobblestones	Asphalt
Number of polygons drawn	9	9	9
Total number of pixels selected	2716	1032	2325

The thermal radiance coefficients of these three distinct types of ground coverings, are represented in the boxplots in Figure 36.

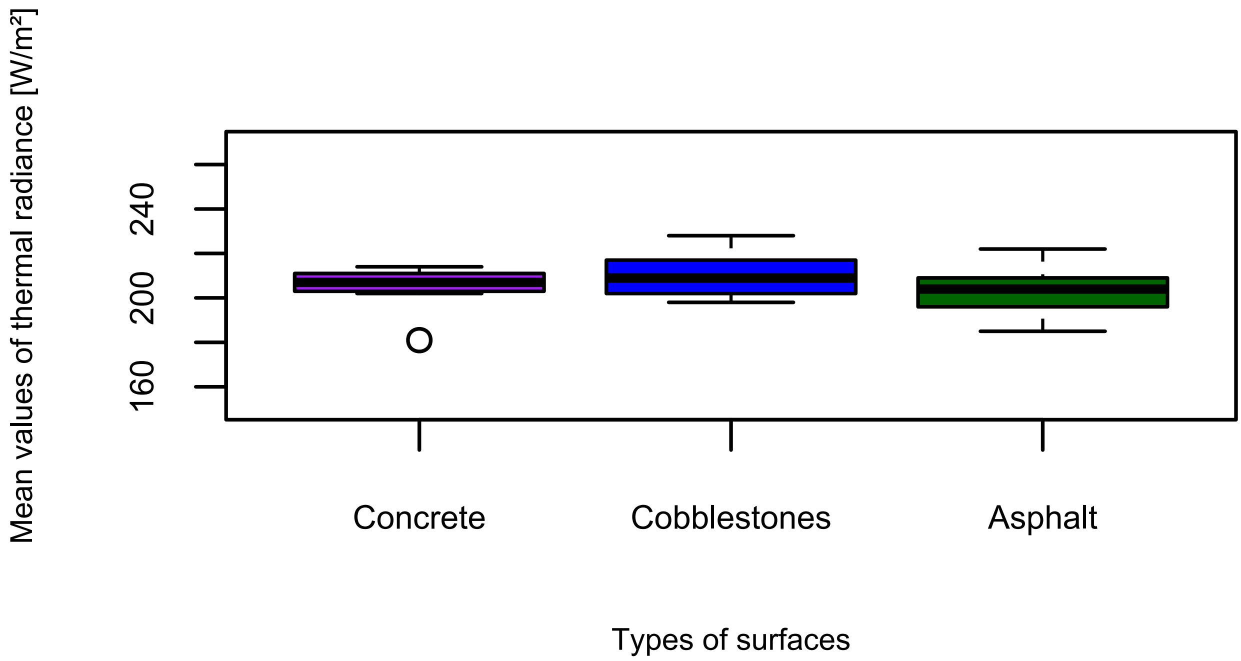

Figure 36 : Boxplot of the different ground covering surfaces

Table 14 presents the mean values and the 95% confidence interval measured for each ground covering type.

Table 14 : Mean thermal radiance value and 95% confidence intervals for each ground covering type

Ground covering type	Concrete	Cobblestones	Asphalt
Mean thermal radiance value [W/m²]	205.11	210.72	202.61
CI 95%	[197.5;212.7]	[202.2;219.2]	[194.1;211.1]

Three means need to be analysed statistically. As mentioned earlier, two conditions are required to conduct an ANOVA test. Upon testing, the homogeneity of variance was satisfactory for asphalt, concrete, and cobblestones. However, the normality of the distribution for concrete wasn't met, because of a p-value of 0.01. Therefore, it was not possible to conduct an ANOVA test on the three ground covering surfaces.

A Kruskal-Wallis test was therefore carried out. The Kruskal-Wallis test evaluates differences in the means of concrete, asphalt and cobblestone and obtained a p-value of 0.3691, which is greater than 0.05, indicating insufficient evidence to reject the null hypothesis (H0). According to this test, it appears that the differences between the mean thermal radiance values of concrete, asphalt and cobblestones are not significant, which suggests that they react in a similar way from a thermal point of view. It may therefore be appropriate to combine these 3 types of road surfacing into a single category: ground covering, with a mean thermal radiance value of 206.15 [W/m²].

5.2.3 Final results for all surface materials found in Louvain-la-Neuve

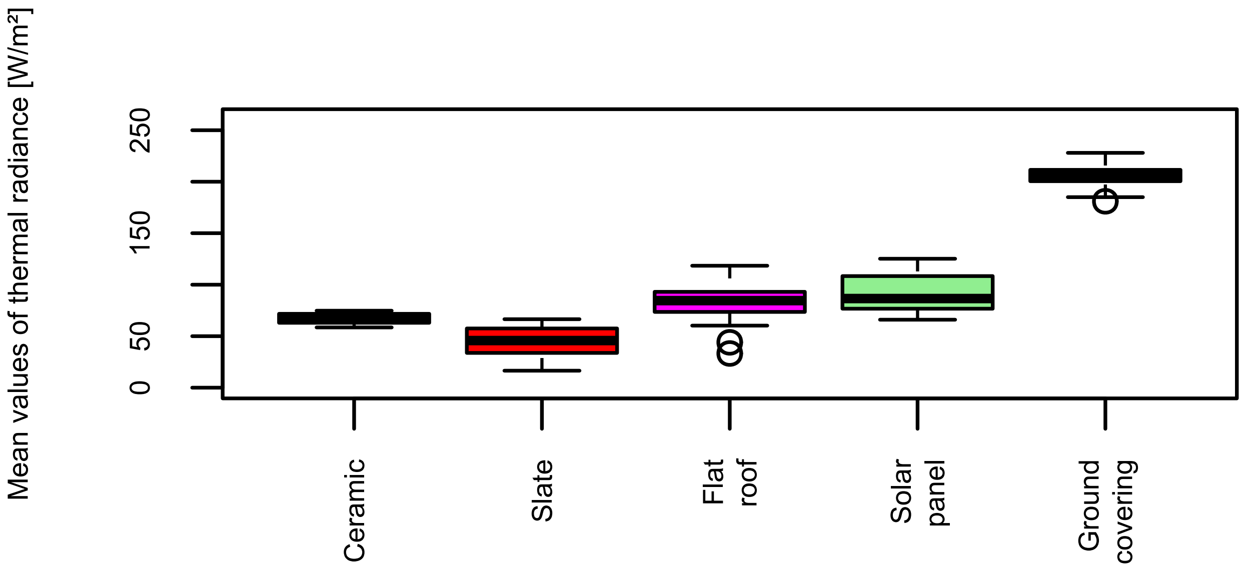

Figure 37 : Final categories for surface materials in Louvain-la-Neuve.

5.2.4 Analysis of other surfaces thermal signal

Several notable observations were made regarding thermal characteristics of various surfaces, it provides further clear evidences :

Metal

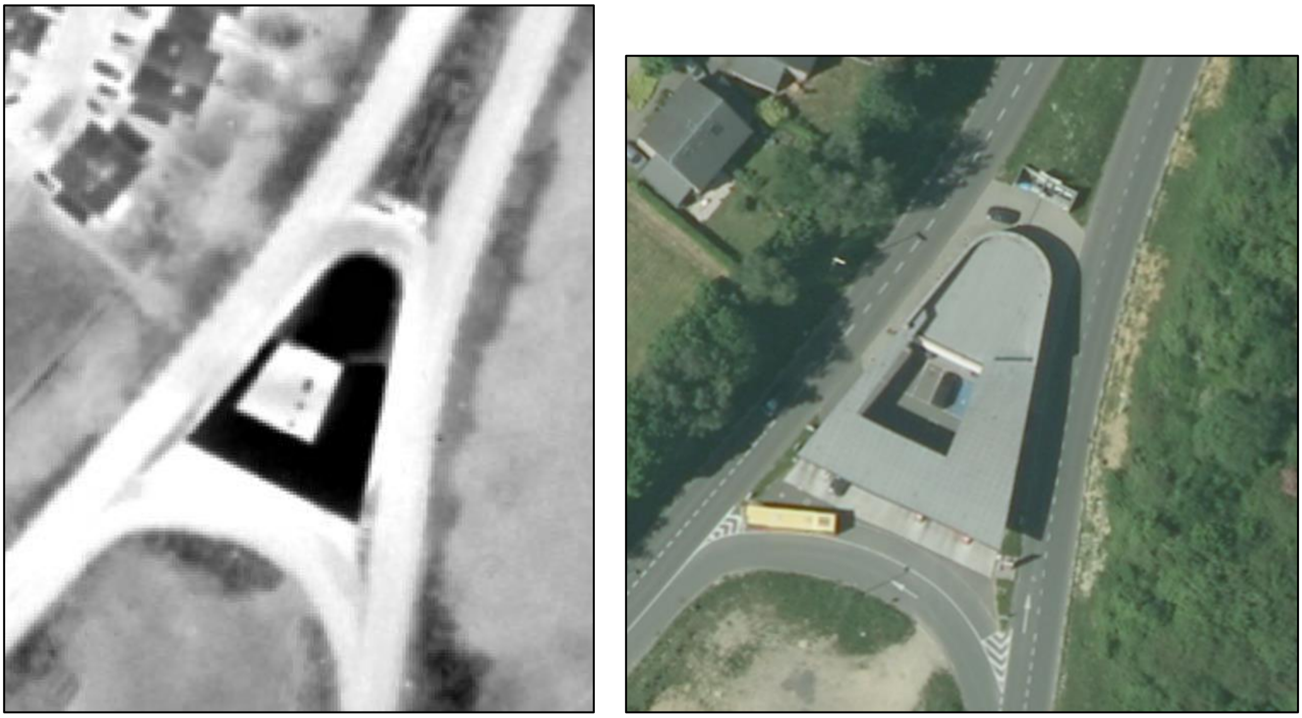

Figure 38: TIR vs optical (WalOnMap, 2012) image of the gas station located at "Boulevard de Wallonie" in LLN.

The Figure 38 shows that on a TIR image, the roof of the Total gas station appears darker. Metal surfaces, such as the roof of the Total gas station, shown in Figure 39, exhibit significantly lower thermal radiance values, indicating higher levels of darkness in the infrared spectrum. Thermal radiance measurements taken on metal surfaces give low values close to 0. The whiter area in the centre of the roof of the gas station in the TIR image is due to the fact that the roof does not cover the entire surface, exposing the asphalt ground below. The difference in materials between the metal roof and the asphalt ground causes this variation in thermal radiance values.

Figure 39 : Image of the roof of the Total gas station situated in Boulevard de Wallonie, LLN (Googlemaps, 2019).

Road – railway line

The comparison between the thermal radiance of roads and railway line shows values of 188.26 for the roads and 129.47 for the railway line. The Figure 40 shows the "Boulevard du Sud" aligned with the railway line.

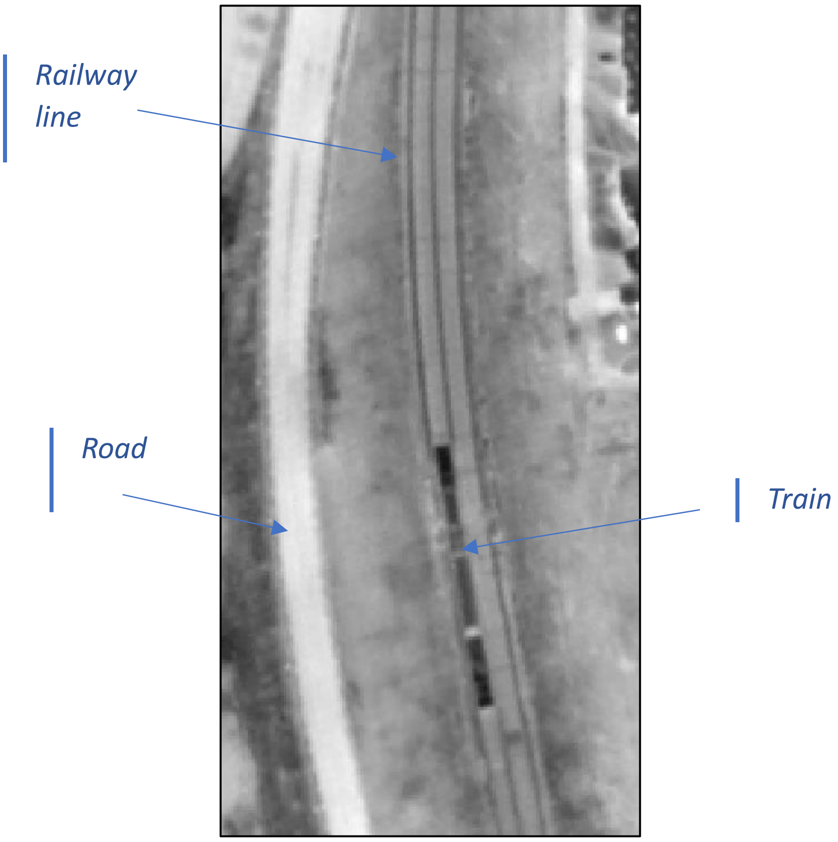

Figure 40 : Infrared image of the "Boulevard du Sud" and the railway line in the centre of Louvain-la-Neuve.

Footbridges

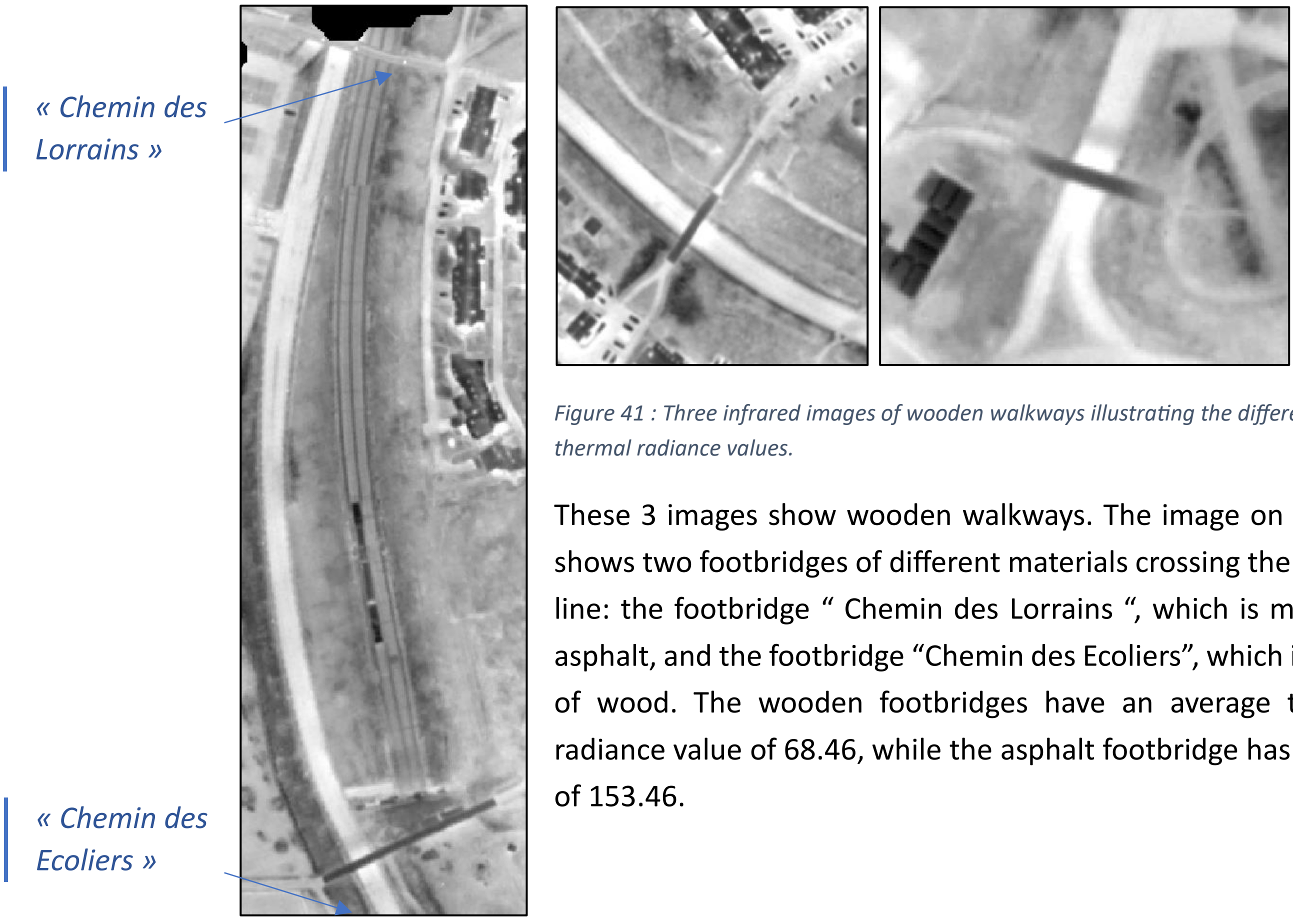

Figure 41 : Three infrared images of wooden walkways illustrating the difference in thermal radiance values.

These 3 images show wooden walkways. The image on the left shows two footbridges of different materials crossing the railway line: the footbridge " Chemin des Lorrains ", which is made of asphalt, and the footbridge "Chemin des Ecoliers", which is made of wood. The wooden footbridges have an average thermal radiance value of 68.46, while the asphalt footbridge has a value of 153.46.

Chapter 6. Discussion

This section analyses and interpret the results presented in the previous sections, exploring their implications, potential limitations, and relevance to the research objectives.

In the following chapters, the text in *italic* highlights briefly the assumptions and the results of the study which are the base of the below associated discussions.

The following discussions have been developed by addressing the three following questions:

- Is there a reasonable scientific explanation to the finding observed? (§6.1/6.2)
- Could the findings of the study indicate that the use of IR image is an interesting way or not to determine (some of) the covering surface types – knowledge of which is an essential input parameter for UHI investigations? (§6.1.2.1/6.2)
- Based on the current study, is there any recommendation to further develop in the future new aspects of the study? (§6.1.2/6.2)
- Is there a link between thermal radiance obtained for materials and the theorical emissivity of materials? (§6.3)

The Chapter 6.4 highlights the limitations of the study and finally the Chapter 6.5 briefly discusses possible strategies to mitigate UHI effects in the city of Louvain-la-Neuve.

6.1 Impact of external factors on thermal radiance

6.1.2 Uniformity of surface temperature

Assumption 2: "Surface temperature remains uniform across the city "

As explained in Chapter 5.1.2, *this assumption facilitates a direct correlation between the thermal radiance value and the emissivity of surface materials.*

The current study is based on infrared image captured at 3 AM in March, in a period marked by reduced human activity and allowing buildings to cool overnight. Additionally, it was presumed that residents do not excessively heat their homes during this nocturnal period.

In general this assumption was confirmed when analysing the infrared image, although with some exceptions which are describes in Chapter 6. These exceptions are related to heat release caused by defecting insulation and shading effect. In those cases the choice of the polygon location has avoid to consider such exceptions.

However, in order to completely confirm the assumption, it could be interesting to evaluate the results on the basis of infrared images to be taken when human activities are negligible and when the ambient temperatures are particularly stable during several days.

Hence, further research based on an infrared image captured in stable summer period could enhance the confidence in this assumption and therefore the possible link between the thermal radiance value and the emissivity of the materials. Such study based on IR image in summer stable period would particularly make sense as it could also be a typically period for UHI.

6.1.2.1 Insulation effect

The results of the study provide compelling evidence of the significant impact of insulation on the thermal radiance values of slate roofs. The importance of the pixel selection is crucial to determine accurate thermal radiance values associated with roof types.

These results were expected but also confirm the quality and the sensibility of thermal dataset. This finding on the effect of insulation reinforces the idea of using aerial inspections to determine the presence of insulation in buildings. However, given the differences in thermal radiance values between roof materials, it is essential that companies assessing roof insulation take into account the materials used. Therefore, it is necessary to classify materials correctly before assessing thermal insulation to avoid incorrect insulation estimates.

For example, in 2023, the Inbw companies conducted a flight across the Brabant Wallon region to determine heat loss from homes. During the data processing of infrared sensor captures, metal surfaces were excluded and all other roof types were categorized together. The separation between metallic and non-metallic surfaces appears crucial due to the differing emissivity values of the materials (see Table 3 and Chapter 5.2.4). The lack of distinction between roof types such as slate and ceramic could lead to errors, implying that ceramic surfaces may be less insulated than slate surfaces at the same temperature.

6.1.2.2 Shading effect

The significant difference in thermal radiance values between areas with and without car shadow is not negligible.

The assumption of a shading effect due to cars being parked all day makes sense, as the car park analysed is often full, especially when students have lessons. It is located in the centre of the town, near the auditoriums and is cheap all year round. The 19 March 2012, the day before the thermal image was taken, a Monday, was indeed such typical day. Furthermore, from the sunrise, the sun had been shining most of the day before (*Cfr* Figure 20) the TIR image was captured, casting shadows on the ground due to objects directly blocking its light, thus preventing sunlight from hitting the asphalt. This shading effect will be further described hereunder. Moreover, the car park is uniformly made of asphalt, excluding material composition as a cause for differing radiance values. Finally, parking spaces that were not in a darker shade are more rarely used because they are further away from the car park exit, as observed on regular visits on-site. As demonstrated by this car park, the shading effect can be highly spatially dynamic

The shading effect of buildings was therefore analysed to validate this assumption. In fact, the orientation of the sunlight during the afternoon could cause shading of the ground surface, affecting thermal radiance values depending on their insolation.

The figure 42 shows "Place du Plat Pays" situated in Louvain-la-Neuve on a TIR image and on an optical image. The images are oriented with North at the top and South at the bottom. The shadow is visible on the optical image.

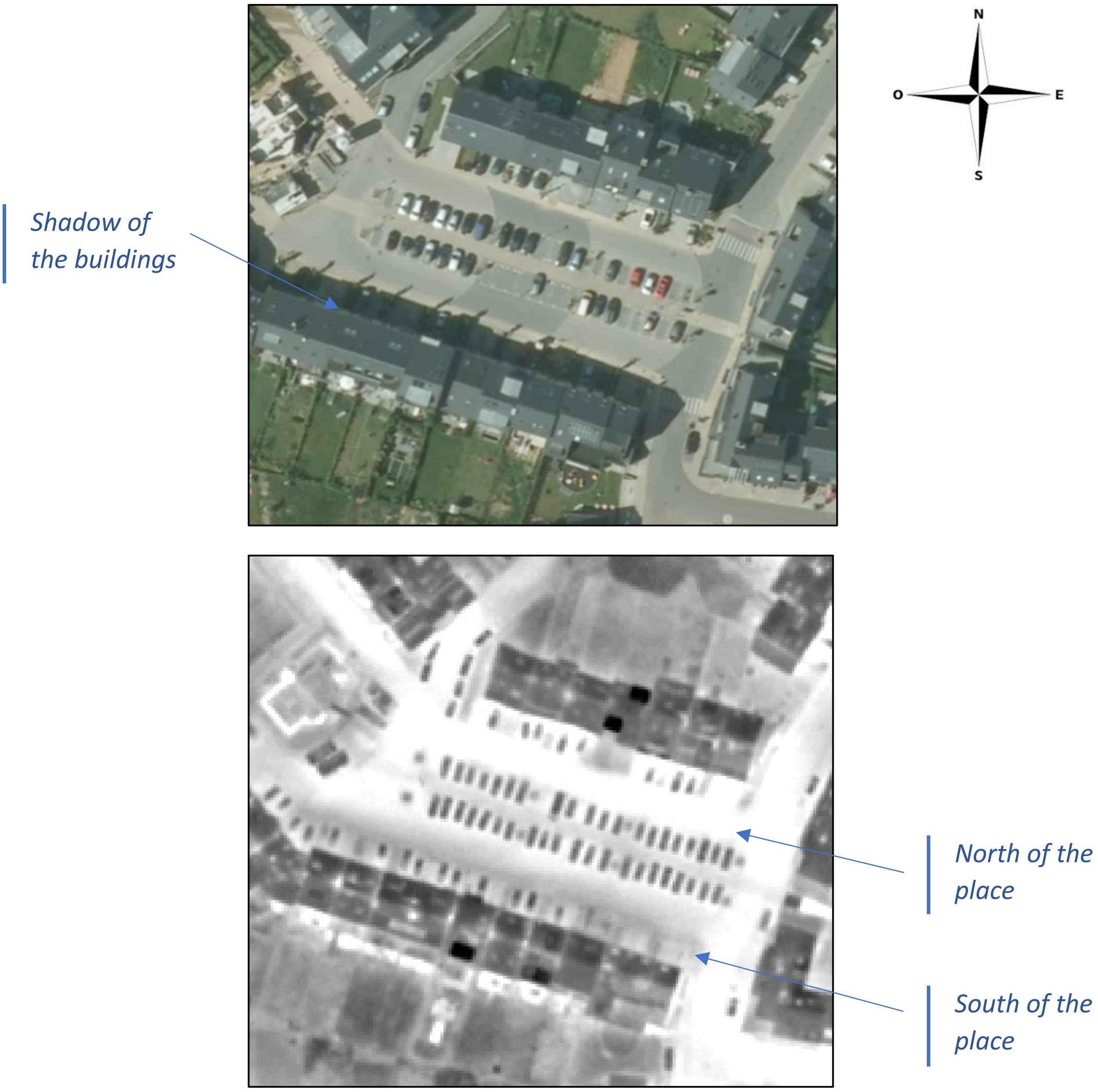

Figure 42: Thermal infrared and optical images of the "Plat du Plat Pays" in LLN.

The results show a clear difference in thermal radiance value, with a value of 159 in north of buildings and a value of 229 in the south of buildings. As the TIR image was captured on the 20th of March 2012, the sun was near its position during the spring equinox, as shown on Figure 43 (Siret, 1997). At midday, the sun is at its highest point in the sky. Later in the afternoon, as the sun moves westward, it casts the shadows of buildings towards the east. The shadows grow longer and can cover significant portions of the ground as the sun is lower in altitude. It is interesting to note that the shadowing has a significant effect on the absorbed energy even in Winter.

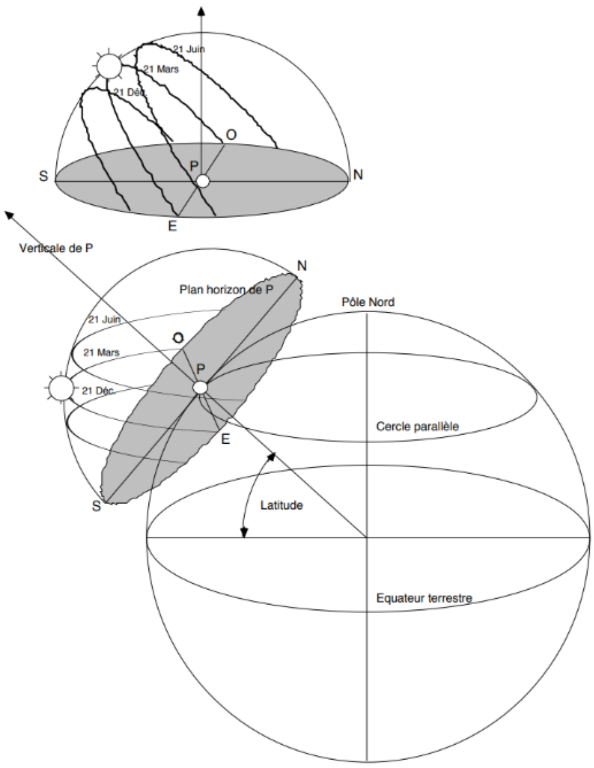

Figure 43 : Apparent solar trajectories at a point P on Earth (Siret, 1997)

The observed difference in thermal radiance value between roads in the north and in the south of the place can then be attributed to the shading effects caused by the buildings. It confirms the assumption that the relative position and height of these structures casting shadows significantly influence the thermal radiance captured in the image and therefore that this shadowing factor must be taken into account for the following analyses.

In summer, and particularly in July, as the sun is higher in the sky, shadows are shorter. The UHI effect is intensified during the summer period, with a higher difference in temperature between urban and rural areas, notably because there is less shade and more direct sunlight on the ground (Sidiqui *et al.*, 2016). This reduced shading effect may influence thermal radiance values compared to other seasons. Therefore, it may be interesting to investigate TIR images of Louvain-la-Neuve across different seasons to evaluate the impact of shading on the thermal radiance during these periods and particularly in early summer hence indirectly on the UHI. Alternatively, a 3D model of the city would allow to estimate the proportion of casted shadows over materials with high emissivity, according to the different seasons.

The vegetation also plays a role in shading. Understanding the shading effects caused by cars, buildings and vegetation is crucial to urban planning and mitigating the UHI effect. The strategic location of vegetation and the design of urban structures can help reduce heat accumulation and improve the urban microclimate.

These findings highlight the importance of carefully selecting pixels from surfaces to avoid external factors, such as shading, which are not inherent to the material itself.

6.1.3 Homogeneity of the environment

Assumption 3: The environment in Louvain-la-Neuve is homogeneous; the city's microclimate has no influence on materials "

The results of the sensitivity analysis carried out to assess assumption 3 suggest that the microclimate of Louvain-la-Neuve does not significantly influence the thermal radiance values of materials such as concrete and asphalt in different areas of the city. Therefore, the thermal properties of materials can be considered relatively homogeneous across Louvain-la-Neuve.

6.1.3.1 Microclimate

This assumption was taken when considering that the city of Louvain-la-Neuve which is a relatively small city of around 9 km^2. The maximum difference in elevation across the city is about 56 m, with an elevation of 103 m at the level of the lake and 147 m at the level of Boulevard Baudoin 1er (Topographic-map, n.d). Although the different in elevation and the repute local climate (Lauzelle is called "La petite Sibérie") there is no significant observation about any microclimate discrepancies. The lake does not seem to significantly influence the thermal radiance value in its surrounding areas, this lack of effect may be attributed to the cold air temperature experienced in March 2012.

6.1.3.2 Platform effect

The results show that there is an influence of the platform on the thermal values. The thermal radiance is higher on the platform compared to off the platform, with a mean value of 243 and 218 respectively.

This results indicates that the platform in the centre of Louvain-la-Neuve seems to contribute to the potential UHI. This difference in thermal radiance values may be due to the materials underneath the cobblestones. Under the platform is either a car park or a tunnel, and therefore air. Whereas the cobblestones outside the platform rest on an infinite layer of natural soil. The platform is surrounded by air, air which enters from outside in the tunnel and air which tends to stagnate in the car parks. In the period when the IR image was captured, the air which comes from outside had a maximum temperature of 11°C during the day and a minimum of 2°C at night (Figure 17). Stagnant air in poorly ventilated areas such as car parks benefits from anthropogenic heat sources, such as the heating of buildings above and car traffic in the car park (Santamouris, 2020). On the other hand, the soil layer is presumed to have a temperature of around 1°C, as it was the end of winter (Çuhac *et al.*, 2020).

Cobblestones laid on a layer of soil therefore benefit from good heat dissipation thanks to the heat of the soil, which is fairly low, and its thermal conduction. When thermal energy is collected by the cobblestone layer, the temperature rises, causing a temperature gradient that drives a heat flux through the soil, according to Fourier's law, $\phi = -k\nabla T$, where k is the thermal conductivity [W/m K] and T is the temperature [K]. By transferring this energy to the soil, the temperature of the cobblestones tends to decrease (Çuhac *et al.*, 2020) and have a damper daily temperature profile.

On contrary, the platform being 39 cm thick, allows a large amount of heat to be stored during the day and released at night, increasing thermal radiance compared to location outside the platform at that moment where the IR image was captured. Therefore, cobblestones of Bierges in concrete, which are light-coloured, are a suitable choice to compensate the effect of the platform because of their higher albedo.

It might be interesting to analyse the platform effect during the summer period, when the air temperature above the platform will be relatively higher compared to that below the platform. Furthermore, the natural soil layer out of the platform will be at that time warmer than in winter, reducing its impact on the amount of heat transfer from the top surface layer.

6.2 Impact of materials on thermal radiance

6.2.1 Roof surfaces

Different typical surface types have been identified for the roofs in Louvain-La-Neuve-such as ceramic, artificial asbestos slate, artificial slate, natural slate, flat roof and solar panel.

The Table 10, showing the thermal radiance values obtained for the different roofing materials, shows a clear distinction in thermal radiance between materials. Among the roof's surfaces identified, there are finally four distinguishable categories: ceramic, slate, flat roof and solar panels. Indeed, the different types of slate could have been grouped into a single category, which means that there is no great influence between artificial slate and natural slate on the thermal radiation coefficient.

Ceramic and slate

The difference between thermal radiance of ceramic and slate roof is quite consistent with the emissivity data previously presented in the Table 3 of the literature review (Chapter 1.4.3), as slate exhibit lower thermal radiance than the ceramic. The emissivity is approximately 0.92 for ceramic and approximately 0.67-0.80 for slate, with slate having a lower thermal radiance value.

An additional explanation for this difference in thermal radiance value could be given by taking into consideration the difference in conductivity of the two materials. The thermal conductivity is about 2.2 [W/mK] for the slate and around 0.32 [W/mK] for ceramic (Pichot, 2018; Eternit, 2014). The higher thermal conductivity of slate means that slate cools down faster than ceramic. To know whether thermal conductivity has an effect on thermal radiance, it is necessary to know whether the surfaces had time to reach ambient temperature. If the ambient temperature is not reached because materials did not have the time to cool down for the time of the flight, conductivity can affect thermal radiance values. If the surfaces are at ambient temperature, then only the effect of emissivity influences the thermal radiance value.

This underline the importance of assumption 2 , "Surface temperature remains uniform across the city", to analyse the thermal radiance values.

The comparison between survey-based and photointerpretation-based data, shows a remarkable convergence between the two sets of data. This consistency reinforces the credibility of the qualitative data and underlines the accuracy of the visual observations on IR image.

Solar panel

The emissivity of solar panels ranges between 0.70 and 0.90 according to the literature review but the results of the current study showed that solar panel exhibit an even higher thermal radiance value than ceramic and slate roof types.

The study of Barron-Gafford *et al.* (2016) investigated the impact of photovoltaic (PV) installations on UHI effect. PV installation reduces albedo, resulting in a darker, less reflective landscape that absorbs a greater portion of solar radiation. Consequently, PV systems re-emit a significant portion of energy as heat in addition to the amount of electricity produced. Thus, PV systems alter how incoming energy is reflected back into the atmosphere or absorbed, stored, and re-emitted. Additionally, PV systems are thin and have a low thermal capacity. The study observed that the installation of these PV systems had a notable influence on the UHI, resulting in a nighttime temperature increase of 3-4°C compared to wildland. This temperature increase may be attributed to the trapping of sensible heat flux re-emitted beneath the PV arrays at night. Furthermore, the study indicates that during the spring and summer months, the effect of PV systems is even greater than that of urban parking lots (Barron-Gafford et al., 2016). This phenomenon could explain the higher thermal radiance, resulting from a higher surface temperature. Hence, while the emissivity given by the literature review may be correct for static conditions, the inherent transient phenomena linked to the PV should be considered for the PV panels and could explain the results of the current study which is associated with a shiny afternoon (*Cfr* Figure 20) preceding the IR image analysed. This therefore demonstrates an exception to assumption 2, which states that the temperature is uniform across the city, as the solar panels appear to have a higher surface temperature.

Furthermore, the relative wide range of thermal radiance values found in the current study for solar panels is attributed to the fact that they were identified solely by visual inspection, without differentiation between the possible various types, such as PV (monocrystalline, polycrystalline,.) and thermal. It might be interesting, in a future study, to separate these two types of solar panel to see if they react in the same way.

<u>Flat roof</u>

Concerning the characteristics of flat roof materials, bitumen and EPDM exhibited in the literature relatively high emissivity values, with 0.92 and 0.90 respectively (Cfr Table 3). In addition, given that these surfaces are dark, they have a very low albedo, leading to low reflection of solar radiation (Cfr Figure 5). The combination of these two parameters yields in a notably high thermal radiance value.

The variability observed in the current study in thermal radiance values for flat roofs (see figure 32) seems to be due to the influence of building insulation. Despite taking the darkest pixels of the roofs, excluding heat sources, no discernible trend is apparent. The influence of the emissivity of flat roof materials therefore seems to be dominated by the effect of the insulation. In Figure 44, the Lavoisier building, the Science Library, and the Mercator building are depicted. It is evident that two of these buildings have recently been insulated, as they exhibit significantly lower radiance values compared to the others. The nature of their roofing materials seems different from those of the older buildings, it is therefore difficult to separate the insulation effect from material effect. Among the buildings that have not been recently insulated, one is much darker, suggesting that this darker part is more isolated or less heated. The contrast between insulated and non-insulated roofs is quite substantial. This insulation effect is therefore a limitation of the assumption 2 of the homogeneity of surface temperature

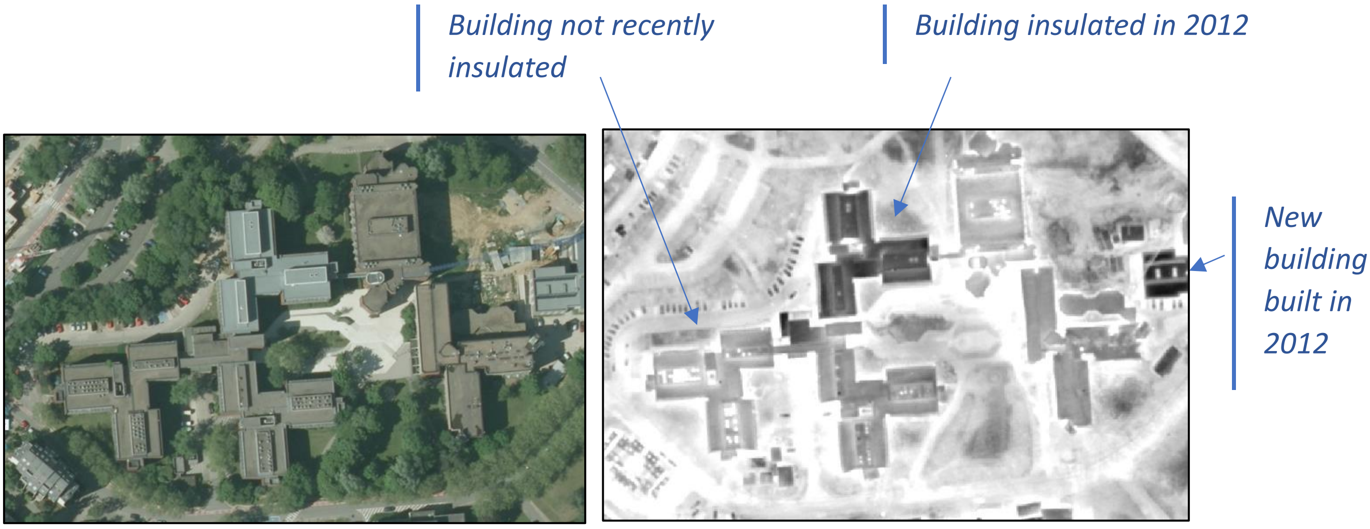

Figure 44: Comparison of insulation of "Lavoisier" buildings, TIR vs optical image (Google maps, 2012).

It would therefore be more relevant to analyse roofs emissivity using a summer thermal infrared image, as this would eliminate the effect of insulation since there would be no heating of the buildings.

<u>Comparison of optical and thermal infrared for differentiating ceramic and slate.</u>

The separability of the classes was found higher in both cases with the optical data. These consistent results from both the Mahalanobis and Bhattacharyya distances indicate that optical data (RGB) offer better separability for differentiating between ceramic and slate roofs compared to thermal infrared (TIR) data.

This robust finding across different statistical measures reinforces the conclusion that optical imaging is more effective for this purpose. The difference in thermal radiance between the two materials, although theoretically distinct, was not as decisive as the differences observed in the visible band. The effectiveness of optical imaging can be attributed to the distinct colour between the two materials in this case. This can also be due to the higher spatial resolution of optical image (4 cm) compared to the infrared image (50 cm).

6.2.2 Ground covering

The three main ground surface coverings in Louvain-la-Neuve, namely asphalt, concrete, and cobblestones, exhibit similar thermal radiance values. In fact, the Kruskal-Wallis test, which returned a p-value of 0.3691, indicates that the mean thermal radiance values for asphalt, concrete, and cobblestones are statistically similar, suggesting that they react in a similar way thermally.

This is quite coherent with their emissivity value presented in the table 1 of the literature review (Chapter 1.4.1). In fact, the emissivity value is 0.93 for asphalt and 0.91 for concrete. Concerning the cobblestones, it depends on the material of the stones, but it turns between 0.67-0.95.

Despite the similarities in terms of thermal radiation, materials do not have the same albedo. As Figure 5 (Chapter 1.2.2) shows, dark-coloured asphalt has a lower albedo (0.1) than light-coloured surfaces. Stone surfaces, such as paving stones, have a higher albedo and therefore reflect more heat. The albedo value is 0.4 for basalt, 0.5 for granite and 0.7 for limestone. Concrete has an albedo value of around 0.5 (Moretti et al., 2021). This would mean that asphalt absorbs more heat during the day compared to the two other materials.

It is therefore intriguing that the cobblestones exhibit similar thermal radiation than asphalt. The study by Moretti et al (2021) assessed the impact of cobblestones roads, as opposed to asphalt roads, on the UHI effect in the centre of Rome. This study revealed a significant improvement in daytime air temperature reduction attributed to the cobblestones (up to 0.6°C). However, this positive impact was exclusively noticeable during daylight hours, as there were no observed changes in air temperature during the early morning. This study underscores a possible explanation for why the cobblestones appear in similar thermal radiance values compared to asphalt and concrete during the night, despite their significant mitigating effect on the UHI phenomenon during daytime.

Unlike impermeable materials such as concrete and asphalt, cobblestone roads, have sandy interstices that allow water to seep into the ground. Over a longer period, this infiltration promotes a cooling effect through evapotranspiration. Permeable surfaces allow water to run off into the sewer system. As a result, cobblestones are better suited to mitigating the UHI effect because they release heat more slowly than impermeable surfaces (Mohammad & Goswami, 2021).

6.2.3 Analysis of others surfaces

Other surfaces were analysed with the aim of highlighting the advantages of thermal imaging over optical imaging for identifying materials.

Metal

Metallic surfaces appear very dark in the infrared image, with a lower thermal radiation value. The measured thermal radiance value was close to 0.

This is because, as Figure 5 in Chapter 1.2.2 shows, metals (aluminium and steel) have a high albedo and low emissivity. These materials therefore re-emit most of the solar radiation received, absorb little heat and re-emit little thermal infrared radiation, due to their low emissivity.

Unlike optics, with which it is difficult to discern metal materials, thermal imaging is a great tool for spotting areas where metal is used, thanks to its very strong dark colour on infrared images.

Road – railway

The comparison between the thermal radiance of roads and railways shows values of 188 for roads and 129 for railways.

This disparity in thermal radiance may stem from the fact that railways are primarily constructed from grey gravel rock, which tends to be lighter in colour compared to asphalt, resulting in a higher albedo. The emissivity of the two materials appears to be fairly similar, as shown in Table 3 in Chapter 1.5.

The environment may have an impact on the radiance values. The railway's location in a hollow area may limit access to direct sunlight, leading to lower radiance values. Additionally, the presence of vegetation surrounding the tracks can contribute to cooling the environment, which may affect surface temperatures and alter the thermal radiance values observed.

The difference in thermal infrared radiation between roads and railways creates a slight distinction between the two materials, which may be more visible on thermal imagery than on optical imagery, as the materials are more or less the same colour in visible range. Railway tracks also contain metal, which can be seen in darker shades on thermal images. However, it is important not to overlook other features that generally make it easier to identify railway tracks, such as their straight alignment. So, although the difference in thermal radiance between roads and railways can play a role, other predominant aspects such as the geometry of railways are also important in their identification.

Footbridge

A difference in thermal radiance is observed between wooden and asphalt footbridge. Wood has lower radiance values, around 68, while the asphalt footbridge has a value of 153.46.

This difference shows that wood reacts differently from asphalt. This variation in thermal radiance stems from the distinct compositions of these materials. This can be confirmed by the lower emissivity of the wood presented in the Table 1 in Chapter 1.4. Furthermore, this lower value of thermal radiance for wood has been verified by the thermal radiance of 99 captured at “Place des Sciences”, which is a large wooden terrace.

Wooden walkways are therefore easily discernible from a thermal point of view, compared with an optical point of view, where the difference between the colour of wood and that of asphalt is less perceptible.

This also underscores the advantage of using wood for footbridges, particularly in mitigating urban heat island effects, due to their low heat emission, which contributes to cooler urban environments and promotes sustainability in infrastructure development.

An interesting observation is that the thermal radiance of the asphalt footbridge has a value of 153.46, which is quite low compared to the average value for asphalt observed in Chapter 5.2.2. This lower thermal radiance value could be due to the presence of opaque barriers on the footbridge, shading the ground, which limit the access of sunlight to the surface, thus reducing its thermal radiance. An alternative explanation could be the possible heat dissipation on both sides of the asphalt and concrete structure of the footbridges.

6.3 Comparison between thermal radiance obtained and theoretical emissivity for surface materials.

This section compares the emissivity values from the literature review (*Cfr* Table 1 and Table 3) with the ranking obtained for the thermal radiance of each material.

The following table compares the two variables qualitatively (from 0 (---) to 1(+++) for the emissivity and from 0 (---) to 270 (+++) for the thermal radiance). It gives the coherence between the equivalent emissivity-thermal radiance values.

Table 15 : Qualitative comparison of thermal radiance and emissivity values of materials

Materials	Emissivity	Thermal radiance value
Metal	---	---
Slate	+	+
Solar panel	++	++
Natural cobblestones	++	+++
EPDM membrane	++	++
Ceramic	+++	+
Concrete	+++	+++
Asphalt	+++	+++

The comparison between the ranking of thermal radiance values measured and the theoretical emissivity is quite similar, with higher emissivity corresponding to a higher thermal radiance value. However, there is an exception for the ceramic value.

The emissivity value coming from the literature review (Table 3) for ceramic is quite high compared to the thermal radiance value of the ceramic roof measured. This discrepancy can be explained by the fact that the emissivity value selected from the literature review for ceramic roof corresponds to porcelain, which may not be appropriate for the type of ceramic used for the tiles. Instead, the emissivity of the red clay tiles, which is lower (0.5), corresponds much better to the results obtained for the ceramic roofs in this study.

6.4 Main limitations of the study

This section will focus on the several limitations that can be identified in the study conducted.

Firstly, the study was based on a thermal image taken in March 2012. Over the past 12 years, many changes have occurred in the city such as the development of new built up surfaces (e.g., accommodation behind the “Esplanade”, Martin’s hotel).

Secondly, the reliance on a single thermal image taken at specific moment may raise some questions. Weather conditions prior to the time the image was taken may have impact on the thermal radiance values. For example, if the day before the thermal image was taken would have been more sunny, the surfaces would have captured more heat and would have had a warmer surface temperature. The effect of shade would have been even greater in such conditions. Additionally, as noted in the study by Zhong et al. (2022), the thermal emissivity and radiance of surfaces can be influenced by recent precipitation. If it had rained locally before the thermal infrared images were taken, the moisture content of the surfaces could have alter the results, possibly leading to variations in the observed thermal radiance values (Zhong et al., 2022). Fortunately, for this study, Figures 17, 18, 19, and 20 in Chapter 3.4 demonstrate that there was low cloud cover, 6.5 hours of insolation, and negligible precipitation the day preceding the flight. It had rained a few days before, so it is possible that some water had infiltrated permeable surfaces. Hence, the image used seems quite representative for the purpose of this study.

Another limitation is related to assumption 2, which considers that the surface temperatures remain uniform across the city as discussed in chapter 6.1. However, it is important to take into account the activities of the city, as localised sources of heat (such as residual heat from industrial activities or buildings) may still introduce variations in surface temperature. Another factor such as building insulation, can also influence surface temperature. Therefore, local temperature variations are possible and should be taken into consideration. Some limitations to this assumption 2 are solar panels, insulation effect and shading effect.

As seen in Chapter 6.2.1 on flat roof, it would therefore be more relevant to analyse roofs emissivity using a summer TIR image, as this would eliminate the effect of insulation since there would be no heating of the buildings. Moreover, as explained in discussion 6.1.2.2 with the shading effect, a TIR image of the summer period would allow to limit the shading effect when the sun is at its highest in the sky, causing buildings to cast less shadow.

In this study, only the ground surfaces were taken into account, given the TIR aerial image. It could also take into account all the 3D obstacles that impede ventilation of the city, and which also absorb heat from the sun's rays.

6.5 Perspectives for UHI in Louvain-la-Neuve

This section discusses possible strategies to mitigate UHI effect in the city of Louvain-la-Neuve.

Choosing the right materials is a crucial strategy for mitigating the UHI effect. It is essential to use low-albedo materials, favouring light-coloured materials, (Moretti et al., 2021) as they have a high solar reflectance, absorbing a small amount of heat when exposed to solar radiation (Di Giuseppe et al., 2017).

The adoption of such materials can therefore have a significant impact. For example:

- in the case of roof surfaces, the use of metal compared with traditional tiles (ceramic or slate);
- in the case of ground surfaces, the use of light-coloured gravel compared to asphalt under the same weather conditions;
- in the case of LLN, the use of light-coloured Bierges cobblestones was typically a good choice during the city's construction.

This is effective in reducing the effect of UHI and also on the cooling requirements of buildings.

Moreover, impermeable materials must be avoided to allow water infiltration into the soil, facilitating cooling by evapotranspiration thereafter. Permeable materials should therefore be preferred.

In order to mitigate UHI, the addition of vegetation in the city is crucial, as it offers multiple benefits, including shading effect and a cooling effect through evapotranspiration. This can be done with green infrastructures (such as green roofs, green walls…) and green areas. These alternatives contribute to cooling of the environment, due to the evapotranspiration process, by both reducing air temperatures and reducing surface temperatures of the buildings (Moretti et al., 2021).

General conclusions

In the context of urban heat island (UHI) phenomenon, which is becoming increasingly widespread and has many consequences, this study has analysed the various materials used in the city of Louvain-la-Neuve. The aim of the study was to measure the thermal radiance value of each surface material and then to evaluate if the differentiation between surfaces materials according to their thermal radiance value was possible. The thermal radiance value of each material used has been measured based on a thermal infrared image.

As the thermal radiance value of materials in winter at night was found driven mainly by the emissivity, the thermal radiance of the TIR image can be considered as directly proportional to their impact on the UHI effect. This study explores the diversity of existing surfaces and their related effects in mitigating the UHI effect.

The results show that the analysis of TIR images can establish a clear distinction between thermal radiances for ceramic, slate, flat roof and solar panel. All different types of slate roof; natural, artificial and artificial with asbestos, exhibited similar thermal radiance values and therefore were grouped into a single category of slate. The ceramic roof exhibited a higher thermal radiance value (67W/m^2) compared to slate roof (46 W/m^2). The flat roof and solar panel exhibited higher thermal radiance values, with a value of 84 W/m^2 for flat roof and 92 W/m^2 for solar panel. However, the level of insulation having an effect on the thermal radiance, this highlights the importance of selecting the darkest pixels to ensure valid estimation of the thermal radiance of roof types.

Concerning the ground covering, asphalt, concrete and cobblestones exhibit similar thermal radiance values in winter time, with a mean of 210 W/m^2. Hence, there is a noticeable difference in the thermal radiance values of ground covering materials compared to roofs materials, with ground covering materials exhibiting higher values. Therefore, the ground can easily be identified from the roof covering based on the TIR images. Given the high thermal radiance of ground covering surfaces, it is crucial to pay attention to these types of surfaces to mitigate the UHI effect.

Nevertheless, this study identified a significant potential shading effect impacting the thermal radiance values on the ground. It is therefore essential, when selecting pixels on the ground, to verify the location of pixels compared to surrounding infrastructures.

The study reveals that, in general, the TIR image appears to be relevant in distinguishing surfaces materials, as the different thermal radiance values are quite discernible. Compared to optical images, TIR appears to be even better for identifying some surfaces. For example, it is particularly advantageous in discriminating metallic and wood surfaces. However, optical images are more relevant for identifying the differences between ceramic (red) and slate (grey), due to their colour differences in the case of Louvain-la-Neuve.

The particularities of a city subject to such study should however carefully be taken into account as possibly impacting the thermal radiance values. In the current study, the platform on which the centre of the city of Louvain-la-Neuve is built has a slight effect causing an increase of the thermal radiance value. This indicates that the platform might be creating a microclimate in this specific area. However, it appeared that there is no significant effect on the overall microclimate of the city in winter time.

Quite interesting results were observed in this study although they are based on a single thermal infrared (TIR) image captured in March. The findings are therefore applicable to the winter period of the image analysed. Numerous observations were possible during this period due to the specific weather conditions with gradients in temperature outside/inside or on a daily basis. However, the analysis of a TIR image of Louvain-la-Neuve captured during a summer period could be also interesting for several reasons :

- First, this summer TIR image would limit the insulation effect, as people are not heating their homes during this period, thus providing a more stable measure of thermal radiance on roof surfaces.
- Second, it would allow for the analysis of a limited shading effect, which is weaker in summer due to the higher position of the sun in the sky.
- Third, the weather conditions and the associated soil and ambient temperatures would be even more relevant because UHI should take place during this period.
- Additionally, it would allow for a quantitative assessment of the cooling effect of the vegetation.
- Finally, it would allow for the analysis of the microclimate during this period to see if it has any influence during the summer period, for example from the lake of Louvain-la-Neuve.

It may therefore be relevant to conduct a similar study with a more recent TIR image of Louvain-la-Neuve captured during the summer period and, if possible, after a stable temperature period without rainy conditions. This recent TIR image would allow comparing the current study, providing insights into seasonal variations and the current state of urbanisation of the city.

References

Akbari, H., & Rose, L. S. (2008). Urban surfaces and heat island mitigation potentials. *Journal of the Human-environment System*, *11*(2), 85-101. https://doi.org/10.1618/jhes.11.85

Ana-Maria, B., Mihai-Ionut, D., Stelian, G. M., & Ștefana, B. (2016). Challenges regarding the study of urban heat islands. Rule set for researchers. *Proceedings of the Risk Reduction for Resilient Cities, Bucharest, Romania*, 3-4. Retrieved from https://www.researchgate.net/publication/309740257_Challanges_regarding_the_study_of_urban_heat_islands_Ruleset_for_researchers

Antoine, R., & Lopez, T. (2017). *Télédétection dans l'infrarouge thermique*. Master's thesis, International Space Science Institute (ISSI) Bern, Switzerland. https://hal.science/hal-02865102/file/Antoine%20and%20Lopez_MecaRoch_2017.pdf

Barron-Gafford, G., Minor, R., Allen, N., Cronin, A., Brooks, A. & Pavao-Zuckerman M. (2016)The Photovoltaic Heat Island Effect: Larger solar power plants increase local temperatures. *Sci Rep* 6, 35070. https://doi.org/10.1038/srep35070

Becosan. (2020). *Matériaux de construction et revêtements*. Becosan. Retrieved 25 May 2024, from https://www.becosan.com/fr/materiaux-de-construction-revetements/

Candoré, J. C., Bodnar, J. L., Szeflinski, A., Ibos, L., Datcu, S., Candau, Y., ... & Frichet, J. C. (2008, July). Helps with the thermal diagnosis of the building: Detection of defects of insulation by stimulated infra-red thermography. In *9th International Conference on Quantitative Infrared Thermography, Krakow, Poland*. http://dx.doi.org/10.21611/qirt.2008.05_01_08

Choi, Y., Lee, S., & Moon, H. (2018). Urban physical environments and the duration of high air temperature: Focusing on solar radiation trapping effects. *Sustainability*, *10*(12), 4837. https://doi.org/10.3390/su10124837

Choi, E., & Lee, C. (2003). Feature extraction based on the Bhattacharyya distance. *Pattern Recognition*, *36*(8), 1703-1709. https://doi.org/10.1016/S0031-3203(03)00035-9

Chui, A. C., Gittelson, A., Sebastian, E., Stamler, N., & Gaffin, S. R. (2018). Urban heat islands and cooler infrastructure–measuring near-surface temperatures with hand-held infrared cameras. *Urban climate*, *24*, 51-62. https://doi.org/10.1016/j.uclim.2017.12.009

Çuhac, C., Mäkiranta, A., Välisuo, P., Hiltunen, E., & Elmusrati, M. (2020). Temperature measurements on a solar and low enthalpy geothermal open-air asphalt surface platform in a cold climate region. *Energies*, *13*(4), 979. https://doi.org/10.3390/en13040979 de Loor, G. P. (1970). The Electromagnetic Spectrum from an Equipment Point of View. *Geoforum*, *1*(2), 9-18. https://doi.org/10.1016/0016-7185(70)90025-4

De Maesschalck, R., Jouan-Rimbaud, D., & Massart, D. L. (2000). The mahalanobis distance. *Chemometrics and intelligent laboratory systems*, *50*(1), 1-18. https://doi.org/10.1016/S0169-7439(99)00047-7

Di Giuseppe, E., Pergolini, M., & Stazi, F. (2017). Numerical assessment of the impact of roof reflectivity and building envelope thermal transmittance on the UHI effect. *Energy Procedia*, *134*, 404-413. https://doi.org/10.1016/j.egypro.2017.09.590

Ducay Stephane, (2017-2018). *Cours de statistique : tests non paramétriques*. Université de Picardie Jules Verne UFR des Sciences. Retrieved from https://www.lamfa.u-picardie.fr/ducay/Statistiques%2020172018/Cours%208.pdf

Dubuisson, P., & Minvielle, F. (2017). Température et rayonnement infrarouge. *Météorologie, (99), 1*. Retrieved 29 October 2023, from https://lameteorologie.fr/admin/api/public/api/meteo/website/downloadArticlePDF/meteo_2017_99_17

Eternit. (2014). *Tuiles plates en terre cuite*. Retrieved 28 May 2024, from https://files.defrancq.be/?id=a2067b64-d3f2-4f67-a1cf-0899112a6abe

Green D. W. & Perry. R. H. (2008) *Perry's Chemical Engineers' Handbook*, Eighth Edition.

Hafiz, A. M., & Bhat, G. M. (2020). A survey on instance segmentation: state of the art. *International journal of multimedia information retrieval*, *9*(3), 171-189. https://doi.org/10.1007/s13735-020-00195-x

Hassani, N. (2023). *Caractérisation des îlots de chaleur de saison chaude dans les territoires de l'Eurométropole de Metz (France) et du Grand Casablanca (Maroc): observation, perception, vulnérabilité*. Doctoral dissertation, Université de Lorraine. https://hal.univ-lorraine.fr/tel-04469142v1/file/DDOC_T_2023_0242_HASSANI.pdf

Iaria, J., & Susca, T. (2022). Analytic Hierarchy Processes (AHP) evaluation of green roof- and green wall-based UHI mitigation strategies via ENVI-met simulations. *Urban Climate*, *46*, 101293. https://doi.org/10.1016/j.uclim.2022.101293

Kim, H. Y. (2014). Analysis of variance (ANOVA) comparing means of more than two groups. *Restorative dentistry & endodontics*, *39*(1), 74. https://doi.org/10.5395%2Frde.2014.39.1.74

Kjellstrom, T., Butler, A. J., Lucas, R. M., & Bonita, R. (2010). Public health impact of global heating due to climate change: potential effects on chronic non-communicable diseases. *International journal of public health*, *55*, 97-103. https://doi.org/10.1007/s00038-009-0090-2

Laaidi, K. (2012). *Rôle des îlots de chaleur urbains dans la surmortalité observée pendant les vagues de chaleur*. Synthèse des études réalisées par l'Institut de veille sanitaire sur la vague de chaleur d'août 2003. Santé Publique France. Retrieved from *http://www. invs. sante. fr/Publications-et-outils/Rapports-etsyntheses/Environnement-et-sante/2012/Role-des-îlots-dechaleur-urbains-dans-la-surmortalite-observee-pendant-les-vagues-de-chaleur*.

Marr, J. M., & Wilkin, F. P. (2012). A better presentation of Planck's radiation law. *American Journal of Physics*, *80*(5), 399-405. https://doi.org/10.1119/1.3696974

Michael E. O'Neill, Ky L. Mathews. (2002). Levene Tests of Homogeneity of Variance for General Block and Treatment Designs, *Biometrics*, Volume 58, Issue 1, Pages 216–224. https://doi.org/10.1111/j.0006-341X.2002.00216.x

Mievis Philippe (2012). *Bilan climatologique du mois de mars 2012 à la station d'Uccle*. Météo Belgique Retrieved 5 June 2024, from https://www.meteobelgique.be/article/84-annee-2012/1757-releves-mars-2012

Mohammad, P., & Goswami, A. (2021). Quantifying diurnal and seasonal variation of surface urban heat island intensity and its associated determinants across different climatic zones over Indian cities. *GIScience & Remote Sensing, 58(7), 955-981.* http://dx.doi.org/10.1080/15481603.2021.1940739

Moretti, L., Cantisani, G., Carpiceci, M., D'Andrea, A., Del Serrone, G., Di Mascio, P., & Loprencipe, G. (2021). Effect of sampietrini pavers on urban heat islands. *International journal of environmental research and public health*, *18*(24), 13108. https://doi.org/10.3390/ijerph182413108

Oke, T. R. (1982). The energetic basis of the urban heat island. *Quarterly journal of the royal meteorological society*, *108*(455), 1-24. https://doi.org/10.1002/qj.49710845502

Oke, T. R. (1988). The urban energy balance. Progress in Physical geography, 12(4), 471-508. http://dx.doi.org/10.1177/030913338801200401

Olln. (2024). *Une ville piétonne*. Office du tourisme- Inforville. Retrieved 19 May 2024, from https://www.olln.be/fr/office-du-tourisme-inforville/decouvrez/les-raisons-de-venir/une-ville-pietonne

Olln. (n.d) *Histoire : D'Ottignies à Ottignies-Louvain-la-Neuve*. Olln Retrieved 25 May 2024, from https://parcours.tourisme-olln.be/fr/la-ville-et-son-universite/histoire.html#:~:text=D'Ottignies%20%C3%A0%20Ottignies-Louvain,Ottignies%207%20ans%20plus%20tard.

Omega engineering (n.d). *Table of Total Emissivity.* Omega engineering. Retrieved 23 December 2023, from https://www.omegaengineering.cn/temperature/Z/pdf/z088-089.pdf

Optris, G. (n.d). Basic principles of non-contact temperature measurement. Innovation Infrared Technology, 1, 39. Retrieved from https://infrarougekelvin.com/wp-content/uploads/2016/06/4A-IR-Basics-2.pdf

Pichot Emilie. (2018). *Ardoise PEB-012*. La matériauthèque. Retrieved 28 May 2024, from https://materiautheque-laplace.second-degre.ac-normandie.fr/spip.php?article68

Pierre & Sol. (n.d.). *Pavé grès*. Pierre & sol. Retrieved 25 May 2024, from https://www.pierreetsol.com/Pages/Vente/pave-gres

Pierre & Sol. (n.d.). *Pavé porphyre*. Pierre & sol. Retrieved 25 May 2024, from https://www.pierreetsol.com/Pages/Vente/pave-porphyre

Pigeon, G., Lemonsu, A., Masson, V., & Hidalgo, J. (2008). De l'observation du microclimat urbain à la modélisation intégrée de la ville. *La Météorologie, (62), PP-39.* http://dx.doi.org/10.4267/2042/19174

Phelan, P. E., Kaloush, K., Miner, M., Golden, J., Phelan, B., Silva III, H., & Taylor, R. A. (2015). Urban heat island: mechanisms, implications, and possible remedies. *Annual Review of Environment and Resources*, *40*, 285-307. https://doi.org/10.1146/annurev-environ-102014-021155

Plachý, J., & Vysoká, J. (2019). Surface temperature of bitumen sheets in the flat roof structure. In *MATEC Web of Conferences* (Vol. 279, p. 02017). EDP Sciences. https://doi.org/10.1051/matecconf/201927902017

Robert H. Riffenburgh (2006). *Kruskal-Wallis test*. in Statistics in Medicine (Second Edition). Retrieved 20 May 2024, from https://www.sciencedirect.com/topics/mathematics/kruskal-wallis-test#:~:text=The%20Kruskal%E2%80%93Wallis%20test%20is,or%20more%20members%20per%20sample.

Sachindra, D. A., Ng, A. W. M., Muthukumaran, S., & Perera, B. J. C. (2016). Impact of climate change on urban heat island effect and extreme temperatures: a case-study. *Quarterly Journal of the Royal Meteorological Society*, *142*(694), 172-186. https://doi.org/10.1002/qj.2642

Santamouris, M., Synnefa, A., & Karlessi, T. (2011). Using advanced cool materials in the urban built environment to mitigate heat islands and improve thermal comfort conditions. *Solar energy*, *85*(12), 3085-3102. https://doi.org/10.1016/j.solener.2010.12.023

Santamouris, M., Cartalis, C., Synnefa, A., & Kolokotsa, D. (2015). On the impact of urban heat island and global warming on the power demand and electricity consumption of buildings—A review. *Energy and buildings*, *98*, 119-124. https://doi.org/10.1016/j.enbuild.2014.09.052

Santamouris, M. (2020). Recent progress on urban overheating and heat island research. Integrated assessment of the energy, environmental, vulnerability and health impact. Synergies with the global climate change. *Energy and Buildings*, *207*, 109482. https://doi.org/10.1016/j.enbuild.2019.109482

Schwertman, N. C., Owens, M. A., & Adnan, R. (2004). A simple more general boxplot method for identifying outliers. *Computational statistics & data analysis*, *47*(1), 165-174. https://doi.org/10.1016/j.csda.2003.10.012

Shi, L., Kloog, I., Zanobetti, A., Liu, P., & Schwartz, J. D. (2015). Impacts of temperature and its variability on mortality in New England. *Nature climate change*, *5*(11), 988-991. https://doi.org/10.1038/nclimate2704

Sidiqui, P., Huete, A., & Devadas, R. (2016, July). Spatio-temporal mapping and monitoring of Urban Heat Island patterns over Sydney, Australia using MODIS and Landsat-8. In 2016 4th International Workshop on Earth Observation and Remote Sensing Applications (EORSA) (pp. 217-221). IEEE. http://dx.doi.org/10.1109/EORSA.2016.7552800

Siret, D. (1997). *Propositions pour une approche déclarative des ambiances dans le projet architectural: Application à l'ensoleillement* (Doctoral dissertation, Université de Nantes). Retrieved from https://www.researchgate.net/publication/50280515_Propositions_pour_une_approche_declarative_des_ambiances_dans_le_projet_architectural_application_a_l%27ensoleillement

Ibrahim, S.H., Ibrahim, N.I.A., Wahid, J., Goh, N.A., Koesmeri, D.R.A., Nawi, M.N.M., 2018. The Impact of Road Pavement on Urban Heat Island (UHI) Phenomenon. *International Journal of Technology*. Volume 9(8), pp. 1597-1608 https://doi.org/10.14716/ijtech.v9i8.2755

Sobrino, J. A., Oltra-Carrió, R., Jiménez-Muñoz, J. C., Julien, Y., Sòria, G., Franch, B., & Mattar, C. (2012). Emissivity mapping over urban areas using a classification-based approach: Application to the Dual-use European Security IR Experiment (DESIREX). *International Journal of Applied Earth Observation and Geoinformation*, *18*, 141-147. https://doi.org/10.1016/j.jag.2012.01.022

Susca, T., Gaffin, S. R., & Dell'Osso, G. R. (2011). Positive effects of vegetation: Urban heat island and green roofs. *Environmental pollution*, *159*(8-9), 2119-2126. https://doi.org/10.1016/j.envpol.2011.03.007

Stewart, I. D., & Mills, G. (2021). The Urban Heat Island. Elsevier Science. 182 pages. Retrieved from https://books.google.be/books?hl=fr&lr=&id=uOgGEAAAQBAJ&oi=fnd&pg=PP1&dq=The+Urban+Heat+Island+:+Iain+D.+Stewart+and+Gerald+Mills&ots=5JtpO6jzsY&sig=nA2LuldjCJ_aesmYO-EErLzqDPA#v=onepage&q=The%20Urban%20Heat%20Island%20%3A%20Iain%20D.%20Stewart%20and%20Gerald%20Mills&f=false

Subedi, I., Silverman, T. J., Deceglie, M. G., & Podraza, N. J. (2019). Emissivity of solar cell cover glass calculated from infrared reflectance measurements. *Solar Energy Materials and Solar Cells*, *190*, 98-102. https://doi.org/10.1016/j.solmat.2018.09.027

Thermometer.eu. (2024). Tableau d'émisivité Retrieved 20 May 2024, from https://www.be.thermometer.eu/blogs/guide-thermometre/tableau-demissivite

Topographic-map. (n.d) Carte topographique Louvain-la-Neuve. Retrieved 1 June 2024, from https://fr-be.topographic-map.com/map-8r5tf/Louvain-la-Neuve/

Vlcek, J. (1982). A field method for determination of emissivity with imaging radiometers. Photogrammetric Engineering and Remote Sensing. Retrieved 27 May 2024, from https://www.asprs.org/wp-content/uploads/pers/1982journal/apr/1982_apr_609-614.pdf

Weather Spark. (2012). Historique de la météo en 20 mars 2012 pour Aéroport de Bruxelles. Retrieved 15May 2024, from https://fr.weatherspark.com/h/d/147989/2012/3/20/M%C3%A9t%C3%A9o-historique-le-mardi-20-mars-2012-%C3%A0-A%C3%A9roport-de-Bruxelles-Belgique#Figures-Temperature

Wikipedia. (2024). Louvain-la-Neuve. Retrieved 1 June 2024, from https://fr.wikipedia.org/wiki/Louvain-la-Neuve

Wong, K. V., Paddon, A., and Jimenez, A. (March 21, 2013). "Review of World Urban Heat Islands: Many Linked to Increased Mortality." ASME. *J. Energy Resour. Technol*. June 2013; 135(2): 022101. https://doi.org/10.1115/1.4023176

Wyard, C., Marion, R., & Hallot, E. (2023). WaRM: a roof material spectral library for Wallonia, Belgium. *Data*, *8*(3), 59. https://doi.org/10.3390/data8030059

XLSTAT. (2023) "Quelle est la différence entre un test paramétrique et non-paramétrique ?" Retrieved 20 May 2024, from https://help.xlstat.com/fr/6739-quelle-est-la-difference-entre-un-test-parametrique-et.

Yow, D. M. (2007). Urban heat islands: Observations, impacts, and adaptation. *Geography Compass*, *1*(6),1227-1251. https://doi.org/10.1111/j.1749-8198.2007.00063.x

Zhong, X., Zhao, L., Zhang, X., Yan, J., & Ren, P. (2022). Investigating the effects of surface moisture content on thermal infrared emissivity of urban underlying surfaces. *Construction and Building Materials*, *327*, 127023. https://doi.org/10.1016/j.conbuildmat.2022.127023

Appendix

7.1 Appendix on the homogeneity of the environment

7.1.1 Results of the Kruskal-Wallis test evaluating the effect of the zone on the materials (asphalt and concrete)

```
        Kruskal-Wallis rank sum test

data:  Value by Zone
Kruskal-Wallis chi-squared = 7.6298, df = 8, p-value = 0.4704
```

7.2 Appendix on shading effect

Shadow of the cars

7.2.1 Results of the Levene test for the homogeneity of variance of data of shadow and not shadow caused by the car

```
Levene's Test for Homogeneity of Variance (center = median)
      Df F value  Pr(>F)
group  1  4.8909 0.03945 *
      19
---
Signif. codes:  0 ‘***’ 0.001 ‘**’ 0.01 ‘*’ 0.05 ‘.’ 0.1 ‘ ’ 1
```

7.2.2 Result of the Welch test for the shadow of the car on the Leclercq parking

```
        Welch Two Sample t-test

data:  donnee_ombre$X_mean and donnee_pas_ombre$X_mean
t = -2.3301, df = 15.947, p-value = 0.03327
alternative hypothesis: true difference in means is not equal to 0
95 percent confidence interval:
 -28.12312  -1.32435
sample estimates:
   Mean for shadow Mean for no shadow
          145.0118           159.7355
```

Shadow of the Buildings

7.2.3 Results of the Levene test for the homogeneity of the data of the shadow and not shadow caused by the buildings

```
Levene's Test for Homogeneity of Variance (center = median)
      Df F value   Pr(>F)
group  1   14.54 0.006601 **
       7
---
Signif. codes:  0 ‘***’ 0.001 ‘**’ 0.01 ‘*’ 0.05 ‘.’ 0.1 ‘ ’ 1
```

7.2.4 Result of the welch test for the shadow of the buildings

```
        Welch Two Sample t-test

data:  donnees_ombre_building and donnees_soleil_building
t = -10.561, df = 3.0809, p-value = 0.001611
alternative hypothesis: true difference in means is not equal to 0
95 percent confidence interval:
 -90.41690 -49.01595
sample estimates:
   Mean for shadow of buildings Mean for no shadow of buildings
                       159.5429                        229.2593
```

7.3 Appendix on insulation effect

7.3.1 Results of the Shapiro-Wilk test :

```
        Shapiro-Wilk normality test

data:  valeurs_emissivite_isolation
W = 0.97875, p-value = 0.9581
```

```
        Shapiro-Wilk normality test

data:  valeurs_emissivite_sans_isolation
W = 0.9326, p-value = 0.474
```

7.3.2 Results of the Barlett test :

```
        Bartlett test of homogeneity of variances

data:  list(valeurs_emissivite_sans_isolation, valeurs_emissivite_isolation)
Bartlett's K-squared = 7.3264, df = 1, p-value = 0.006795
```

7.3.3 Results of the Wilcoxon test :

```
        Wilcoxon signed rank exact test

data:  valeurs_emissivite_sans_isolation and valeurs_emissivite_isolation
V = 55, p-value = 0.001953
alternative hypothesis: true location shift is not equal to 0
```

7.4 Appendix on platform analysis

7.4.1 : Comparison of thermal radiance coefficients on and off the platform (platform in red and off-platform in blue)

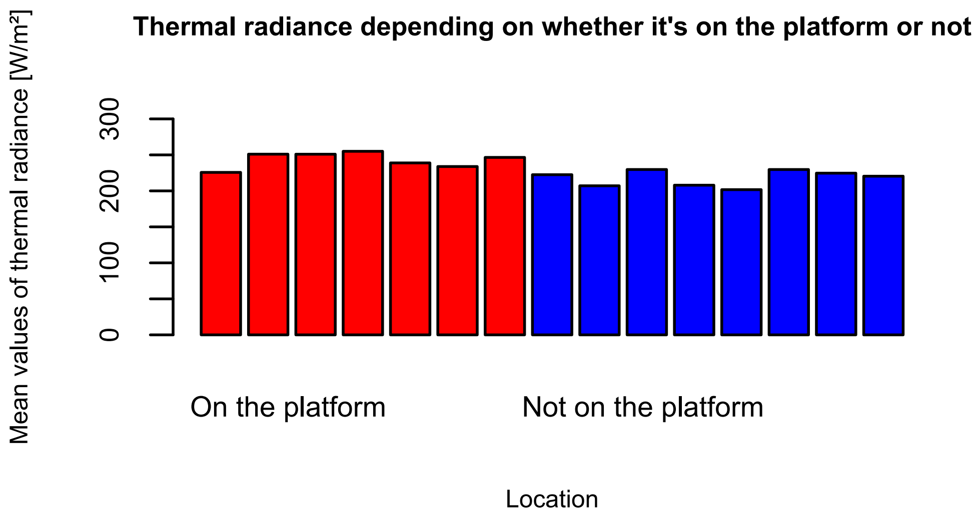

7.4.2 Results of the Levene test:

```
Levene's Test for Homogeneity of Variance (center = median)
      Df F value Pr(>F)
group  1  0.0076 0.9319
      13
```

7.4.3 Results of the Shapiro-Wilk test :

```
        Shapiro-Wilk normality test

data:  donnee_dalle$X_mean
W = 0.92582, p-value = 0.5159
```

```
        Shapiro-Wilk normality test

data:  donnee_pas_dalle$X_mean
W = 0.88719, p-value = 0.2203
```

7.4.4 Results of the Student's t-test :

```
        Two Sample t-test

data:  donnee_dalle$X_mean and donnee_pas_dalle$X_mean
t = 4.5074, df = 13, p-value = 0.0005893
alternative hypothesis: true difference in means is not equal to 0
95 percent confidence interval:
 13.10569 37.23285
sample estimates:
mean of x mean of y
 243.1343  217.9650
```

7.5 Appendix on roof surfaces

Result of the tests for the roofs surfaces

7.5.1 statistic table for each roof type (ceramic, artificial slate, artificial slate with asbestos, natural slate, flat roof and solar panel respectively) for the survey-based approach

```
> print(tableau_statistiques_ceramique)
   Moyenne  Médiane Écart.type Minimum Maximum
1 67.37987 68.66667   5.317985    58.5   74.75
```

```
> print(tableau_statistiques_ardoiseArtif)
  Moyenne Médiane Écart.type Minimum Maximum
1  50.125      51   2.852468      46    52.5
```

```
> print(tableau_statistiques_ardoiseAA)
   Moyenne  Médiane Écart.type  Minimum Maximum
1 44.42308 43.66667   15.83609 17.16667      64
```

```
> print(tableau_statistiques_ardoiseNatu)
   Moyenne Médiane Écart.type Minimum Maximum
1 44.96296      44   17.99904    16.5    66.5
```

```
> print(tableau_statistiques_toits_plats)
  Moyenne  Médiane Écart.type  Minimum  Maximum
1 83.6067 84.51282   20.18024 33.20588 118.4211
```

```
> print(tableau_statistiques_solaire)
   Moyenne Médiane Écart.type Minimum Maximum
1 92.08443   86.55   19.27885      66   125.2
```

7.5.2 Results of the Shapiro-Wilk test to assess the normality of the residuals :

```
        Shapiro-Wilk normality test

data:  mean_ardoiseArtif
W = 0.85864, p-value = 0.2554
```

```
        Shapiro-Wilk normality test

data:  mean_ardoiseNatu
W = 0.9018, p-value = 0.2626
```

```
        Shapiro-Wilk normality test

data:  mean_ardoiseAA
W = 0.91456, p-value = 0.2117
```

7.5.3 Results of the Levene test to assess the homogeneity of the variances :

```
Levene's Test for Homogeneity of Variance (center = median)
      Df F value  Pr(>F)  
group  2  3.3715 0.05199 .
      23                  
---
Signif. codes:  0 ‘***’ 0.001 ‘**’ 0.01 ‘*’ 0.05 ‘.’ 0.1 ‘ ’ 1
```

7.5.4 Results of the ANOVA test on the three types of slate :

```
              Df Sum Sq Mean Sq F value Pr(>F)
types_ardoise  2    103   51.62   0.211  0.811
Residuals     23   5626  244.59               
```

7.5.5 statistic table for the three types of slate

```
> print(tableau_statistiques_slate)
   Moyenne Médiane Écart.type Minimum Maximum
1 45.48718   45.75    15.1377    16.5    66.5
```

7.5.6 statistic table for slate and ceramic of the photointerpretation-based approach

```
> print(tableau_statistiques_ardoise50)
  Moyenne Médiane Écart.type  Minimum Maximum
1 41.9856  42.025   12.46563 13.57143    67.5
```

```
> print(tableau_statistiques_ceramique50)
   Moyenne  Médiane Écart.type Minimum  Maximum
1 64.84653 63.79167   9.112686      49 89.66667
```

Results of the tests for the comparison of qualitative and quantitative approaches :

7.5.7 Results of the Shapiro-Wilk test

```
> # Vérification de la normalité des résidus : Test de Shapiro-Wilk
> shapiro.test(mean_slate)

        Shapiro-Wilk normality test

data:  mean_slate
W = 0.9386, p-value = 0.1244

> shapiro.test(mean_ardoise50)

        Shapiro-Wilk normality test

data:  mean_ardoise50
W = 0.98584, p-value = 0.8071

> shapiro.test(mean_ceram)

        Shapiro-Wilk normality test

data:  mean_ceram
W = 0.95373, p-value = 0.6918

> shapiro.test(mean_ceram50)

        Shapiro-Wilk normality test

data:  mean_ceram50
W = 0.9818, p-value = 0.6552
```

7.5.8 Results of the Levene test : first slate and then ceramic

```
Levene's Test for Homogeneity of Variance (center = median)
      Df F value Pr(>F)
group  1  1.6732 0.1998
      74
```

```
Levene's Test for Homogeneity of Variance (center = median)
      Df F value Pr(>F)
group  1  2.6511  0.109
      57
```

7.5.9 Results of the Student's t-test : first slate and then ceramic

```
        Two Sample t-test

data:  mean_slate and mean_ardoise50
t = 1.0785, df = 74, p-value = 0.2843
alternative hypothesis: true difference in means is not equal to 0
95 percent confidence interval:
 -2.967660  9.970813
sample estimates:
mean of x mean of y
 45.48718  41.98560
```

```
        Two Sample t-test

data:  mean_ceram and mean_ceram50
t = 0.88437, df = 57, p-value = 0.3802
alternative hypothesis: true difference in means is not equal to 0
95 percent confidence interval:
 -3.202837  8.269522
sample estimates:
mean of x mean of y
 67.37987  64.84653
```

Results of the Mahalanobis distance for the comparison of TIR and optical data for differentiate ceramic and slate

7.5.10 Distance of Mahalanobis

```
[1] "La distance de Mahalanobis des données infrarouge est de 2.09375383319048
 alors que la distance de Mahalanobis des données optiques est de 4.26871308962
557 . La séparabilité est meilleure avec les données optiques (RVB)."
```

7.5.11 Distance of Bhattacharyya

```
[1] "La distance de Bhattacharyya des données infrarouge est de 0.5721247924677
93 alors que la distance de Bhattacharyya des données optiques est de 2.7902952
0654804 . La séparabilité est meilleure avec les données optiques (RVB)."
```

7.6 Appendix on ground covering

7.6.1 Results of the test for the ground covering

```
        Kruskal-Wallis rank sum test

data:  list(valeurs_emissivite_beton, valeurs_emissivite_paves, valeurs_emissivite_aspha
lte)
Kruskal-Wallis chi-squared = 1.9933, df = 2, p-value = 0.3691
```

Impact of artificial surfaces on Urban Heat Island (UHI) effect on the city of Louvain-la-Neuve. Study of the thermal radiance of materials and possible differentiation of surfaces from a TIR image

Romane Maroye

The global climate has shown signs of change, such as increasing temperatures, altered precipitation patterns and a higher frequency of extreme events. In addition to rising temperatures and the increasing frequency of heat waves, cities will be more vulnerable due to the urban heat island (UHI) effect. The UHI effect is characterised by higher air temperature in urban areas compared to surrounding rural areas. This difference in temperature is mainly due to the transformation of natural surfaces into artificial ones, anthropogenic heat release, and urban design that alters the energy balance. The disruption of the energy balance varies according to the types of urban development and the properties of their materials. Given the several impacts of this phenomenon on human health, energy consumption, biodiversity and so on, it is crucial to understand the factors contributing to this effect. This study aims to contribute to a better understanding of these factors in Louvain-la-Neuve.

Therefore, this study focuses on the different surface materials used in the city of Louvain-la-Neuve. The main objective of this study is to assess the thermal radiance of different types of artificial surfaces that contribute to the urban heat island effect. This is done using a thermal infrared (TIR) map. The study also aims to determine whether it is possible to recognise surface materials based on their thermal radiance from a thermal infrared image.

The current study has analysed the possible effect of the particularities of the city of Louvain-la-Neuve on the thermal radiance values. The platform on which the centre of the city is built has a slight effect, causing an increase in the thermal radiance value. However, it appears that there is no other effect of microclimate. Nevertheless, shading effect and insulation effect have been observed and must be taken into account when selecting pixels to determine valid thermal radiance values.

The results of the study show that the analysis of TIR images can establish a clear distinction between thermal radiances of different roof types, including ceramic, slate, flat roof and solar panel. The ceramic roof exhibits a higher thermal radiance value compared to slate roof. The flat roof and solar panel exhibits higher thermal radiance values than the two other roof types. Concerning the ground coverings, asphalt, concrete and cobblestones exhibit a similar thermal radiance value, which is significantly higher compared to the value of roof materials. Therefore, based on the TIR images, ground covering can easily be identified compared to roof coverings.

The study reveals that, in general, the TIR image appears to be relevant in distinguishing surface materials, thanks to the different thermal radiance values . TIR appears to be particularly advantageous in discriminating metallic and wood surfaces compared to optical images.

UNIVERSITÉ CATHOLIQUE DE LOUVAIN
Faculté des bioingénieurs
Croix du Sud, 2 bte L7.05.01, 1348 Louvain-la-Neuve, Belgique | **www.uclouvain.be/agro**